SURFACE AND DUAL-DOPPLER RADAR ANALYSIS OF 23-24 JUNE 1985 OK PRE-STORM HEAT BURSTS

by Ben C. Bernstein

Colorado State University

DEPARTMENT OF ATMOSPHERIC SCIENCE

PAPER NO. 474

SURFACE AND DUAL-DOPPLER RADAR ANALYSIS OF 23-24 JUNE 1985 OK PRE-STORM HEAT BURSTS

by

Ben Carter Bernstein

Department of Atmospheric Science
Colorado State University
Fort Collins, CO 80523

This research was supported by the National Science Foundation
under Grant No. ATM–8711649.

Atmospheric Science Paper No. 474

November 1990

ABSTRACT

SURFACE AND DUAL-DOPPLER RADAR ANALYSIS OF 23-24 JUNE 1985 OK PRE-STORM HEAT BURSTS

Doppler radar data are used to investigate heat bursts which accompanied a mesoscale convective system that traversed the OK PRE-STORM mesonetwork on 23-24 June 1985. The three dimensional structure of the precipitation and wind fields are discussed in an effort to uncover the cause of strong downdrafts which lead to the formation of heat bursts. Surface mesonetwork data are presented to depict the changes in temperature, dew point, relative humidity, θ_e, wind speed and wind direction which characterize them. Digitized WSR-57 radar data are used to detail the progression of the MCS, and a sounding is used to give an indication of the vertical structure of the temperature, dew point and wind fields in the vicinity of the heat bursts.

The 23-24 June MCS formed along a dry line in western Kansas. As the system matured, an area of stratiform precipitation developed behind a line of convective towers which moved southeast with time. Southwesterly flow at upper levels caused the stratiform precipitation to extend northeastward, allowing it to become isolated from the convective line. A broad surface mesohigh was observed beneath the core of the stratiform region. This feature was flanked by sharp pressure gradients and mesolows to its northwest, north and northeast. It was within these mesolows that the heat bursts occurred.

Time series of surface mesonetwork data show that heat bursts are characterized by sudden dramatic rises in temperature and falls in dew point. Strong, gusty winds and modest falls in θ_e also accompanied the bursts. These changes are attributed to the removal of a shallow, moist stable layer at the surface by an intrusion of warm, dry air from aloft.

A 600 km^2 area of winds greater than 15 $m\ s^{-1}$ was detected near the surface by the CP-3 Doppler radar. This wind maximum developed in an area of low reflectivity on the northeastern edge of the stratiform extension. These features moved southeast with time, and passed over one station in the mesonetwork, PAM-12. Their passage corresponded in time with the occurrence of heat bursts at that station.

Dual-Doppler syntheses for 5-10 minutes preceding the onset of the heat bursts reveal an anvil-like structure in the precipitation field over PAM-12. Stratiform precipitation was falling just to the west of the station, and a strong reflectivity gradient existed at the edge of this precipitation. A strong mesoscale inflow entered the anvil cloud region at mid-levels, descended along the base of the anvil and reached the surface in the area of the strong reflectivity gradient. Downdrafts reaching 3 $m\ s^{-1}$ were observed there. The winds detected in this region are used to infer winds which may have existed in the precipitation free portion of the stratiform anvil. It is proposed that this lateral inflow jet warmed dry adiabatically as it descended, deformed the surface stable layer and caused a dramatic warming and drying at PAM-12.

ACKNOWLEDGEMENTS

I wish to give my heartfelt thanks to Dr. Richard H. Johnson, my advisor, who has been extremely patient with me. He has offered helpful and thoughtful criticism at every step of this research. He has also been a good friend.

Additional thanks goes Dr. Steven Rutledge for his guidance in the use of the radar software packages. The advice he has offered was one of the keys to the success of this research. I would also like to thank Dr. Reza Zoughi, who has taken the time to stay involved with this research.

I would also like to acknowledge the assistance of my office mates, James Bresch, William Gallus and Michael Vescio. Their comments and assistance has made a big difference, especially when working with the computers. Thanks also go to Ray McAnelly, Jason Nachamkin, Hans Verlinde and Doug Burks, for their help with the radar processing, to Ian Baker for his aid on figures, and to Ian Wittmeyer for his help with VMS. Scot Randell is also thanked for his tireless and prompt editing of this manuscript.

The final manuscript was prepared by Gail Cordova, who has been an incredible help to me in many ways. This research was supported by the National Science Foundation Grant No. ATM-8711649.

TABLE OF CONTENTS

LIST OF FIGURES

Chapter 1

INTRODUCTION

Studies of Mesoscale Convective Systems (MCSs) by Newton (1950), Fujita (1955), Pedgley (1962), Zipser (1969, 1977), Houze (1977), Rutledge, et. al. (1988), and Johnson and Hamilton (1988) have led to a much clearer understanding of the structure and features associated with these storms. Houze et. al. (1989) have assimilated this research into an idealized model MCS (Fig. 1.1), depicting three distinct branches of storm-relative mesoscale flow: (1) a front-to-rear flow which ascends from the gust front region, forming convective precipitation just behind the gust front and advecting hydrometeors reward to aid in the formation of stratiform precipitation, (2) a rear-to-front flow, or "rear inflow jet" (Houze and Rutledge, 1986; Smull and Houze, 1986), which enters the storm at the rear and descends along the base of the trailing anvil cloud, warming and drying as it approaches the back edge of the stratiform precipitation region, and (3) a low-level return flow (front-to-rear) of cool convective downdraft air, which forms a stable layer behind the convective line (Houze, et. al., 1989).

A number of authors [e.g. Zipser (1969, 1977), Smull and Houze (1985, 1987), Rutledge and Houze (1987), Leary and Rappaport (1987), Rutledge, et. al. (1988), Johnson, et. al. (1989), Stumpf, et. al. (1990)] have analyzed the trailing stratiform region, the rear inflow jet and the features associated with this portion of MCSs. Johnson, et. al. (1989) have determined that the circulations associated with the trailing stratiform region set up an environment that is conducive to the formation of strong localized downdrafts, similar to those which accompany microburst events [e.g. Brown, et. al. (1982), Wakimoto (1983)]. They found that when a shallow surface inversion exists in the trailing stratiform region, these strong downdrafts may penetrate to the ground, producing sudden temperature jumps known as "heat bursts" (Johnson, 1983). Earlier documentations of heat burst

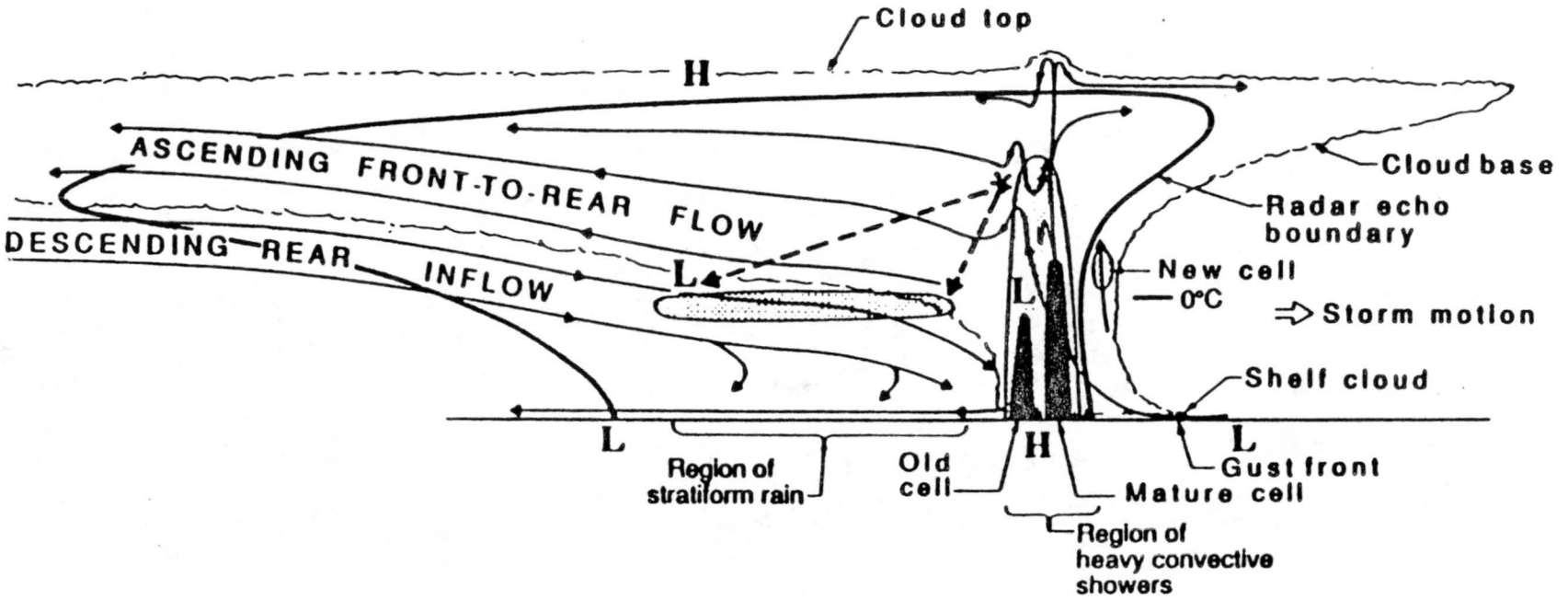

Figure 1.1: Schematic diagram of a typical squall line system having a trailing stratiform region. (From Houze, et. al., 1989)

activity by Williams (1963), Froude and Simmonds (1965), Sloan (1966), Wood (1966), and Fujita and Caracena (1977) have shown that these temperature rises are accompanied by dramatic falls in dew point temperature and pressure at the surface, in addition to strong, gusty winds (in some cases). The pressure falls were likely to have been caused by the nearby impact of a downburst, which resulted in the lateral displacement of the cool, moist layer near the surface and its subsequent replacement with warm, dry air from aloft (Fujita, 1985; Bedard and LeFebvre, 1986). Johnson, et. al. (1989) pointed out that this process was important for the case they studied, as simple heating of the surface layer did not produce pressure falls as large as those experienced during bursts.

A number of authors have noted that soundings released in close proximity to heat burst activity have shown a predominantly dry adiabatic temperature lapse rate, with a shallow, moist stable layer near the surface. The source of the stable layer may vary, although it most likely emanates from thunderstorm downdrafts, nocturnal surface cooling, or a combination of these factors. Johnson (1983) and Johnson, et. al. (1989) have determined that strong downdrafts were necessary to breach the shallow stable layers which exist in their heat burst cases. Such downdrafts have been documented at low levels using 461 m tower data by Johnson (1983), but the source of these downdrafts has yet to be determined. Johnson, et. al. (1989) have tentatively proposed that microbursts (Wakimoto, 1985) descending beneath virga from anvil clouds (Fujita, 1985) may penetrate a shallow, moist stable layer, thus causing warming, drying, and pressure falls at the surface. They also mentioned other possible mechanisms for the production of strong downdrafts, including rear inflow descending at the back edge of the stratiform precipitation region.

The purpose of this study is to attempt to determine the specific causes of the strong, localized downdrafts which produced the heat bursts in the case studied by Johnson, et. al. (1989). To accomplish this, dual-Doppler radar data will be used to analyze the precipitation and wind structures in the area of the burst activity. Further documentation of the surface features associated with the heat bursts will also be performed, with an attempt to relate these features to the proposed downdraft mechanism.

Chapter 2

PREVIOUS STUDIES OF HEAT BURSTS

Heat burst phenomena, although quite dramatic, have been the focus of few scientific investigations. The term "heat burst" was coined by Garrett (Johnson, 1983) as a sudden blast of hot, dry air that occurs in the vicinity of thunderstorms. The first documentation of heat burst (hereafter referred to as HB) activity was performed by Williams (1963) for a nocturnal thunderstorm that occurred on 3-4 May, 1961. This system passed through a network of surface stations that was in place for the National Severe Storms Project. Williams' analysis of this data revealed the existence of rises in temperature and falls in relative humidity and pressure just to the rear of a thunderstorm. This region, which he referred to as the thunderstorm wake, is commonly known as the wake low or wake depression (Fujita, 1955; Pedgley, 1962).

Sudden temperature rises of 8 to 11°C, accompanied by relative humidity falls of up to 45% were recorded within the wake low of the 3-4 May, 1961 storm. With time, these features tracked along with the back edge of the stratiform precipitation, as documented by low elevation scans taken at a nearby National Weather Service (NWS) WSR-57 radar site. Williams (1963) noted that no radar echoes were present at low levels in the regions where the HBs occurred. A single sounding released in the region of the wake low was also presented in this study. It revealed that a shallow, moist inversion existed in the 60 mb layer closest to the ground, with a 400 mb deep, nearly dry adiabatic layer immediately above (see Fig. 2.1). Williams used these data to infer that subsidence in the region contributed to the formation of the wake low and HB activity observed in that case.

Froude and Simmonds (1965) gave a short account of a "hot blast" that occurred near Aden, in southern Yemen. In their case, a temperature jump from 31°C to 42°C,

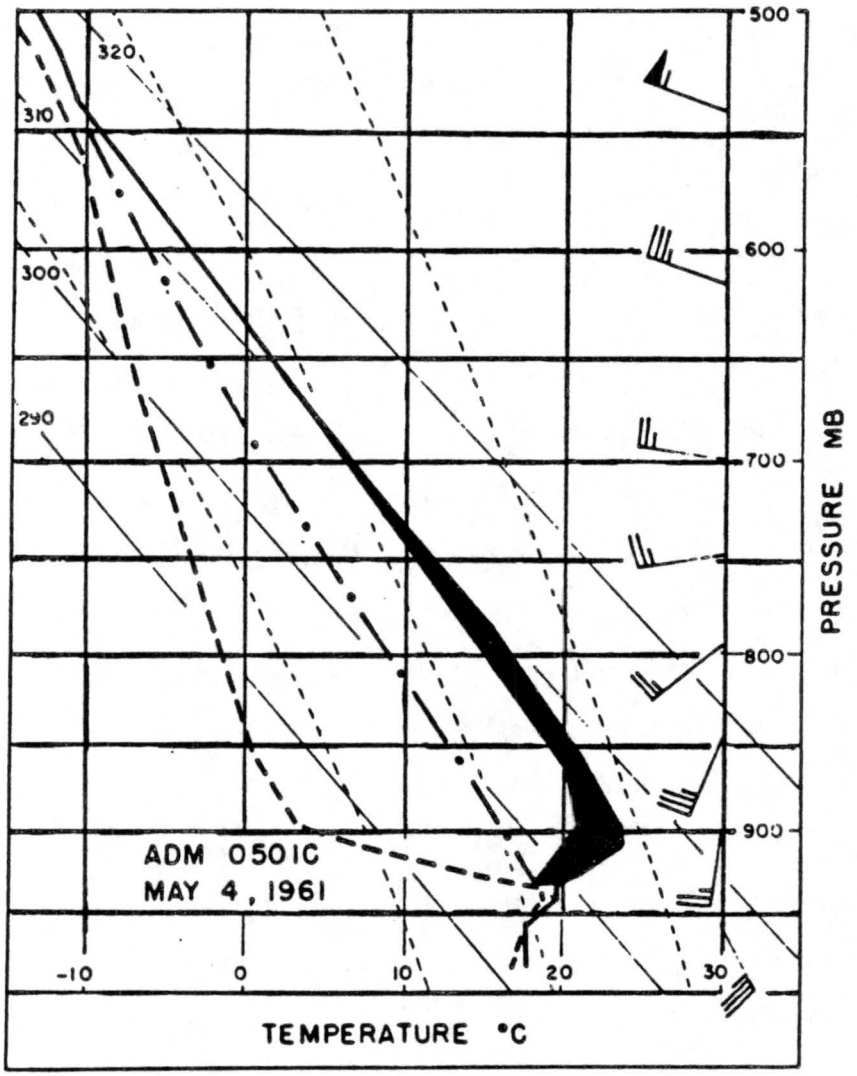

Figure 2.1: Sounding from the surface to 500 mb at Ardmore, Oklahoma, 0501 CST, 4 May 1961. The heavy solid line is temperature, and the heavy dashed line is dew point. The heavy dash-dot-dash line is an assumed coincident curve of temperature and dewpoint from 0357 CST. The shaded area shows the portion of the warming in the lower troposphere due to horizontal advection from 0357- 0501 CST. (From Williams, 1963).

accompanied by a relative humidity drop of nearly 45% and gusty surface winds that measured up to 16 $m\ s^{-1}$, occurred. Also presented in this study was a sounding taken earlier in the day (Fig. 2.2), showing a nearly dry adiabatic column with low moisture values from 850 mb to 530 mb, and a shallow stable layer in the lowest 100 mb. Sloan (1966) documented a similar event with a 6.6°C temperature rise that occurred in the vicinity of a small, dissipating cumulonimbus cloud. This event had a similar thermodynamic sounding structure to those cases reported earlier, but was not accompanied by gusty winds at the surface (Sloan, 1966).

Similar events and sounding structures have been documented by Wood (1966) in the vicinity of both active and dissipating thunderstorms. Fujita and Caracena (1977) also noted the occurrence of a number of warm downdrafts in their investigation of the crash of Continental flight 426 at Stapleton Airport, Denver on 7 August 1975. In this case, the 0000 Z evening sounding at Denver contained a nearly dry adiabatic lapse rate up to approximately 500 mb, and a surface temperature rise of 1.7°C was recorded (Fujita and Caracena, 1977). Cunningham (1989) also described a dramatic HB event in southern England, during which relative humidity dropped from near 100% to 16.5% almost instantaneously. All of these documentations of HBs were brief, and while they have collectively shed some light on the mechanism for strong warming at the surface, namely, the penetration of a shallow inversion by strong downdrafts, the character and source of the downdrafts have not yet been established.

A more comprehensive study of HBs was completed by Johnson (1983) for nocturnal thunderstorms that occurred in central Oklahoma on 29 May 1976. Again, a mesonetwork of surface stations, sounding and WSR-57 radar data were used for the investigation. However, the data set for this program (1976 observational program at the National Severe Storms Laboratory (NSSL)) also employed two unique data sets: an array of 9 rawinsonde sites and a 461 m instrumented tower, which collected vertical velocity data. The rawinsonde network revealed that the air was very dry aloft during the hours preceding the 29 May 1976 storms (Johnson, 1983). As these storms formed and were observed in the mesonetwork, WSR-57 data revealed that only a weak extension of stratiform precipitation existed in the area of HB occurrence. This precipitation area decayed and moved

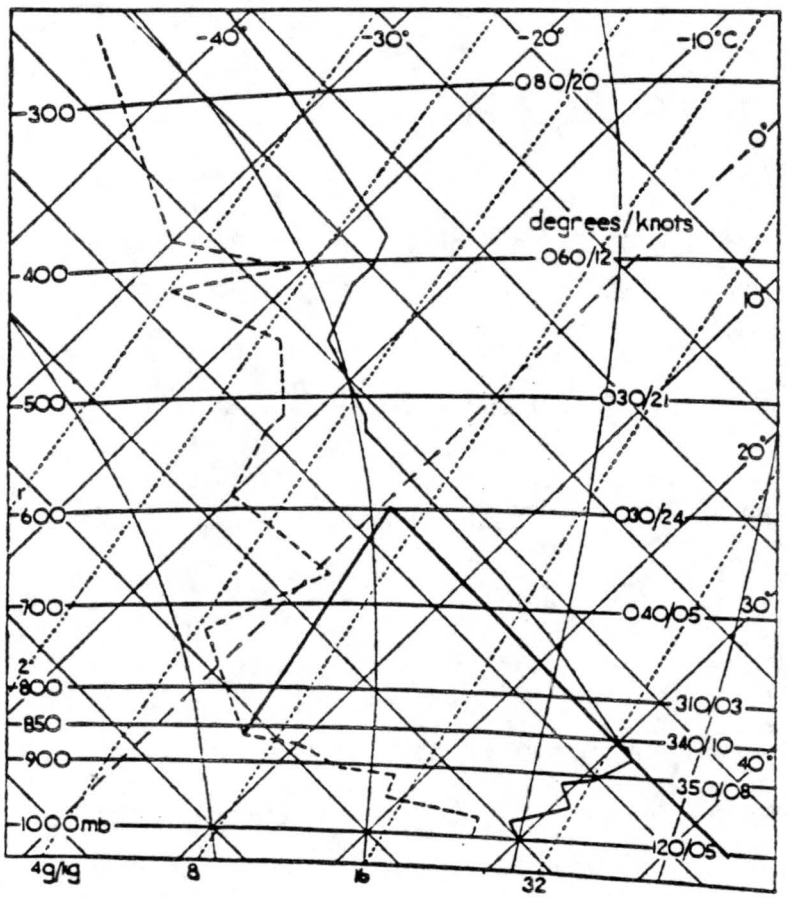

Figure 2.2: Sounding for Khormaksar, Yemen at 2330 UTC, 29 June 1964. The solid line represents temperature, and the dashed line represents dew point. (From Froude and Simmonds, 1965)

across the surface network with time, and a number of the surface stations measured temperature peaks, humidity drops and gusty winds which backed with time, similar to those described in earlier studies of heat bursts (Johnson, 1983). Rawinsonde time-height cross-sections taken during the passage of the decaying precipitation region reveal the existence of a preceding anvil cloud (seen as a layer of high θ_w values aloft), with very dry conditions in the layer just beneath it (see Fig. 2.3). Similar cloud structures were present in close proximity to the heat burst occurrences in the case studied here (see Chapter 5). Rawinsonde wind data presented in Johnson (1983) provide some indication of inflow from mid-levels outside the anvil cloud (see Fig. 2.3). A number of soundings were also presented for anvil regions near other heat bursts recorded on 29 May 1976. These soundings contained similar characteristics to those described earlier (e.g. moist, shallow surface inversion layer, deep dry adiabatic layer aloft). Tower data also collected during the passage of the decaying precipitation band indicated strong downdrafts of up to 8 $m\ s^{-1}$ in the region of HBs at approximately 450 m AGL (Johnson, 1983).

The most recent study of HBs was performed by Johnson, et. al. (1989) for the 23-24 June, 1985 MCS that occurred during the PRE-STORM field project. This case was studied using a mesonetwork of NCAR (National Center for Atmospheric Research) PAM (Portable Automated Mesonetwork - II) surface stations, radiosonde and digitized 10 cm WSR-57 radar data. HBs were detected near the northern and northeastern fringes of an expanding stratiform region that was associated with a convective line to the south (see Fig. 2.4). The bursts were characterized by temperature spikes of 2 to 4°C, dew point falls as great as 10°C, strong winds and relatively low pressure values. A negative correlation was found between the pressure and temperature fluctuations at PAM-3, the station which received the strongest bursts. However, no such correlation was found at station PAM-12, a station which received slightly weaker bursts (Johnson, et. al., 1989). Williams (1963), Johnson (1983) and Johnson, et. al. (1989) note 2 to 4 mb falls in the surface pressure during burst periods.

Differences in pressure changes during bursts may be attributed to the different downdraft impact scenarios described by Bedard and LeFebvre (1986). They point out that the

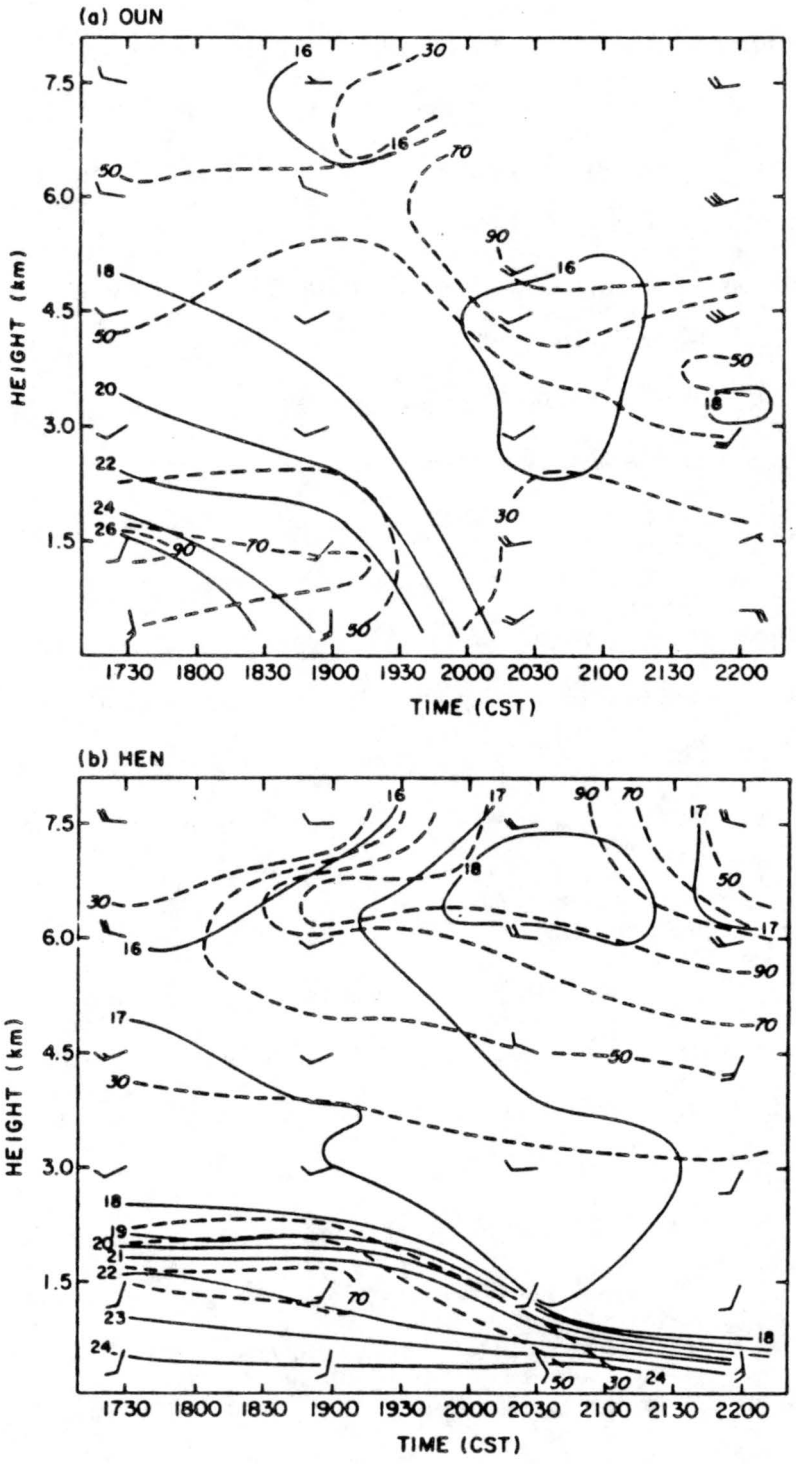

Figure 2.3: Height-time cross-sections at (a) Norman (OUN) and (b) Hennessey (HEN), Oklahoma. θ_w lines at 1°C intervals for OUN and 2°C intervals for HEN and are represented by solid lines. Whole and half wind barbs represent 10 and 5 $m\ s^{-1}$. Dashed lines represent isopleths of relative humidity. (From Johnson, 1983).

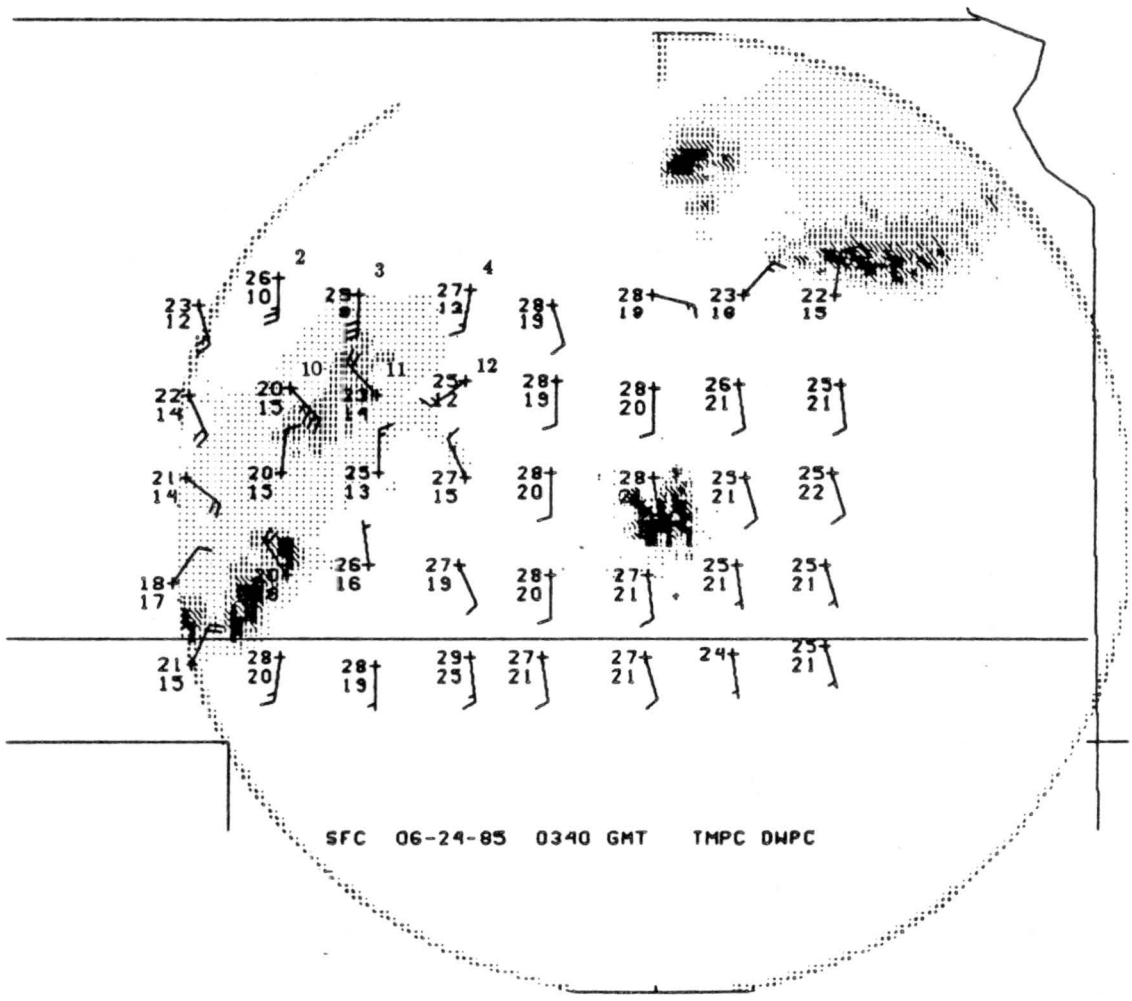

Figure 2.4: Surface mesonetwork analysis overlain with ICT WSR-57 radar data for 0340 UTC on 24 June 1985. Stations which received heat bursts are identified. Temperature and dew point are in °C.

impact of a downburst on a surface stable layer may result in a number of surface pressure responses. Lateral displacement of cool air near the ground by a nearby impacting downburst may result in pressure falls, while direct impact of a downburst may result in pressure rises at the surface.

Johnson, et. al. (1989) also analyzed a single sounding that was released close to the burst activity and pointed out the resemblance of this sounding to those presented by Johnson (1983). They also noted the similarity of their sounding to dry microburst soundings presented by Brown, et. al. (1982) and Wakimoto (1983), with the exception that microburst soundings contain a superadiabatic, rather than stable layer at the surface (see Fig. 2.5). The latter two authors point out that if precipitation aloft is evaporated in a dry environment, an air parcel in this region will cool, causing it to be negatively buoyant. This negative buoyancy will persist in a dry adiabatic environment, and a strong downdraft may be created by the time the parcel reaches low levels (Wakimoto, 1983). If the parcel has enough downward momentum to break through the shallow, moist stable layer near the surface (like those presented in HB soundings), then a dramatic warming and drying at the surface may occur (Johnson, et. al., 1989). Using the nearby sounding and the conditions described by Bedard and LeFebvre (1986) for the penetration of a downburst to the surface, Johnson, et. al. (1989) determined that a downdraft of 6 to 8 $m\ s^{-1}$, similar to those presented by Johnson (1983), would be required to breach the stable layer for the 23-24 June PRE-STORM case.

In none of the above studies were Doppler radar or other data available to document the three-dimensional structure of the precipitation and wind fields associated with the strong downdrafts. It is the purpose of this paper to remedy this situation, and to provide information concerning the source of the downdraft air.

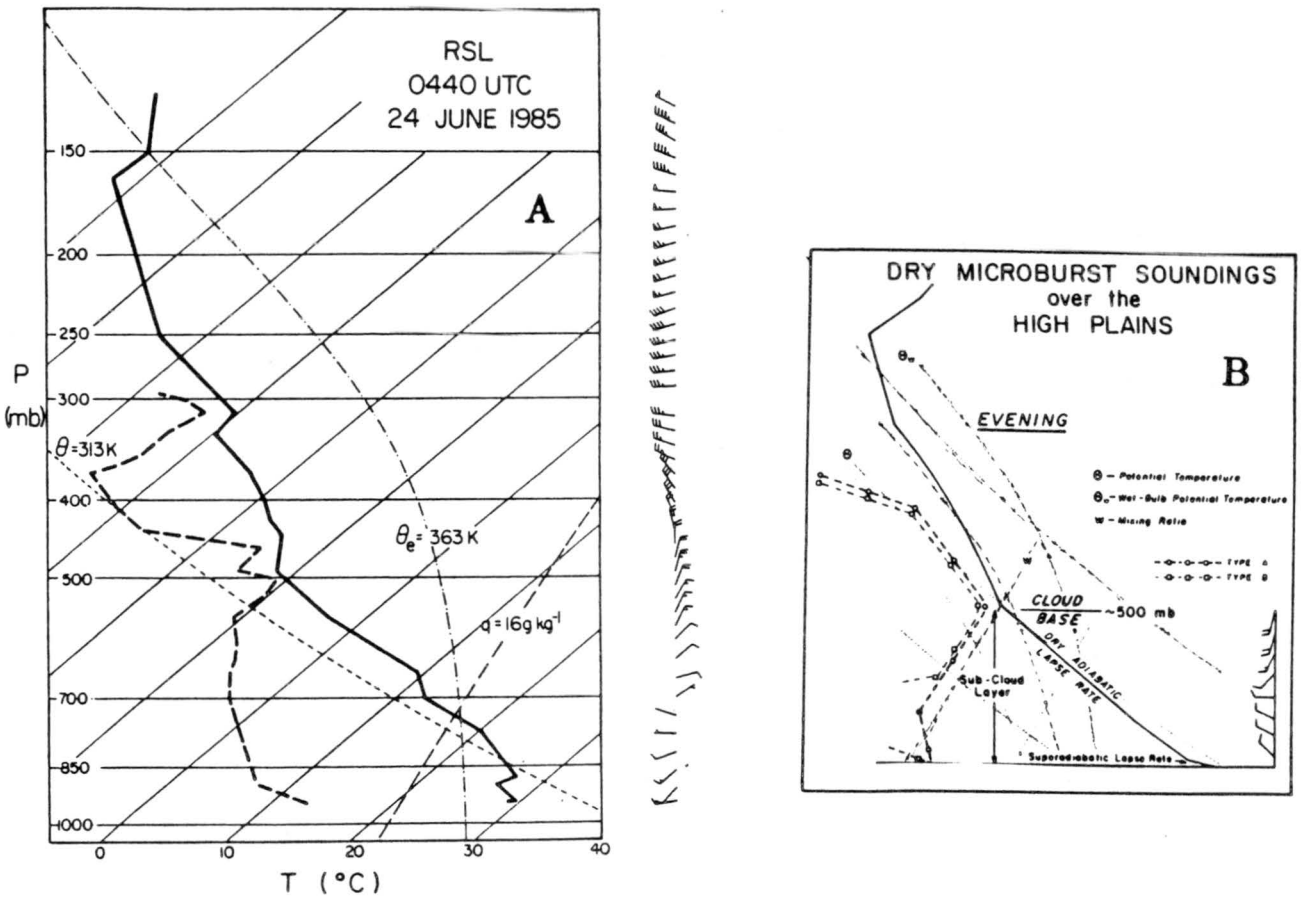

Figure 2.5: Typical soundings for (a) dry-microburst activity over the High Plains (from Wakimoto, 1983) and (b) heat burst activity (from Johnson, et. al., 1989)

Chapter 3

DATA SET AND ANALYSIS TECHNIQUES

3.1 OK-PRE-STORM

The Oklahoma - Kansas Preliminary Regional Experiment for STORM - Central (hereafter referred to as PRE-STORM) was a large field project conducted in the south-central Great Plains of the United States from 1 May to 27 June 1985. The purpose of this program was to study and improve the understanding of midlatitude mesoscale convective phenomena, and more specifically mesoscale convective systems (MCSs). Emphasis was placed on the evolution, structure and surface features associated with these storms. This was achieved through the use of a sophisticated data collection network employed for this experiment. This network included a mesonetwork of surface stations, seven digitized NWS WSR-57 10 cm radars, a network of rawinsonde sites, wind profilers, and four 5 cm Doppler radars (see Fig. 3.1)(Cunning, 1986).

3.2 Surface Data

The PRE-STORM field project employed 84 automatic surface stations. The stations were placed in an 8 by 10 array, with a separation of approximately 50 km between stations. The northern portion of this surface mesonetwork was comprised of 40 NCAR/FOF Portable Automated Mesonetwork - II (hereafter referred to as PAM) stations, while the southern portion of the network was made up of 42 National Severe Storms Laboratory (NSSL) Surface Automated Mesonetwork (SAM) stations (Meitín and Cunning, 1985). Two additional PAM stations were colocated at two SAM station sites. For this study, only data from PAM stations (see Fig. 3.2) will be analyzed, as this portion of the surface mesonetwork encompasses those stations affected by the 23-24 June MCS between 0230

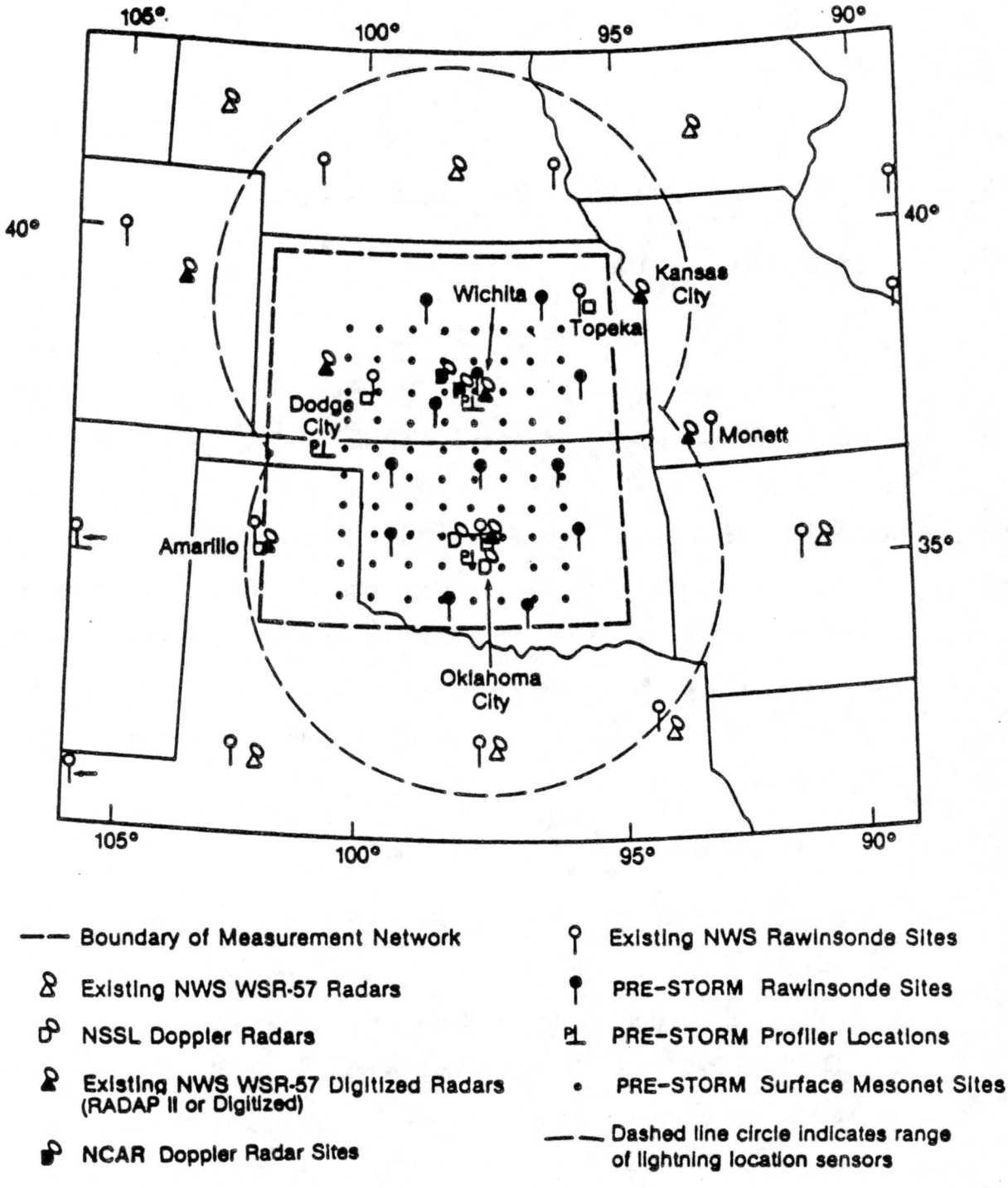

Figure 3.1: Overview of the surface measurement network (From Meitín and Cunning, 1985).

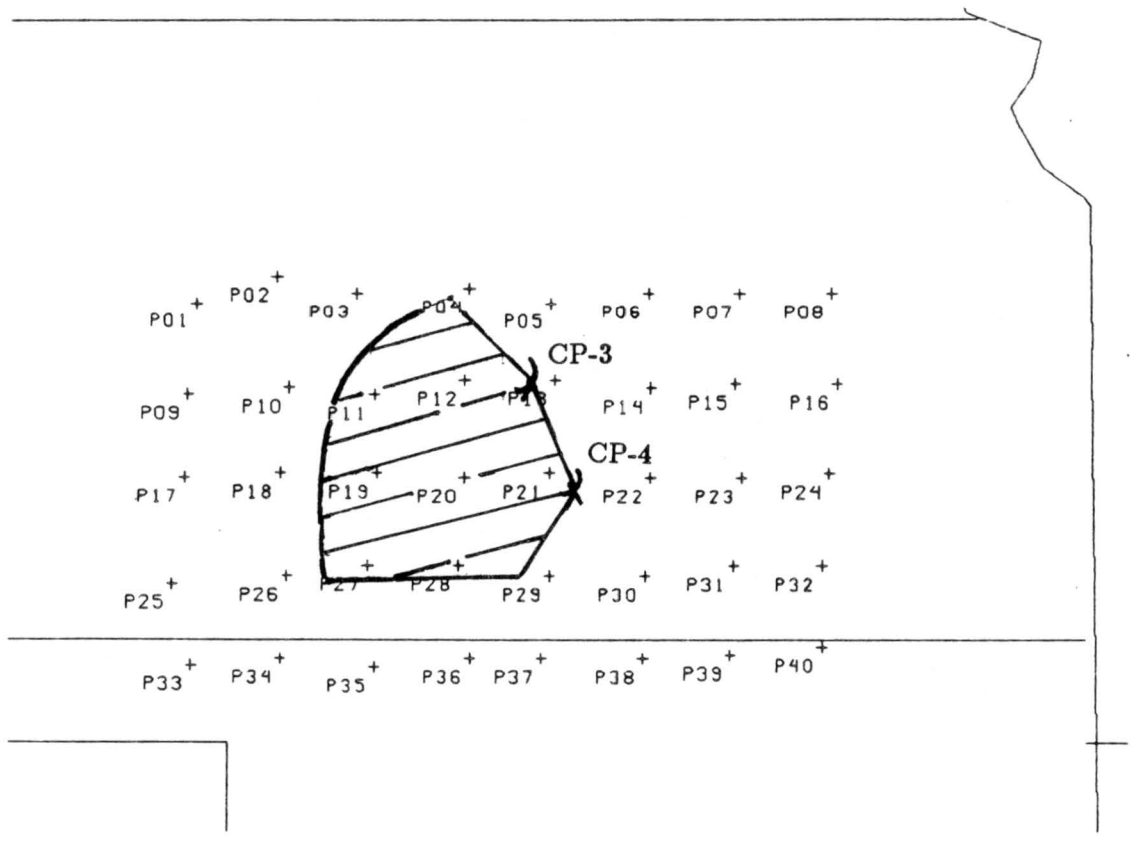

Figure 3.2: NCAR/FOF Portable Automated Mesonetwork - II (PAM) stations 1 through 40, overlain with NCAR CP-3 and CP-4 dual-Doppler radar grid area used in this case (hatched area).

and 0530 UTC, as well as a number of surrounding stations which represented the environmental conditions of the region. The SAM stations were removed from the area of interest, and thus, were not necessary for the complete analysis of surface features associated with this system.

Data measured and recorded at the mesonet stations included 5 minute averages of dry bulb and wet bulb temperature, pressure, and the u and v components of the wind. Peak wind gust and rainfall measurements were also recorded, and variables such as θ_e and θ_w were calculated for each 5 minute period. Sloped topography in the area of the surface mesonetwork required that all pressure measurements be adjusted hydrostatically to the average elevation of 24 stations which surrounded PAM-12, 584.3 m. This adjustment was performed for each station using the following formula:

$$P_{584.3} = P_s exp\left[\frac{g(584.3 - z_s)}{R_d \bar{T}_{vs}}\right] \tag{3.1}$$

where T_{vs}, the surface virtual temperature, is used to approximate the mean virtual temperature in the column from the station elevation to 584.3 m. Station pressure (P_s) and station elevation (z_s) are given in mb and m, respectively. The constants used in (3.1) are gravity (g) = 9.8 $m\ s^{-2}$ and the gas constant for dry air (R_d) = 287 $J\ kg^{-1}\ K^{-1}$. Adjustments were also made for systematic errors in the surface pressure measurements, as outlined by Johnson and Toth (1986).

3.3 Radar Data

The PRE-STORM observational network also featured extensive radar coverage. Large areal coverage of Kansas, Oklahoma and the surrounding region was provided by 7 existing NWS WSR-57 (see Fig. 3.1). The volume scans recorded by these radars were in digitized format, which allowed for more simplified display than the previous method of photography of the radar scope (e.g. Johnson, 1983). The WSR-57 radars had a 10 cm wavelength, a 2° beamwidth and a gate spacing of approximately 2 km (Meitín and Cunning, 1985). Also in place for this experiment were the NCAR CP-3 and CP-4 Doppler radars, located at Nickerson and Cheney Reservoir, Kansas, respectively (see Fig.

3.1 for locations). The relative position of the NCAR radars allowed for extensive dual Doppler coverage in the Kansas region of the PRE-STORM mesonetwork (see Fig. 3.2). These radars performed coordinated scans of common volumes, providing two areas of dual-Doppler coverage (Rutledge, et. al., 1988). Each single Doppler radar volume was corrected for aliasing in the radial wind field, and for false echoes (e.g. second trip echoes from precipitation outside the range of the radar) by hand, using the NCAR RDSS software package. These data were then interpolated to a three-dimensional Cartesian grid, using the NCAR SPRINT software package (Mohr, et. al., 1979). A grid spacing of 2 km in the horizontal and 0.5 km in the vertical was used. All data were repositioned in the grid to account for storm motion over the period of the radar scans. A storm motion vector of 5 $m\ s^{-1}$, from 330°was subtracted from all horizontal winds, giving storm-relative flow (Rutledge, et. al., 1988). This vector was determined using the change in position of an enhanced portion of the stratiform precipitation shield between 0230 and 0530 UTC. A detailed description of the processes used to attain the final reflectivity and u, v and w wind fields can be found in Appendix A.

3.4 Upper Air Data

Another highly valuable data source in place for the PRE-STORM field project was an extensive upper air network. This network was comprised of 15 NWS rawinsonde sites, as well as 12 supplemental sites that were in place specifically for the program. The location of these sites is shown in figure 3.3. Unfortunately, limited upper air data were available for the 23-24 June, 1985 case, and only one rawinsonde (RSL, 0440 UTC) was released in the vicinity, and near the time of the HB activity. Investigation of rawinsonde data for this case is therefore limited to this lone sounding. Equivalent potential temperature, θ_e, was calculated for 27 levels in the RSL 0440 UTC sounding between 300 mb and the surface, using the methods outlined by Bolton (1980).

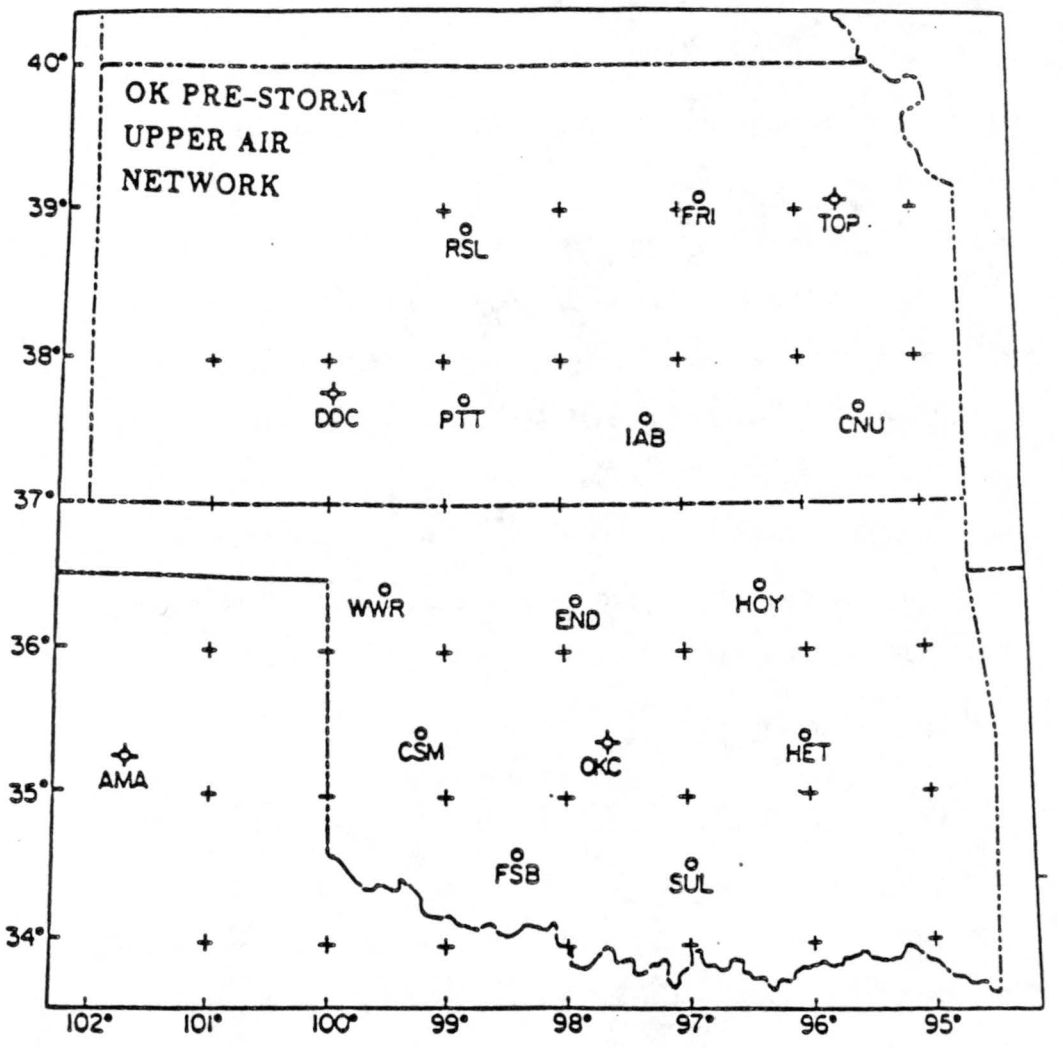

Figure 3.3: The PRE-STORM upper air network. Crossed circles indicate NWS sites. Plain circles indicate supplemental sites. (From Stumpf, 1988)

Chapter 4

SYNOPTIC SITUATION AND STORM OVERVIEW

4.1 Synoptic Conditions Preceding MCS Development

4.1.1 Surface Data Analysis

Analysis of the conditions preceding the development of convection on 23-24 June 1985 reveal a number of important features. Surface measurements taken at 1200 UTC at NWS stations in the Kansas-Oklahoma area on 23 June show that rather warm, moist conditions predominated, with temperatures between 22 and 25°C, and dew points between 16 and 18°C (see Fig. 4.1). A stationary front was positioned across central Nebraska, extending from a deep low pressure system centered near Hudson Bay, Canada, and connected to a weak low pressure center located near the Nebraska-Colorado-Kansas border. A large high pressure system was centered near Cape Hatteras, North Carolina. The combination of these pressure centers and the nearby cold frontal trough led to strong southerly and southwesterly flow over Kansas and Oklahoma. Temperatures and dew points to the south were slightly higher. A dry line was also present near the Colorado-Kansas border at this time. Dew points in eastern Colorado ranged from 0 to 5°C, while winds there were predominantly from the west.

By 0000 UTC (not shown), most temperature and dew point values in Kansas and Oklahoma reached 30°C and 22°C, respectively. Winds there remained strong out of the south, with some stations reporting speeds of 10 $m\ s^{-1}$. The surface low located in western Nebraska at 1200 UTC migrated southeastward by 0000 UTC, and was centered along the western portion of the Kansas-Nebraska border. Its central pressure had fallen slightly. The dryline in western Kansas had not moved detectably during the twelve hour period, according to the synoptic scale data available for this case. It is likely, however, that it

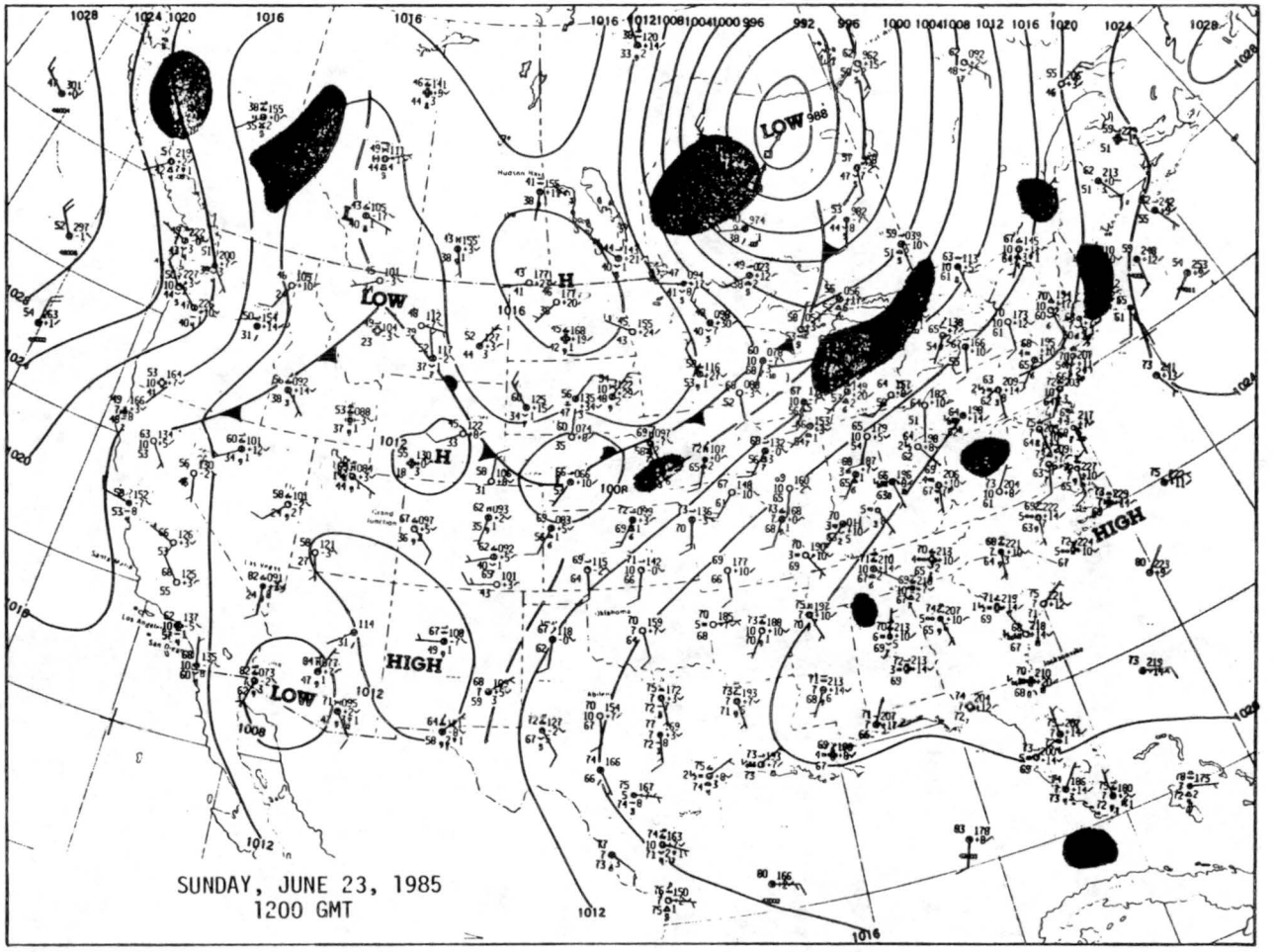

Figure 4.1: Synoptic surface analysis for 1200 UTC, 23 June 1985. (From Meitin and Cunning, 1986)

moved slightly eastward, along with the surface low, and acted as a triggering mechanism for the MCS studied here.

4.1.2 Upper Air Data Analysis

National Meteorological Center (NMC) upper level analyses for 1200 UTC, June 23 (Fig. 4.2) reveal that warm temperatures and southwesterly flow existed over Kansas and Oklahoma at 850 mb. Moisture at this level was plentiful, with dew points of 15 and 16°C reported over the PRE-STORM study area. Cooler conditions existed at higher levels (700 and 500 mb), which brought about a conditionally unstable temperature lapse rate in the region.

The NMC 500 mb height analysis depicted a warm anticyclone over central Oklahoma at 1200 UTC. Temperatures there were around -8°C, while dew points depressions of 30°C were reported at all Kansas and Oklahoma upper air stations. A vorticity maximum approaching western Kansas provided a lifting mechanism over the PRE-STORM area (see Fig. 4.3). The 300 mb analysis reveals an additional lifting mechanism at upper levels, as some directional divergence existed in the winds there. Further discussion of the conditions which existed over Kansas and Oklahoma for the 23-24 June MCS case can be found in Stensrud and Maddox (1988).

4.2 MCS Development and Life Cycle

The convective activity studied in this case first began to form along the dryline in western Kansas, along the southern periphery of the dry line in northeastern New Mexico, and along the synoptic cold front in southeastern Nebraska by 2100 UTC (see Figs. 4.4, 4.5a). Infrared satellite images (Fig. 4.5b,c) depict that this activity intensified, and developed an area of cold cloud tops between 0100 UTC and 0400 UTC on 24 June.

The life cycle of the 23-24 June MCS is most clearly demonstrated by the series of infrared satellite images in Fig. 4.5 and ICT WSR-57 digitized radar reflectivity images (Fig. 4.6). The ICT radar data are presented in approximately 30 minute intervals and are overlain with the Kansas-Oklahoma border to aid in the placement of this data in relation to the surface data to be presented later in this paper (chapter 5).

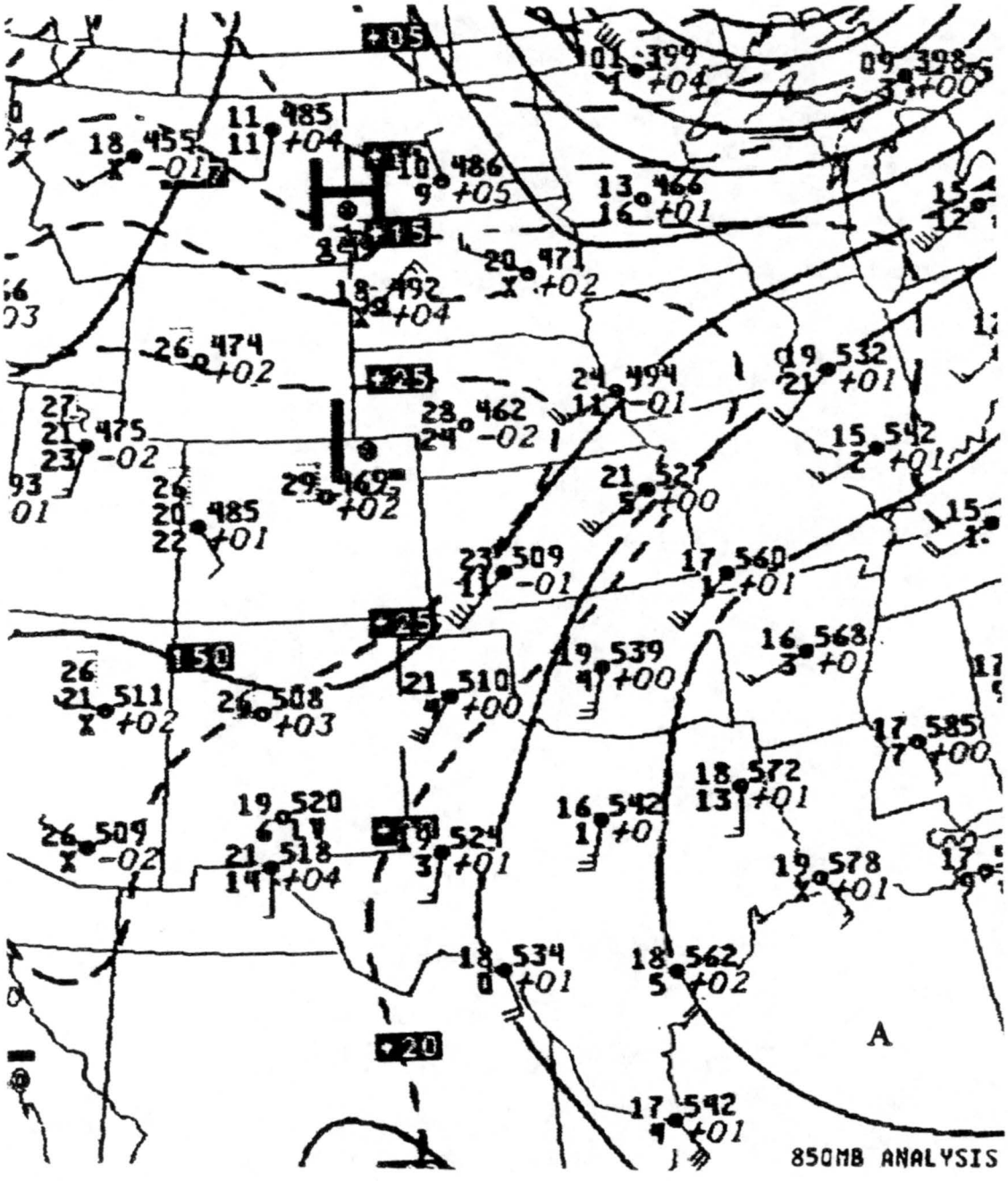

Figure 4.2: NMC upper level charts at (a) 850, (b) 700, (c) 500, and (d) 300 mb for 1200 UTC, 23 June 1985.

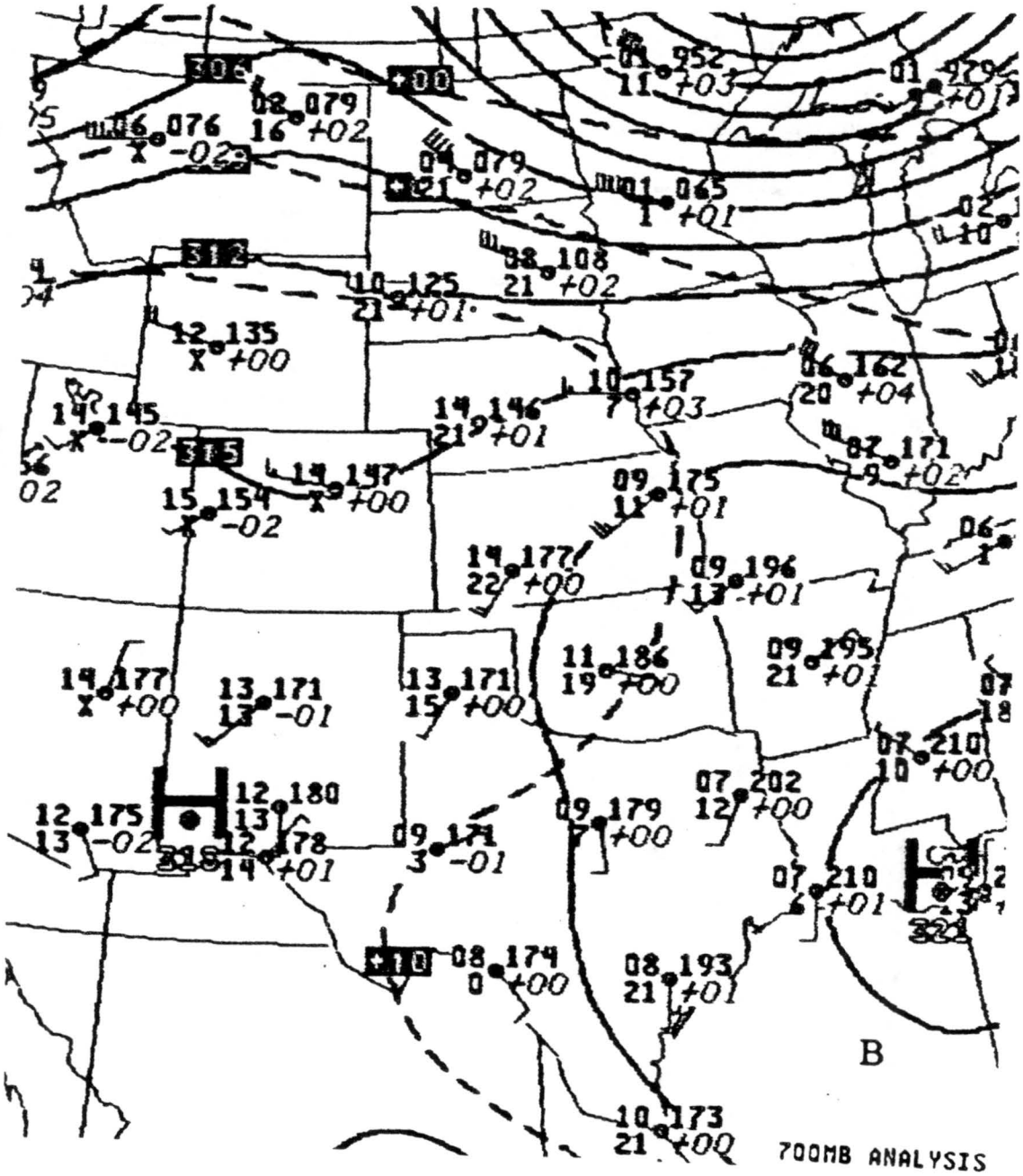

Figure 4.2: continued

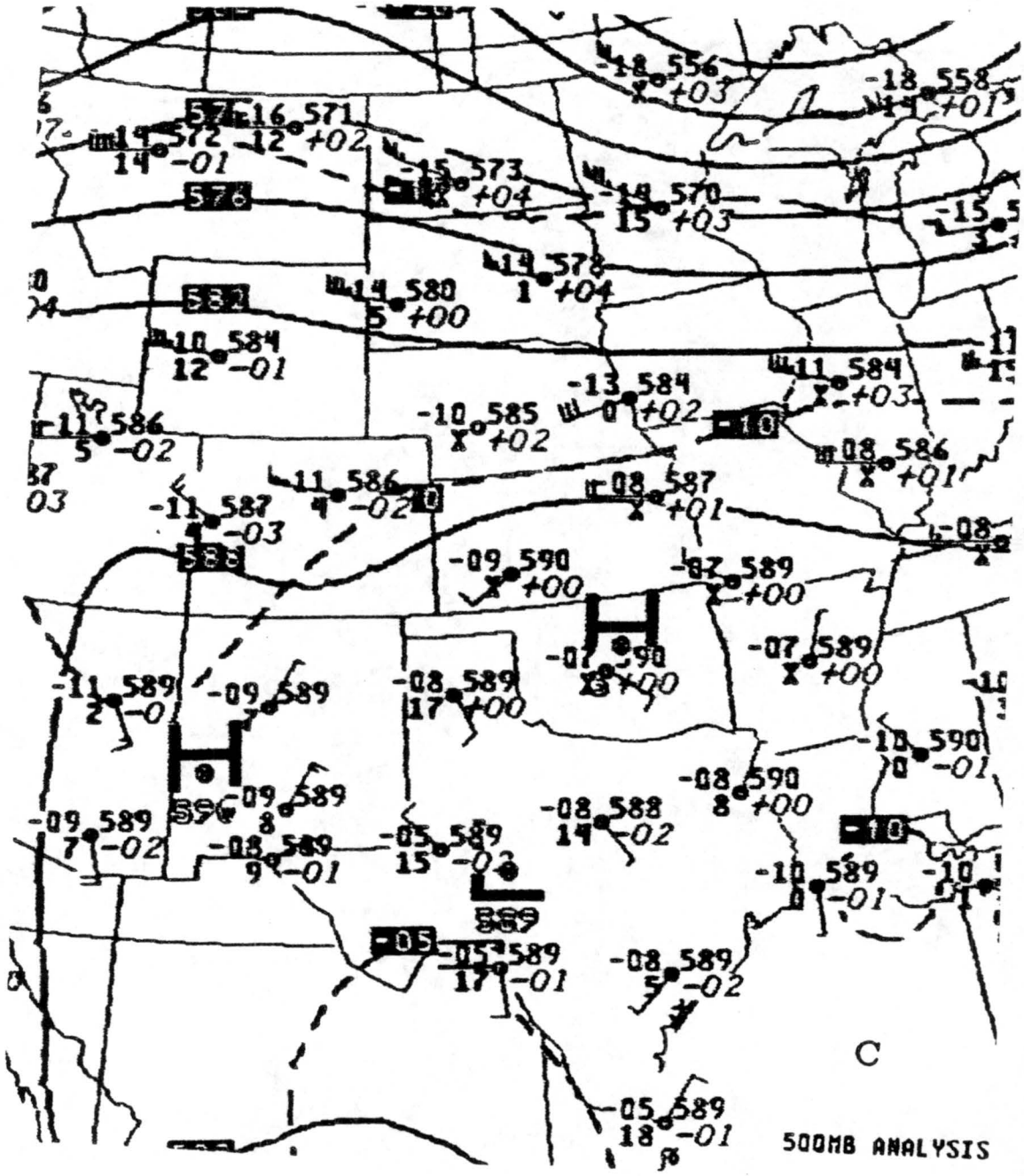

Figure 4.2: continued

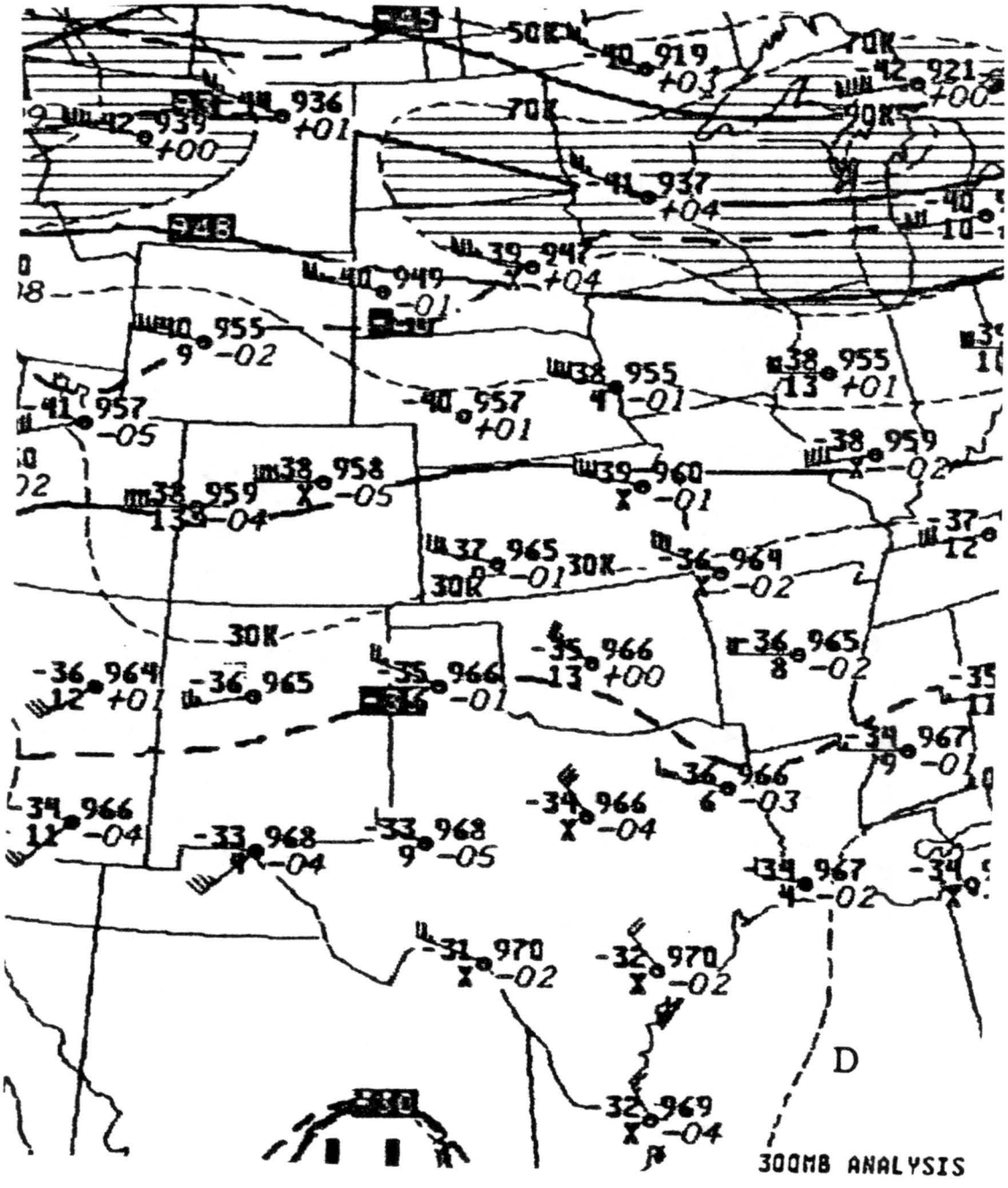

Figure 4.2: continued

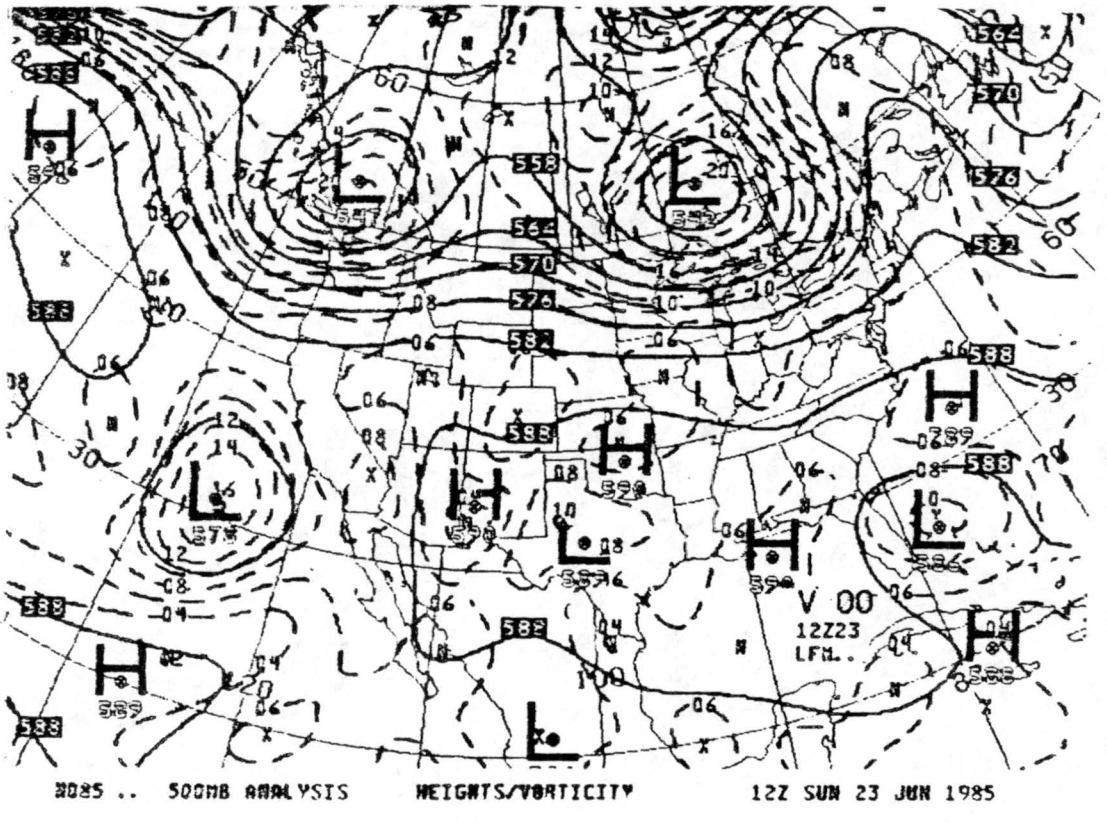

Figure 4.3: 500 mb heights (dam) and absolute vorticity (x 10^{-5} s^{-1}).

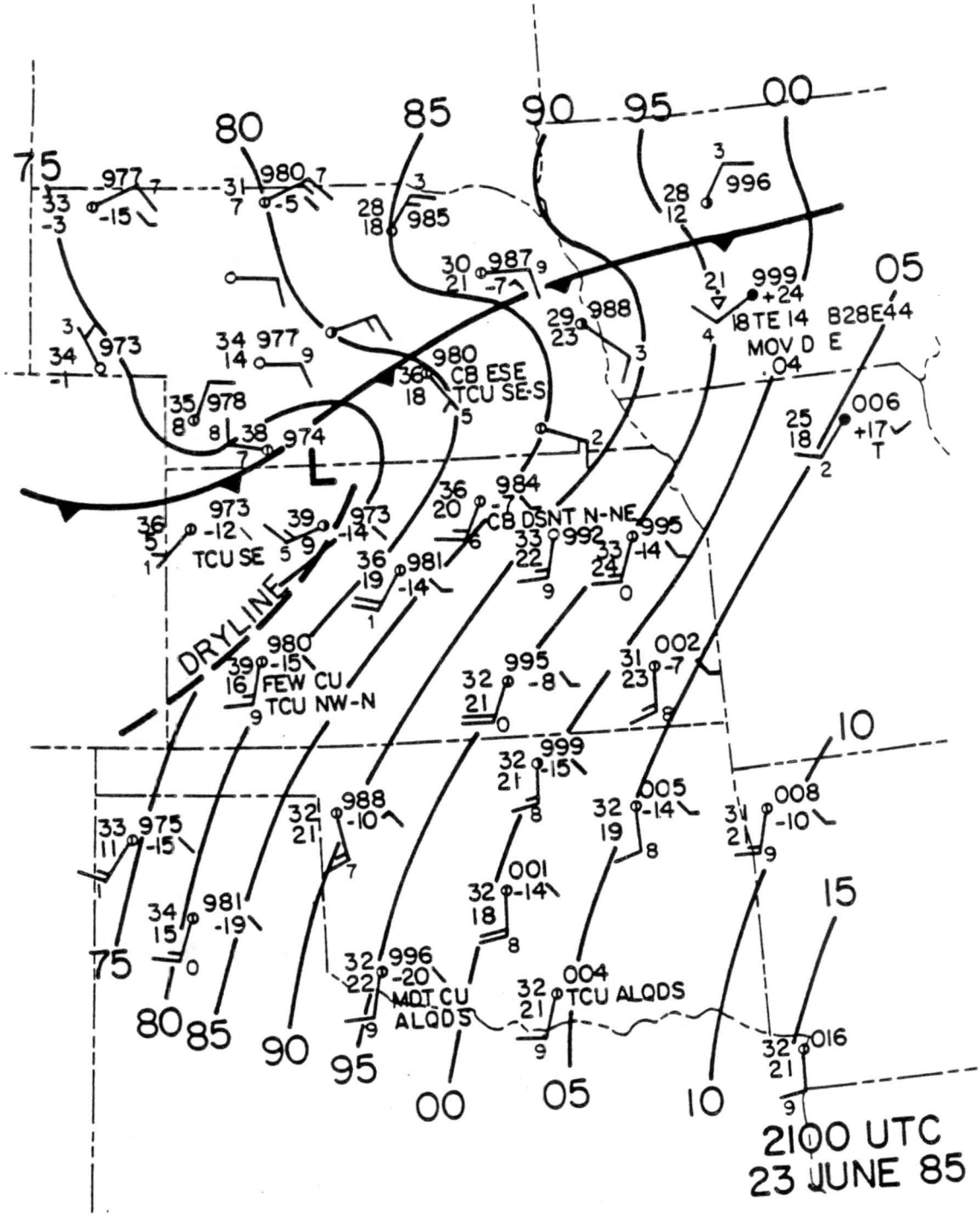

Figure 4.4: Surface analysis for 2100 UTC, 23 June 1985. Contours of pressure are for altimeter settings, adjusted to a mean level of 400 m. Units of contours are in Hg. (From Johnson, et. al., 1989)

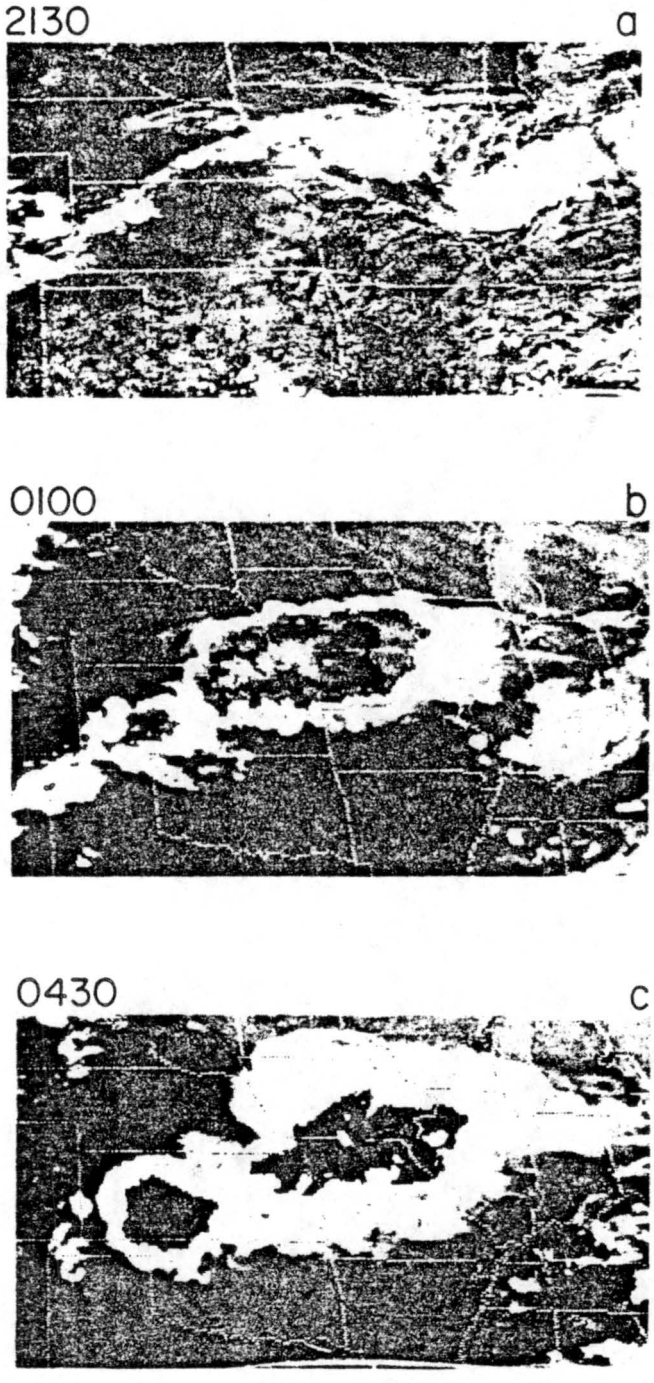

Figure 4.5: Visible and infrared satellite images for (a) 2130 UTC, 23 June, (b) 0100 UTC, and (c) 0400 UTC, 24 June 1985.

The initial frame of the ICT radar sequence (Fig. 4.6a) shows the existence of two distinct systems at 0147 UTC . Convection that formed along the stationary front in southeastern Nebraska (see section 4.1) is visible on the northern periphery of this scan. This system progressed slowly to the south-southeast with time. A second system is visible on the western edge of this scan. This system, the focus of the study, featured a broken line of convective cells which existed just behind a gust front that was progressing in a bow-like fashion toward the south and east. The passage of this gust front, featuring temperature falls, pressure rises and heavy precipitation was detected at many surface stations in the PRE-STORM mesonet. The convective cells had reflectivity greater than 40 dBZ with some cells exceeding 50 dBZ. The strongest of these cells existed on the southern edge of the convective activity, while weaker cells appeared on the southeastern edge (most reflectivity 30-45 dBZ) and eastern edge (most reflectivity 18-30 dBZ) of the MCS. At this time, an extensive stratiform region had already developed. Most reflectivity in the stratiform area was between 18 and 30 dBZ, with a small area of enhanced reflectivity (greater than 30 dBZ) embedded within.

By 0218 UTC, the broken convection assumed a more linear structure, with a nearly continuous line of reflectivity exceeding 30 dBZ (see Fig. 4.6b). The extreme northeastern edge of this convective line continued to be characterized by weak reflectivity, with few echoes exceeding 30 dBZ. During the 30 minute period between scans, the stratiform area expanded, and developed a larger area of enhanced precipitation. The 0256 UTC radar scan shows that the convective line once again became discontinuous, although individual cells attained larger areas of reflectivity exceeding 45 dBZ (see Fig. 4.6c). Two strong cells existed on the southern periphery, while a lone cell existed on the eastern edge of the MCS. Again, the stratiform area and the enhanced precipitation area within expanded. By 0311 UTC (only 15 min. later), the eastern cell had begun to decay, rapidly lost nearly all reflectivity values greater than 50 dBZ, and decreased in size (see Fig. 4.6d). These cells moved very little as they weakened. The southern cells also weakened slightly, but continued to move southward with time. The stratiform region continued to grow, however. By 0340 UTC, the eastern cell had almost completely dissipated, and only remained as a weak extension of the stratiform region (see Fig. 4.6e).

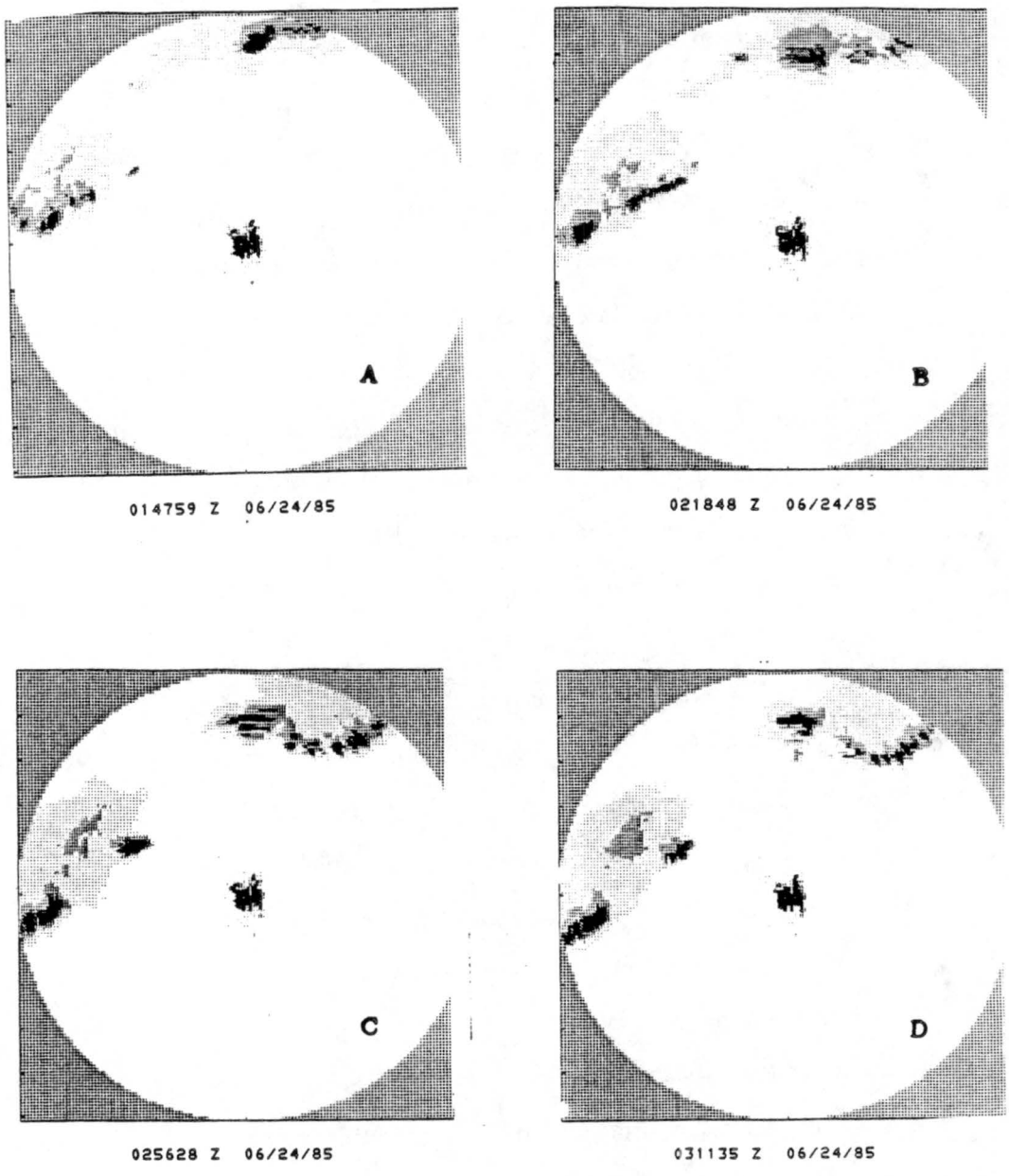

Figure 4.6: WSR-57 radar reflectivity patterns from Wichita, Kansas at (a) 0147, (b) 0218, (c) 0256, (d) 0311, (e) 0340, (f) 0410, (g) 0448, and (h) 0529 UTC, 23 June 1985.

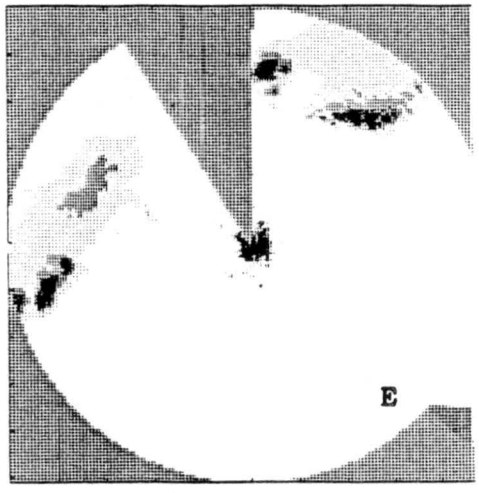

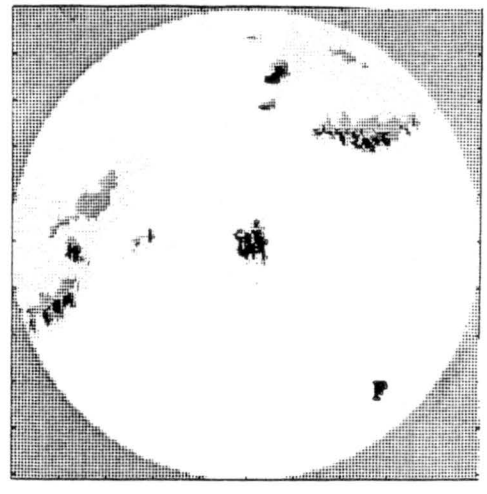

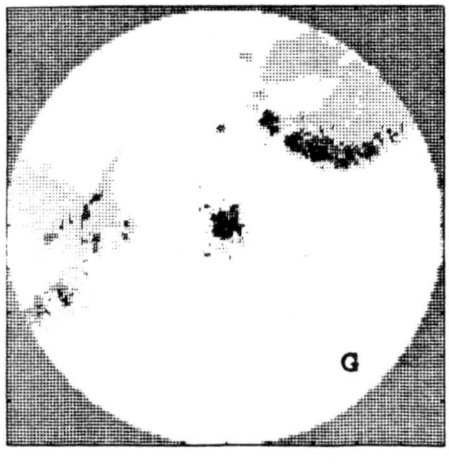

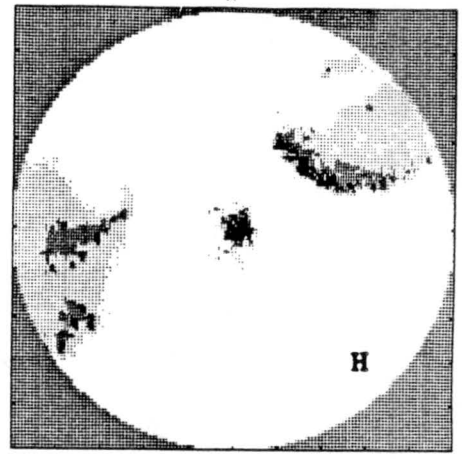

Figure 4.6: continued

The scans recorded between 0400 and 0529 UTC, following the decay of the eastern cell, depict that the convective line soon weakened, leaving only a large area of stratiform rain behind (see Figs. 4.6f-h). This precipitation area drifted slowly south-southeastward, and weak convection occasionally formed on its southern edge. Some growth of the enhanced stratiform area also took place during this period.

Heat burst activity, including extreme events at station PAM-3, occurred along the periphery of the stratiform precipitation area associated with the 23-24 June MCS. This study will concentrate on the activity of this MCS between 0230 and 0530 UTC, the period of the most intense heat burst activity at PAM-12, with special attention lent to the precipitation close to that station.

Chapter 5

SURFACE OBSERVATIONS OF HEAT BURSTS

5.1 Heat Bursts Recorded in the Surface Mesonet

The HB activity that accompanied the 23-24 June MCS was recorded at a number of PAM surface mesonet sites. Figure 5.1 shows the effects this activity had on the temperature and dew point traces of six stations, PAM-2, 3, 4, 10, 11 and 12. Stations 3, 4 and 12 experienced the strongest HBs, with temperature and dew point fluctuations on the order of 3 to 5°C. Dew points at PAM-3 fell as much as 10 to 12°C. The fluctuations in these variables at stations PAM-2, 10 and 11 were nearly all on the order of 1°C. Although stations PAM-3, 4 and 12 all recorded significant HB activity, only station PAM-12 was located close enough to the NCAR CP-3 and CP-4 Doppler radars to allow dual-Doppler investigation of the precipitation and wind structures related to the HB activity there (see Fig. 3.2). Therefore, the investigation of the surface records of the HBs will be limited to this station.

5.2 Heat Burst Activity at PAM-12

The HB activity at PAM-12 is demonstrated using a trace of the surface measurements recorded at this site over time (Fig. 5.2). Such figures have been used in previous studies of HBs by Williams (1963), Froude and Simmonds (1965), Johnson (1983), Johnson, et. al. (1989) and Cunningham (1989) to depict the changes in temperature, dew point, relative humidity, pressure, wind speed and wind direction. These variables will also be investigated here, but will be supplemented by traces of peak wind gust speed and θ_e. The effects of HB activity on temperature, dew point, relative humidity and pressure have been well documented, as discussed in Chapter 2. The impact of HBs on surface winds,

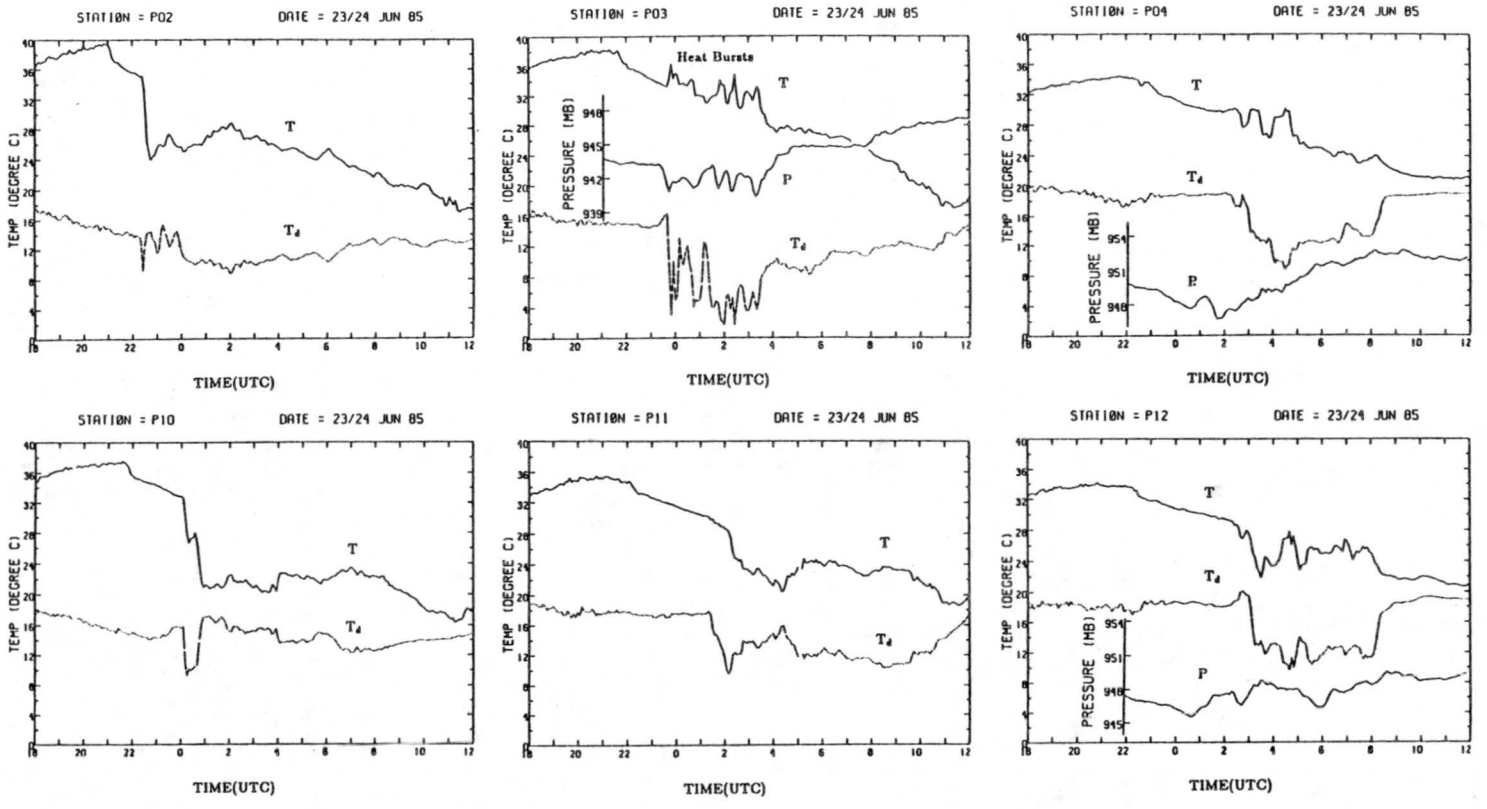

Figure 5.1: Time series of temperature, dew point and pressure at PAM stations 2, 3, 4, 10, 11 and 12 from 1800 UTC, 23 June 1985 to 1200 UTC, 24 June 1985. Heat bursts were most prominent at stations 3, 4 and 12. (From Johnson, et. al., 1989).

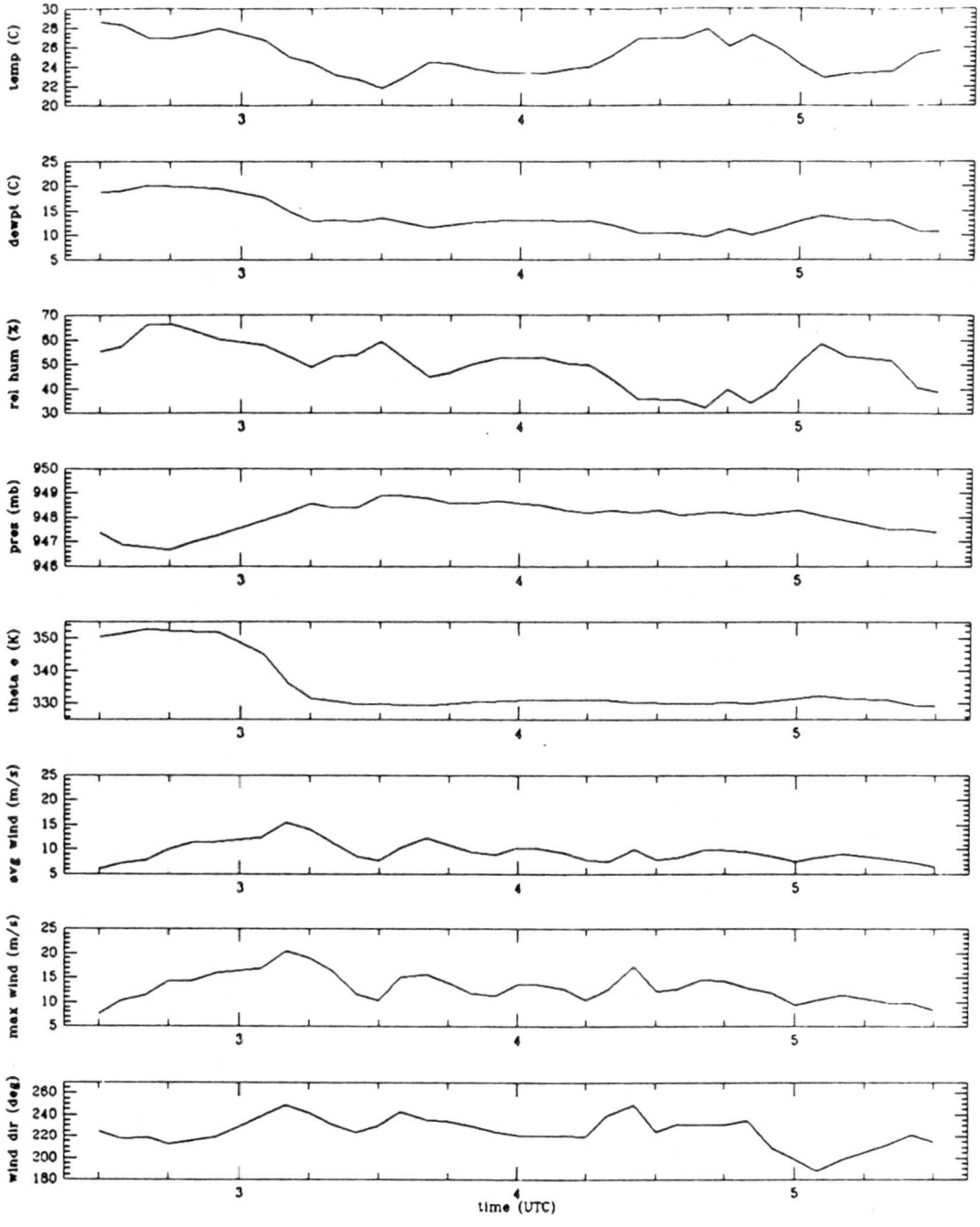

Figure 5.2: Time series of temperature, dew point, relative humidity, pressure, θ_e, average wind speed, peak wind gust speed and wind direction at station PAM-12 from 0230 UTC to 0530 UTC, 24 June 1985.

however, has remained unclear. Surface winds were reported as gusty and variable in some of the cases mentioned above. Johnson (1983) noted that winds backed with time and were gusty during HBs.

Time traces of the above mentioned variables will be used in conjunction with θ_e and peak wind gust speed measured at station PAM-12. θ_e will be used to give an indication of the origin of the air reaching the surface at PAM-12 with the aid of sounding data taken simultaneously with the surface HB occurrence at a nearby site, Russell, Kansas (RSL) (θ_e values were calculated at 27 levels in this sounding (see section 3.4 for calculation method)). WSR-57 radar reflectivity data from Wichita, Kansas (ICT), overlain with PAM surface mesonet data and a surface pressure analysis, will also be presented.

The majority of the HB activity at PAM-12 occurred between 0230 and 0530 UTC on 24 June, and can be broken down into five distinct periods: 1) 0230 - 0330 UTC, the period preceding the first HBs, 2) 0335 - 0350 UTC, the first HB episode, 3) 0355 - 0415 UTC, the period between the two HB episodes, 4) 0420 - 0450 UTC, the second HB episode, and 5) 0455 - 0530 UTC, the period following the first two HB episodes .

5.2.1 Period 1: 0230 - 0330 UTC

The period preceding the occurrence of the first HBs at PAM-12 began at 0230 UTC, near the time of sunset. At this time, the station temperature and dew point were 28.7°C and 18.8°C, respectively (see Fig. 5.2). A composite of ICT WSR-57 radar data and mesoscale pressure analysis for 0240 UTC demonstrates that PAM-12 is located just ahead of a southeastward progressing gust front (see Fig. 5.3a). A broken line of convective cells extended from southwest to northeast along and just behind this front. The strongest cells (reflectivity greater than 45 dBZ) were located about 25 km to the southwest of PAM-12, while a weak extension of this activity (reflectivity between 18 and 30 dBZ) was located immediately southwest of the station.

Analysis of the mesoscale pressure field at this time reveals the existence of a strong mesohigh (P_{adj} = 948.1 mb) just behind the convective line, and relatively low pressure to the northwest, north and northeast of the mesohigh. The pressure gradient between these features was large, with a maximum gradient of 7 mb over 65 km, between stations

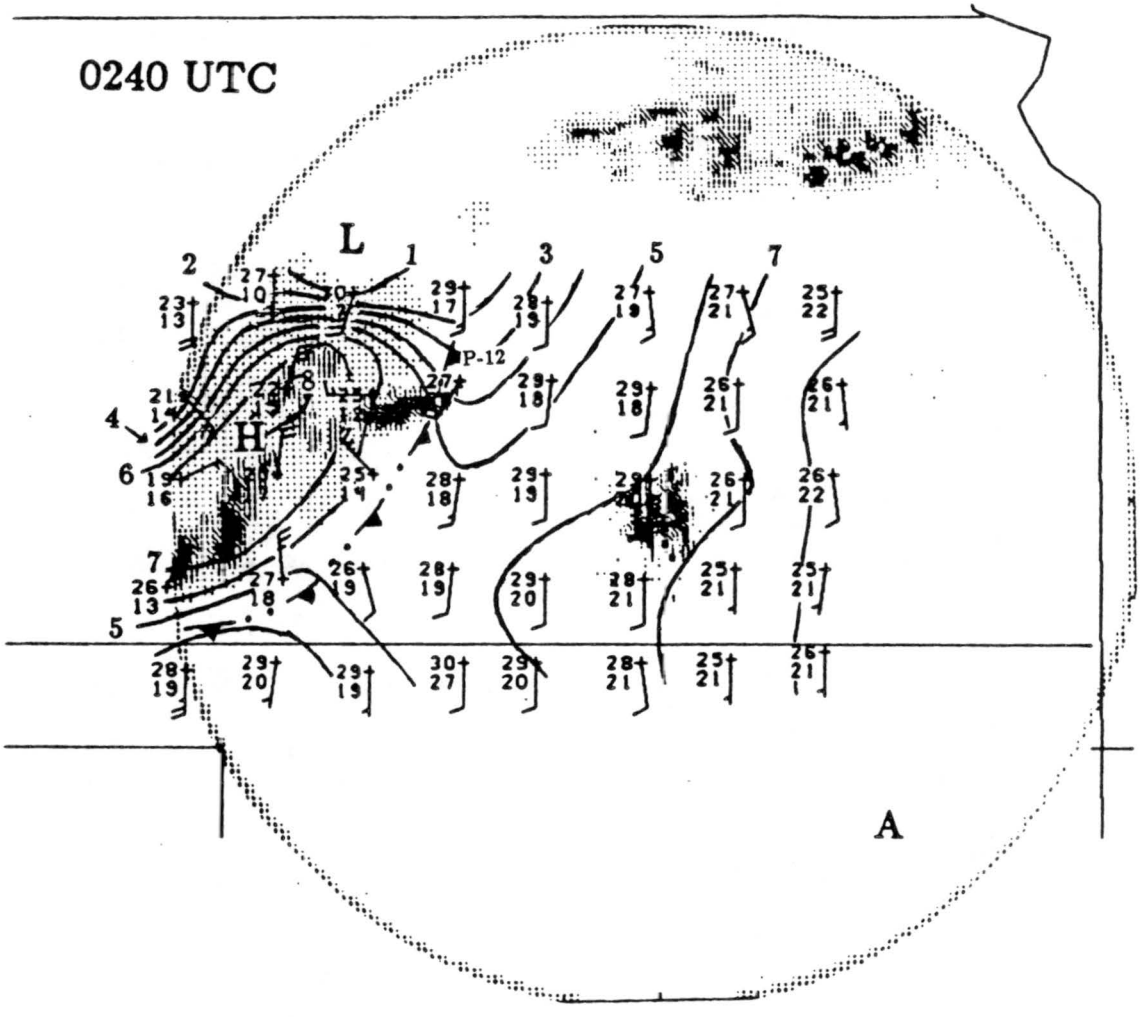

Figure 5.3: Surface mesonetwork analysis at (a) 0240, (b) 0255, (c) 0320, (d) 0340, (e) 0350, (f) 0410, and (g) 0440 UTC, 24 June 1985. Contours represent pressure adjusted to 584.3 m, the elevation of PAM-12. Pressure contour values are given as departures from 940 mb (e.g. 1 = 941 mb). Temperature and dew point are in °C. Reflectivity thresholds are 18, 30, 40, 45 and 50 dBZ. Dashed, double dotted lines indicate the position of a gust front.

PAM-2 and 10. Station PAM-12 was near the axis of a mesoscale trough located just to the east of the northeast extension of precipitation (see Fig. 5.3a).

Rises in dew point temperature, likely associated with precipitation just to the southwest of the station, were recorded between 0230 and 0245 UTC. Winds at PAM-12 were out of the southwest at this time. No rainfall was recorded at the station at any time during the life cycle of the 23-24 June MCS, however. At 0245 UTC, the temperature at the station had fallen to 27°C, while winds averaged 7 $m\ s^{-1}$ at 217°, station pressure had fallen slowly from 947.4 (0230 UTC) to 946.7 mb and θ_e remained approximately 350 K.

A weak gust front appears to have passed PAM-12 at approximately 0300 UTC. This event was characterized by a gradual drop in temperature and dew point of 5.2°C and 5.3°C, respectively, as well as a slow rise in station pressure of 2.2 mb, between 0255 and 0330 UTC. The station wind shifted to approximately 230°, and wind gusts in excess of 20 $m\ s^{-1}$ were recorded. A dramatic fall in θ_e of 20.0 K also occurred. Relative humidity remained near 60%, although it fluctuated slightly during the period.

WSR-57 reflectivity maps overlain with mesoscale pressure analyses for 0255 and 0320 UTC (Figs. 5.3b,c) reveal that the strong convective cells to the southwest of PAM-12 weakened and moved southeastward by 0320 UTC. Reflectivity values associated with these cells were predominantly between 30 and 40 dBZ at 0320 UTC. The pressure field associated with the MCS remained fairly steady through this period, although pressures at PAM-3 fell 1.9 mb by 0320 UTC.

5.2.2 Period 2: 0335 - 0350 UTC

The first HBs at PAM-12 occurred between 0335 and 0350 UTC. During this period, the convective cells to the southwest of the station dissipated considerably (see Figs. 5.3d,e). Only a weak southeastward extension of stratiform precipitation with reflectivity of 18-30 dBZ remained there by 0340 UTC. The occurrence of the first HBs corresponded in time with the decay of this precipitation.

The first bursts at PAM-12 were marked by the following changes between 0330 and 0340 UTC: 1) a rise in temperature of 2.7°C, 2) a fall in dew point of 1.8°C, 3) a fall in relative humidity of 14.6%, 4) a fall in θ_e of 0.4 K, 5) a rise in average wind speed of

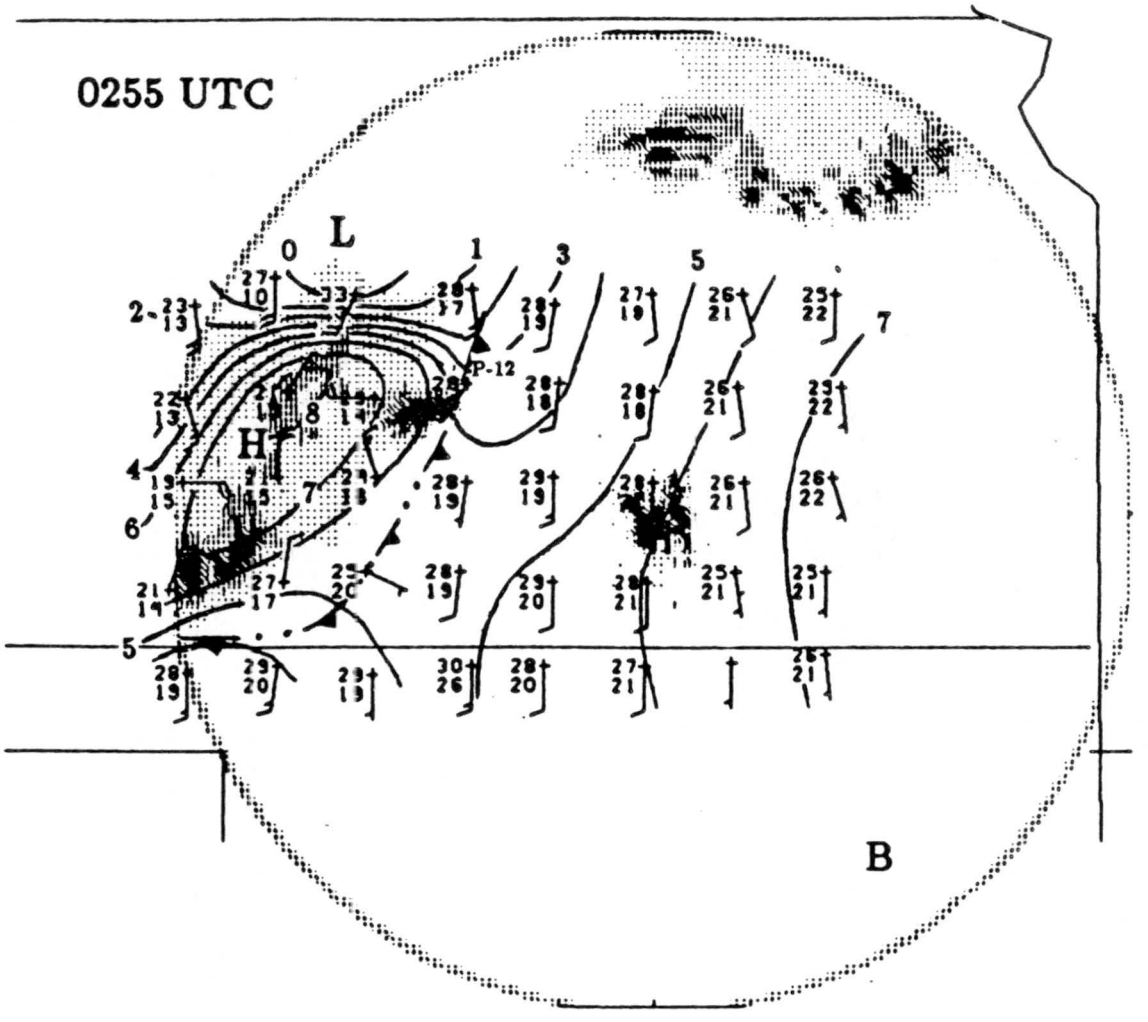

Figure 5.3: continued

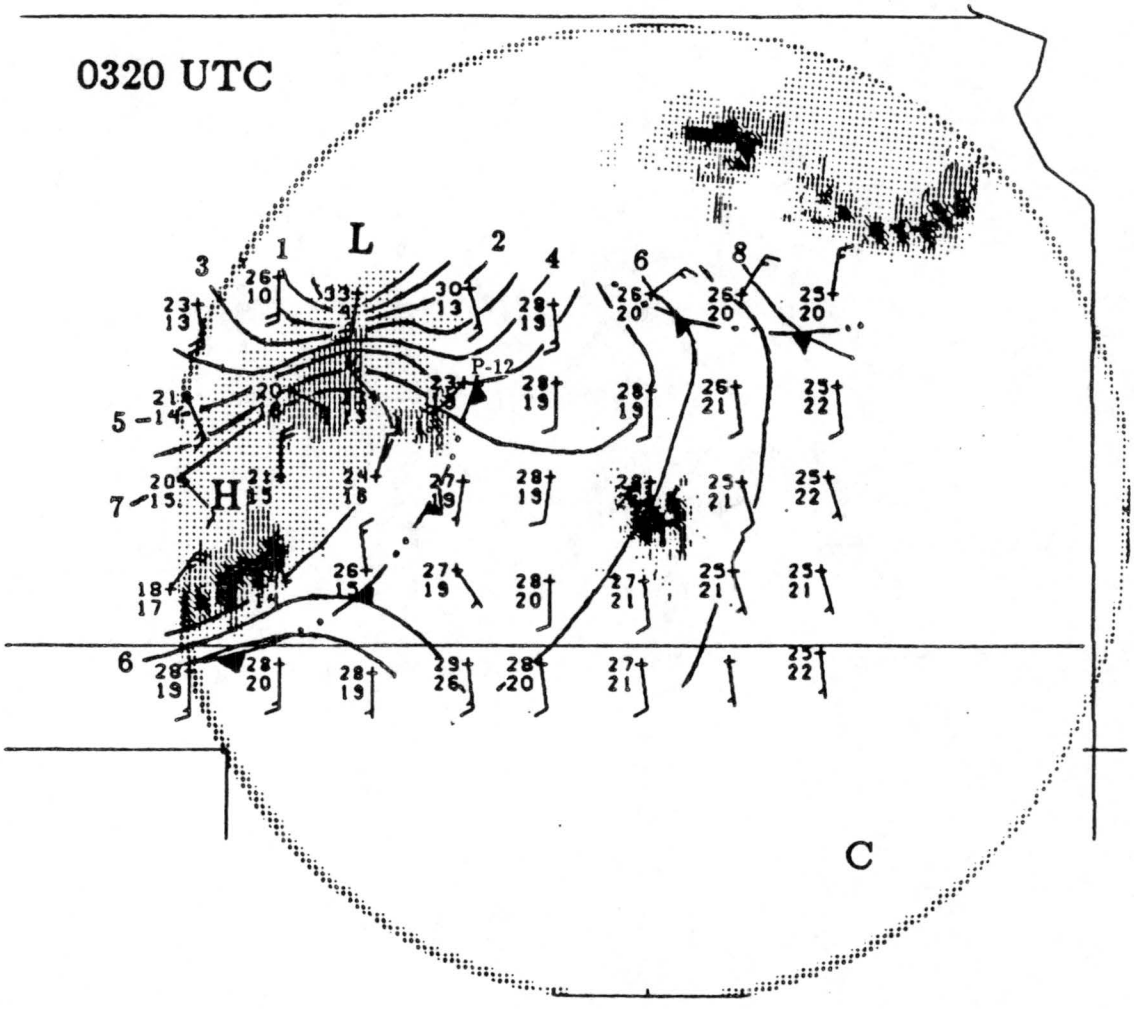

Figure 5.3: continued

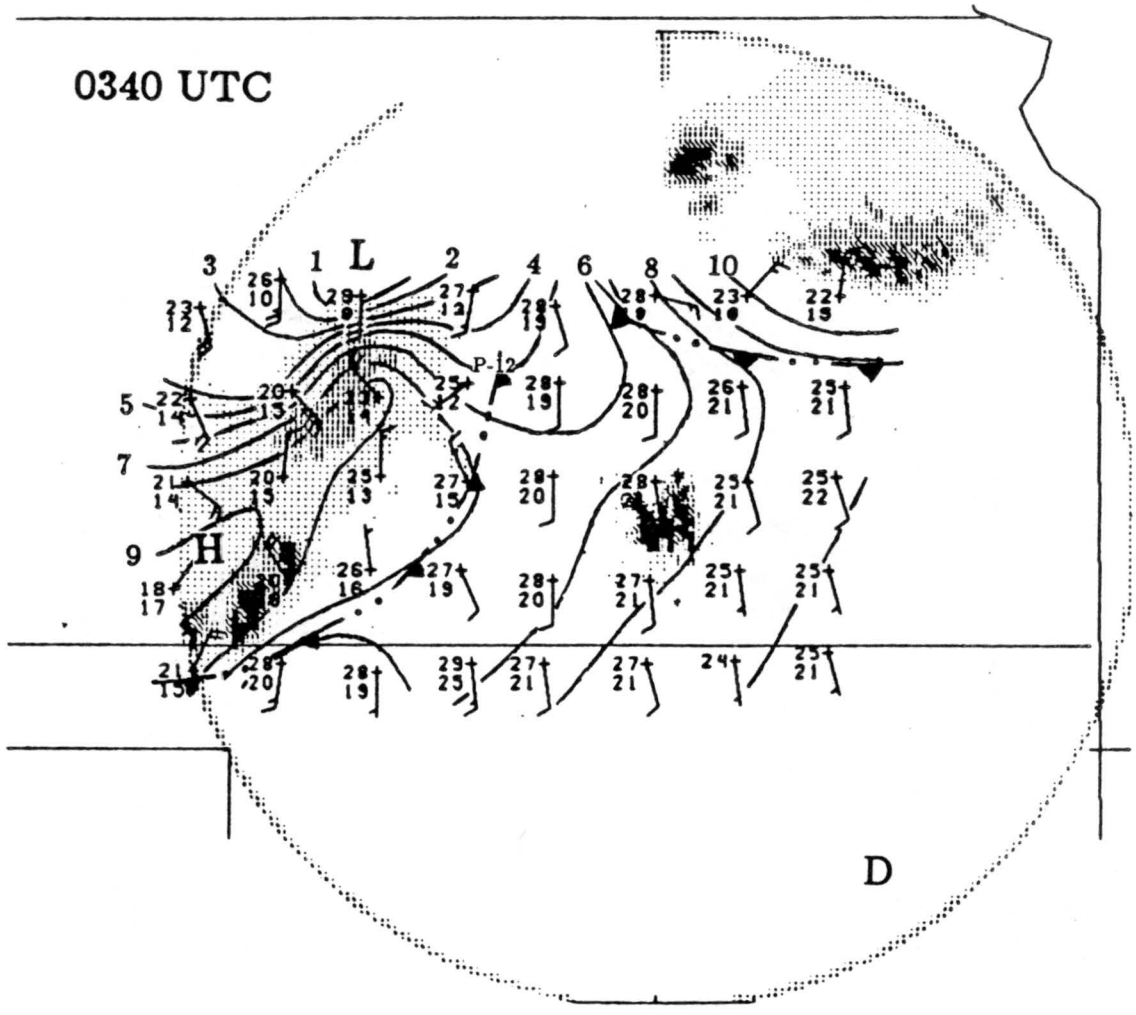

Figure 5.3: continued

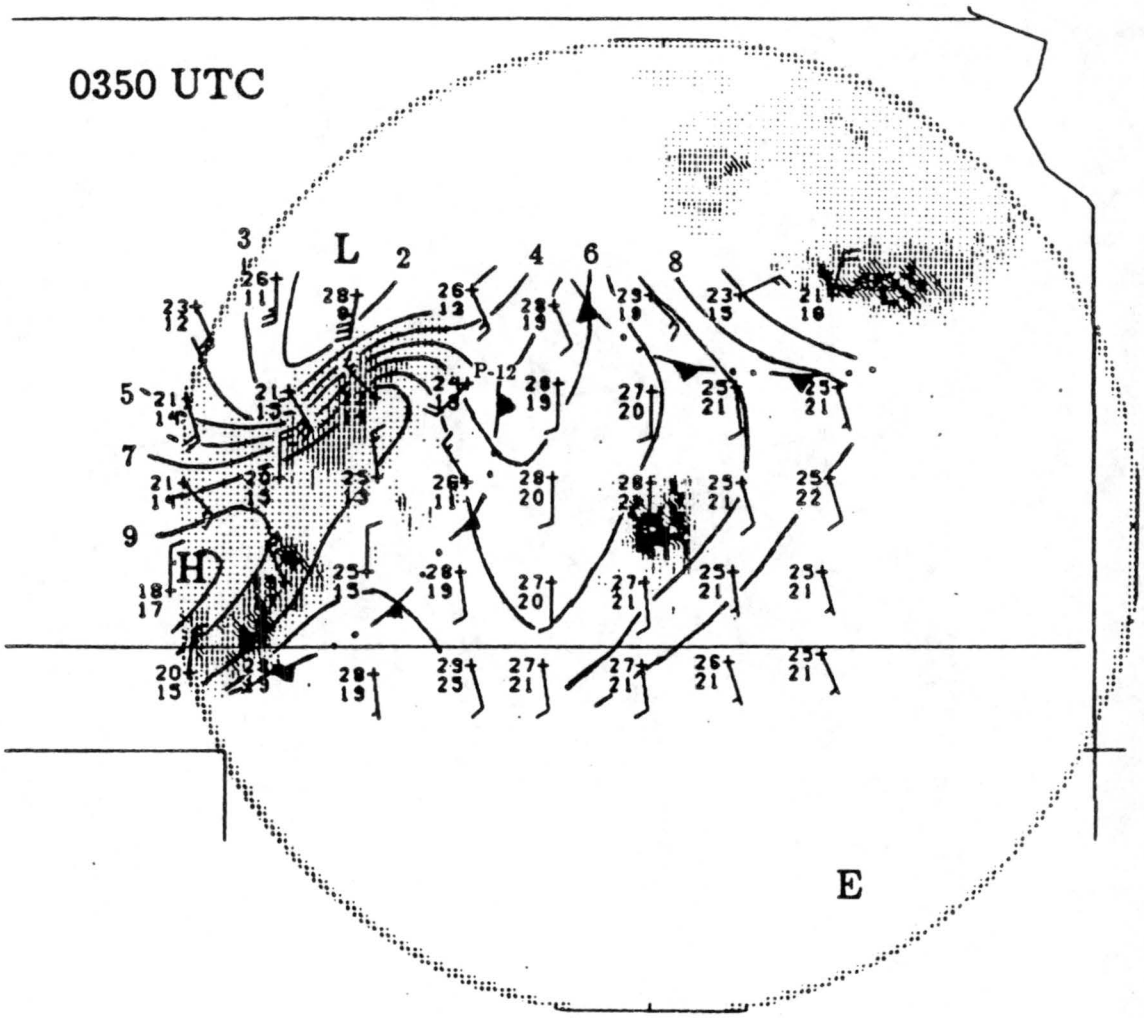

Figure 5.3: continued

4.5 $m\ s^{-1}$, 6) a rise in peak wind gust speed of 5.5 $m\ s^{-1}$, and 7) a veering of the wind direction from 230° to 240° (see Fig. 5.2). Pressure remained nearly constant at 948.8 mb. The majority of these changes are consistent with those reported in earlier studies of HBs (see Chapter 2), with a few exceptions. Pressure falls often accompanied the bursts in previous studies, while pressure changes at PAM-12 were weak and poorly correlated with the bursts.

θ_e has not been previously discussed in relation to these phenomena. During both HB episodes (see section 5.2.4 for second HB episode), θ_e reached minimum values. Two possible explanations for the existence of the low θ_e at PAM-12 are: 1) horizontal advection of low θ_e air by surface winds, and 2) vertical transport of low θ_e values from a mid-tropospheric minimum.

Analysis of surface θ_e values over the PAM mesonetwork (Fig. 5.4) reveals that low θ_e air was only detectable at the surface in areas traversed by some portion of the MCS. These areas are characterized by downdrafts which carry low θ_e air to the surface from aloft. High θ_e air was present over the remainder of the mesonetwork. Therefore, it seems unlikely that horizontal advection was the process which led to the appearance of low θ_e air at PAM-12.

A sounding of θ_e taken at RSL (72 km north-northeast of PAM-12) near this time (Fig. 5.5) clearly shows that the lowest values of θ_e existed in a layer between 700 and 480 mb. Values in this layer ranged from 328.9 K to 331.7 K, with minima of 328.9 K, 329.4 and 329.7 K at 489 mb, 555 mb and 700 mb, respectively. Similar values of θ_e, between 329.5 and 330.5 K were recorded at PAM-12 during HB activity. Winds in this layer were from the north-northeast, possibly indicating that air from this layer was approaching PAM-12 at this time.

The 0°C level in the RSL sounding was approximately 570 mb, or about 4 km AGL. Leary and Houze (1979) and Smull and Houze (1987) have shown that melting of precipitation in the stratiform region can result in considerable cooling, and thus a lowering of the θ_e values of air which pass through this layer. Stumpf, et. al. (1990) showed that this process may have been responsible for the existence of a θ_e minimum just above the ground

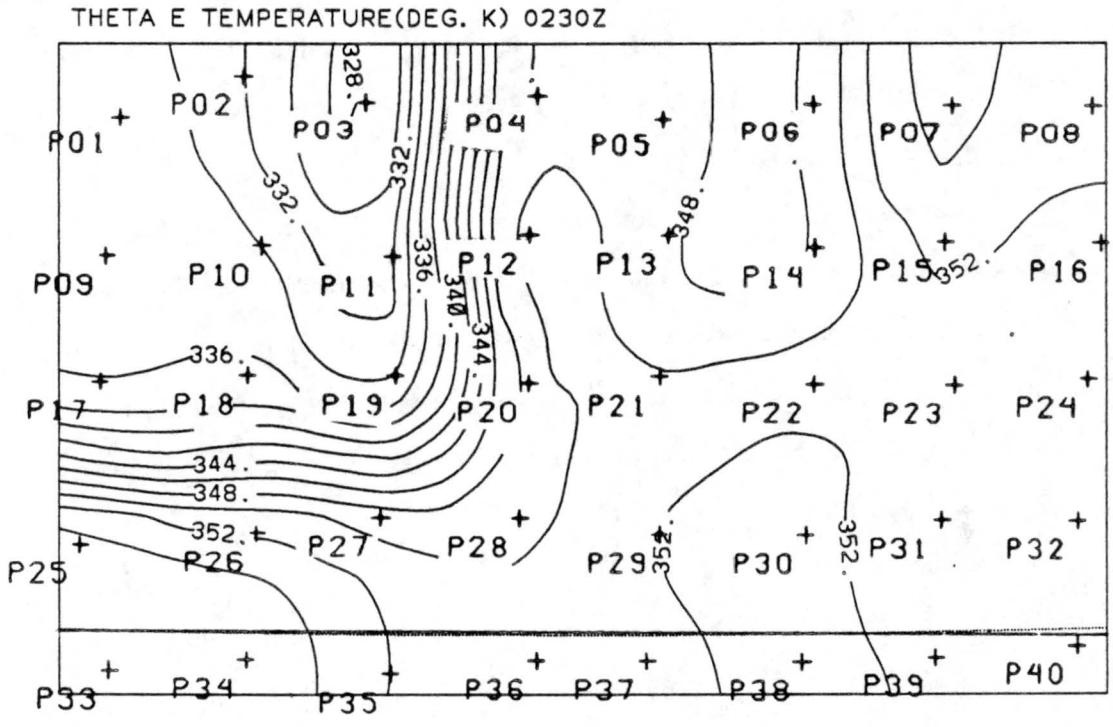

Figure 5.4: Objective analysis of θ_e values measured in the PAM mesonet at 0230 UTC.

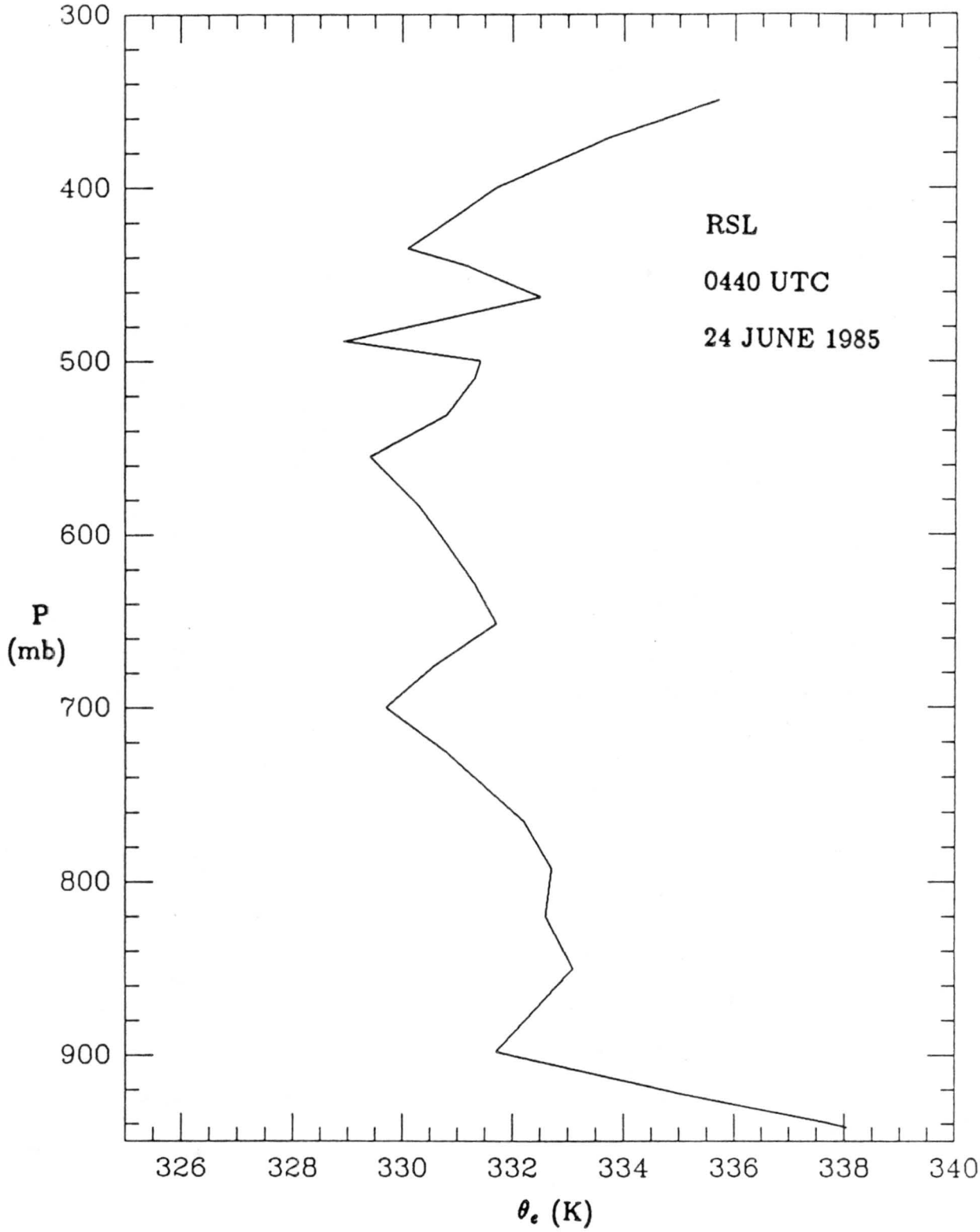

Figure 5.5: Sounding of θ_e values for Russell, Kansas (RSL) at 0440 UTC, 24 June 1985.

at the back edge of the stratiform precipitation in their case. Such processes may have lent to additional lowering of θ_e values of the air which reached PAM-12 during HBs in this case. Descent of air from mid-levels will be later confirmed by dual-Doppler analyses in Chapter 6.

5.2.3 Period 3: 0355 - 0415 UTC

Following the first HB episode was a short, relatively calm period from 0355 to 0415 UTC. During the time span between the strongest HBs of the first episode, 0340 UTC, and 0405 UTC, the following changes were experienced at PAM-12: 1) a fall in temperature of 1.1°C, 2) a rise in dew point of 1.5°C, 3) a rise in relative humidity of 8.2%, 4) a fall in pressure of 0.3 mb, 5) a rise in θ_e of 1.6 K, 6) a decrease in average wind speed of 2.1 $m\ s^{-1}$, 7) a decrease in the peak wind gust speed of 4.4 $m\ s^{-1}$, and 8) a backing in the wind direction of 15°.

A composite of ICT WSR-57 radar reflectivity data and analysis of the mesoscale pressure field for 0410 UTC appears in figure 5.3f. The weak extension of stratiform precipitation located to the southwest of PAM-12 had dissipated further, while the northeast extension of stratiform precipitation continued to exist just to the northwest and southwest of the surface station at this time.

5.2.4 Period 4: 0420 - 0450 UTC

The second episode of HBs at PAM-12 occurred between 0420 and 0450 UTC. During this time period, the remainder of the weak stratiform extension to the southwest of PAM-12 dissipated almost completely (see Figs. 5.3f,g - 0410 and 0440 UTC composites). The stratiform extension close to PAM-12 decreased in areal extent, and very little precipitation with reflectivity exceeding 30 dBZ remained there by 0440 UTC. The mesohigh associated with this extension also dissipated, leaving a north-south pressure gradient over this region. The occurrence of the second episode of HBs corresponded in time with the decay of these features.

The HB activity recorded at PAM-12 between 0420 and 0450 UTC was more intense than that recorded during the first HB episode. Larger changes in the variables recorded

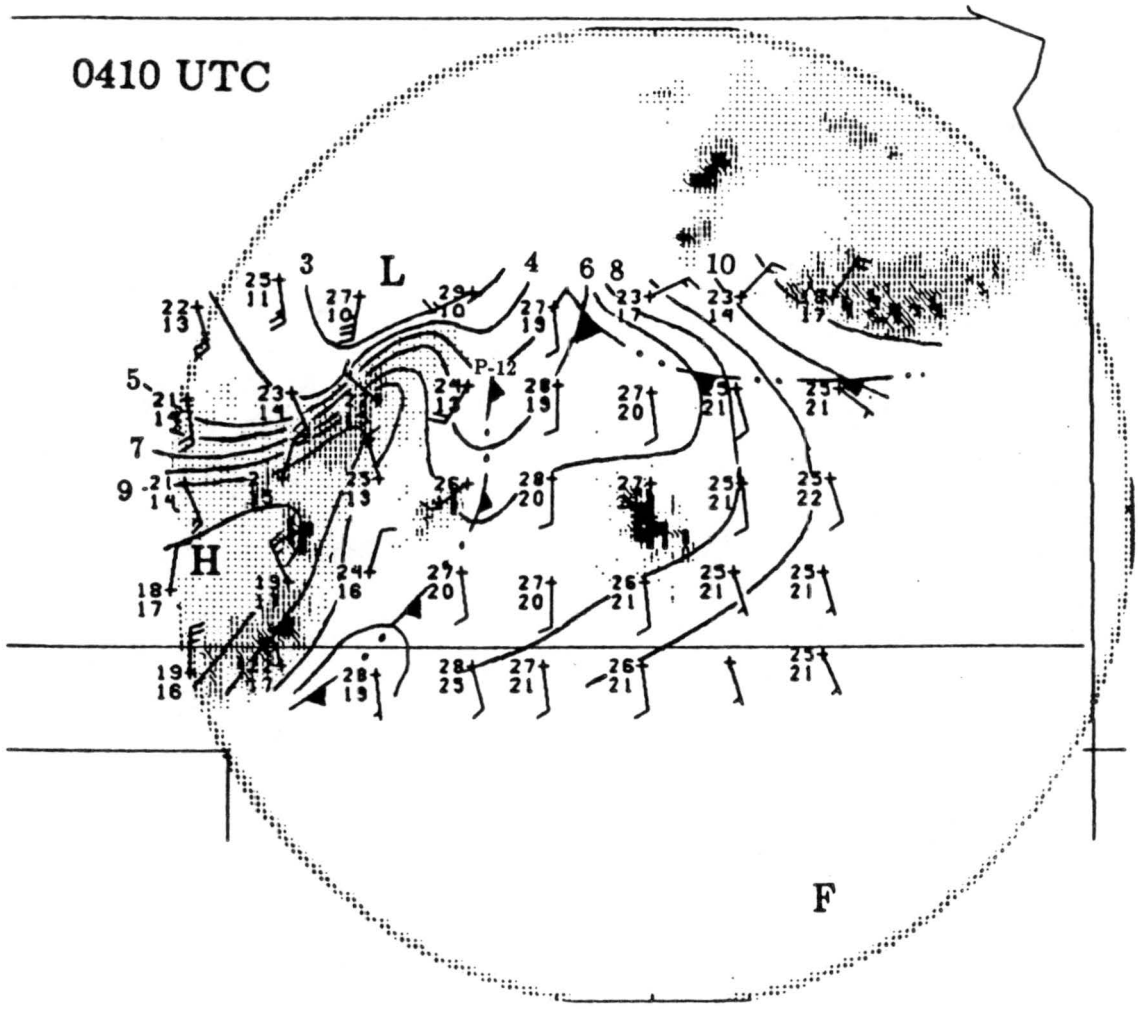

Figure 5.3: continued

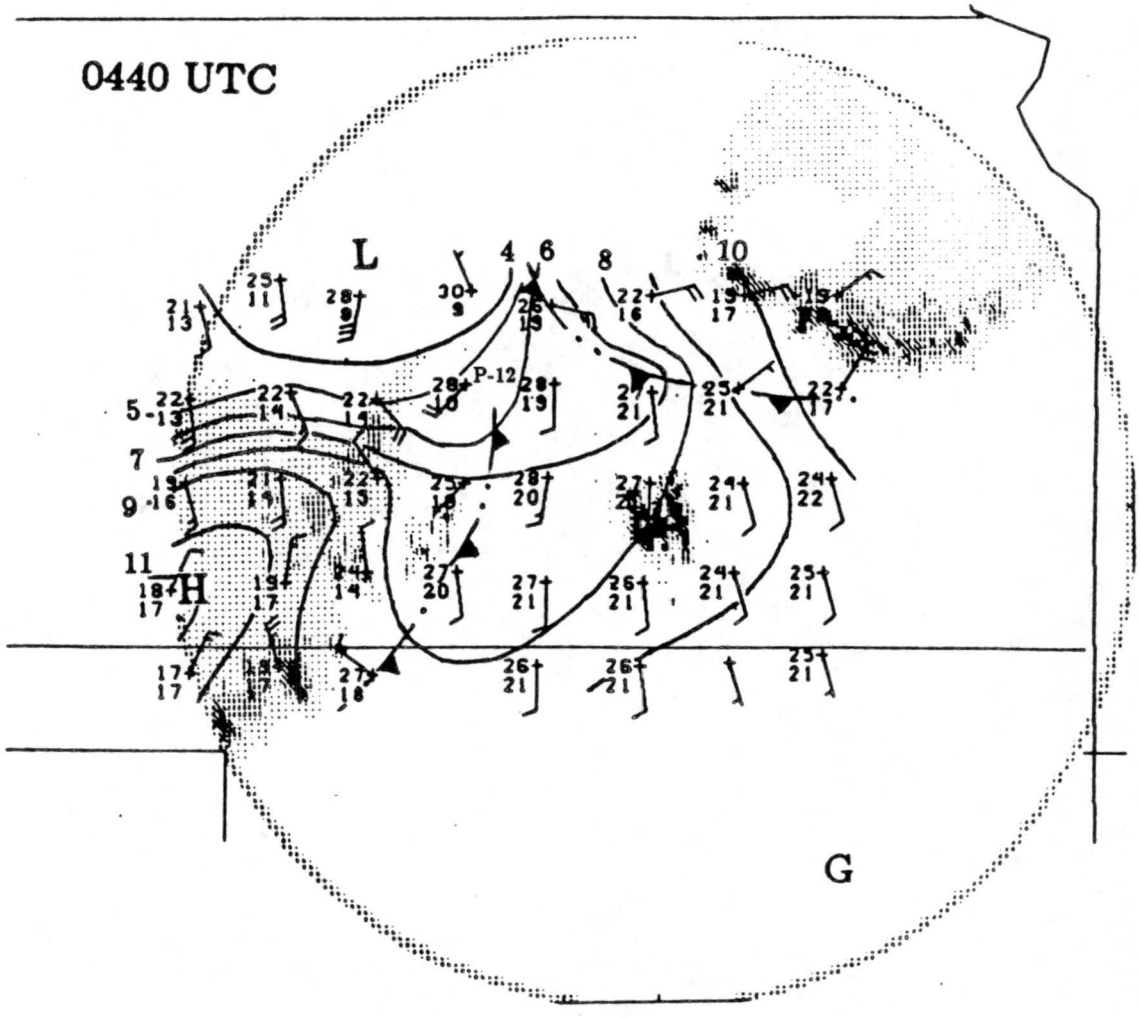

Figure 5.3: continued

at the station between 0415 and 0440 UTC bear this out: 1) a rise in temperature of 3.8°C, 2) a fall in dew point of 3.3°C, 3) a fall in relative humidity of 17.6%, 4) a fall in pressure of 0.3 mb (between 0405 and 0440 UTC), and 5) a fall in θ_e of 1.5 K. The winds at the station went through two periods of change. At the onset of the bursts (0420 - 0425 UTC), 1) the average wind speed rose 2.2 $m\ s^{-1}$, 2) peak gusts increased 6.9 $m\ s^{-1}$ to reach a value of 17.4 $m\ s^{-1}$, and 3) the wind direction veered from 220° to 249°. During the remainder of the burst episode, the winds at the station remained fairly strong, averaging approximately 9 $m\ s^{-1}$, with peak gusts of 14.7 $m\ s^{-1}$ between 0430 and 0450 UTC, but the wind direction backed to 230°.

5.2.5 Period 5: 0455 - 0530 UTC

Immediately following the second HB episode (between 0450 and 0505 UTC), PAM-12 experienced the following changes: 1) a fall in temperature of 5.0°C, 2) a rise in dew point of 4.7°C, 3) a rise in relative humidity of 26%, 4) a rise in θ_e of 2.5 K, 5) a fall in average wind speed of 3.3 $m\ s^{-1}$, 6) a decrease in peak wind gust speed of 6.3 $m\ s^{-1}$, and 7) a back in wind direction of 47°. Station pressure remained nearly constant immediately after the second HB episode, but eventually fell 0.7 mb by 0530 UTC. These changes were quite similar to those experienced between HB episodes, and represent a near return to those conditions which preceded the bursts. A HB, therefore, may be thought of as an interruption of the flow at a station, as wind, temperature and dew point return to their initial state following a burst.

During the hours following the second HB episode, a series of weaker bursts were experienced at the station (see Figs. 5.1 and 5.2). These bursts featured changes in temperature and dew point that were weak when compared with those of the first two HB episodes, and thus were not focused upon in this study.

5.3 Summary of Heat Burst Characteristics

The heat bursts which occurred at PAM-12 had common characteristics. They were marked by a sharp rise in temperature, and falls in dew point, relative humidity and θ_e. Average wind speed and peak gust speed both increased, and wind direction veered at

the onset of the heat bursts at PAM-12. Almost no change in pressure accompanied the bursts, however. This may be attributed to the relative weakness of these bursts when compared to those which occurred at PAM-3 in this case, and those which have been documented in earlier studies.

Chapter 6

DOPPLER RADAR INVESTIGATIONS OF PAM-12 HEAT BURSTS

To further understand the heat burst events which occurred at station PAM-12, a three-dimensional perspective of the precipitation and wind fields associated with them is essential. An earlier study of HBs by Johnson (1983) attempted this through the use of cross-sections of rawinsonde data, but the data used were too sparse to fully resolve the features associated with these phenomena. In the study of the 23-24 June case by Johnson, et. al. (1989), it was indicated that the extreme HBs at PAM-3 were out of dual-Doppler range, so they could not be studied. However, the weaker HBs at PAM-12 were within range of the two NCAR Doppler radars in place for the PRE-STORM field project. Both single and dual-Doppler data were available for the 23-24 June MCS case (see Chapter 3), will be analyzed here and related to the HB activity recorded at the surface.

6.1 Radar Data Available and Times of Observations

Doppler radar data were available throughout the entire period of HB activity, from 0230 to 0530 UTC. Seven Planned Position Indicator (PPI) images of CP-3 single Doppler radial velocity data at a 0.2° elevation angle were taken at twenty minute intervals from 0240 to 0440 UTC. These velocity fields will be used to demonstrate the development of the radial wind field through this period. WSR-57 low level radar scans will be used to locate features in the wind field with respect to precipitation at the surface. These features will be related to the onset of HBs at PAM-12. PAM-12 was located 38 km from the CP-3 radar at 280° (relative to north).

Two dual-Doppler syntheses were also performed at 0324 and 0415 UTC, the times of the last radar volumes which preceded the HB episodes at PAM-12. Figure 6.1 depicts the times of the Doppler data used for this case, and relates them to the periods of

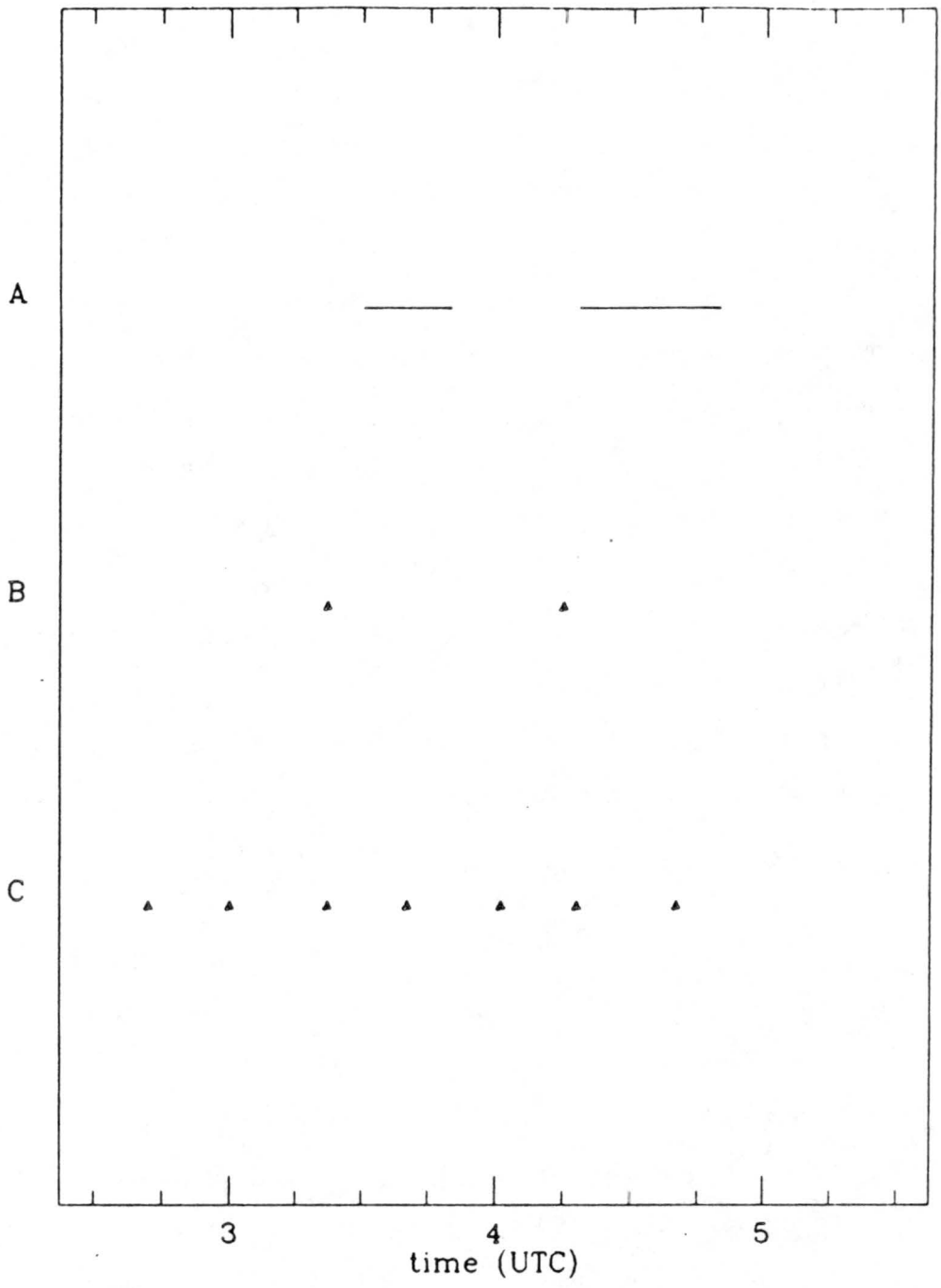

Figure 6.1: Times of (a) heat burst occurrence at surface station PAM-12, (b) dual-Doppler syntheses, and (c) CP-3 PPI images of the radial velocity field.

burst activity at PAM-12. These times were selected as immediately preceding (5-10 min. before) the bursts, to discover the three-dimensional structure of the precipitation and wind fields which led to their occurrence.

6.2 Single Doppler Radial Velocity Fields

At 0242 UTC a line of convective cells was located to the southwest of PAM-12 with a northeastward extension of stratiform precipitation, as described earlier (see Fig. 5.3a). Between these precipitation areas was an area of low reflectivity. The radial wind field (not shown) there was poorly defined at this time, but did indicate southwesterly flow in the vicinity of PAM-12. This corresponded with the 219° wind direction reported at the station at 0240 UTC.

By 0300 UTC, the wind field in this region became more defined, and a 400 km^2 area of radial wind speeds greater than 15 $m\ s^{-1}$ formed to the west and northwest of PAM-12 (see Fig. 6.2a). This wind maximum was detected between 300 and 500 m AGL, and was indicated by areas of folded radial velocities toward the radar (nyquist velocity for the CP-3 radar was set to 15.13 $m\ s^{-1}$ for this experiment [Meitín and Cunning, 1986]). This area of folded velocities increased in size to nearly 600 km^2 by 0322 UTC (see Fig. 6.2b). Some peak radial velocity values measured within this area exceeded 25 $m\ s^{-1}$ at this time. It also extended farther to the east, reaching station PAM-12. As described in Chapter 5, the small group of convective cells that were just to the southwest of this station were decaying, and an area of low reflectivity to the northwest of the station (see Fig. 5.3c) was colocated with the wind maximum at this time. Although the wind maximum was detected in an area of low reflectivity values, the wind pattern was quite coherent. Particles such as blowing dust may have aided in the detection of these winds. The CP-3 radar indicated 15 $m\ s^{-1}$ radial velocities 150 m above that location, while the station measured winds at 11.5 $m\ s^{-1}$ from 232°, with gusts to 16.5 $m\ s^{-1}$. The winds measured at the surface roughly agreed with those detected by the radar, but were apparently retarded by friction.

By 0340 UTC these cells had almost completely dissipated, the low reflectivity area moved over PAM-12, and the first HB episode was occurring there. The areal extent of the

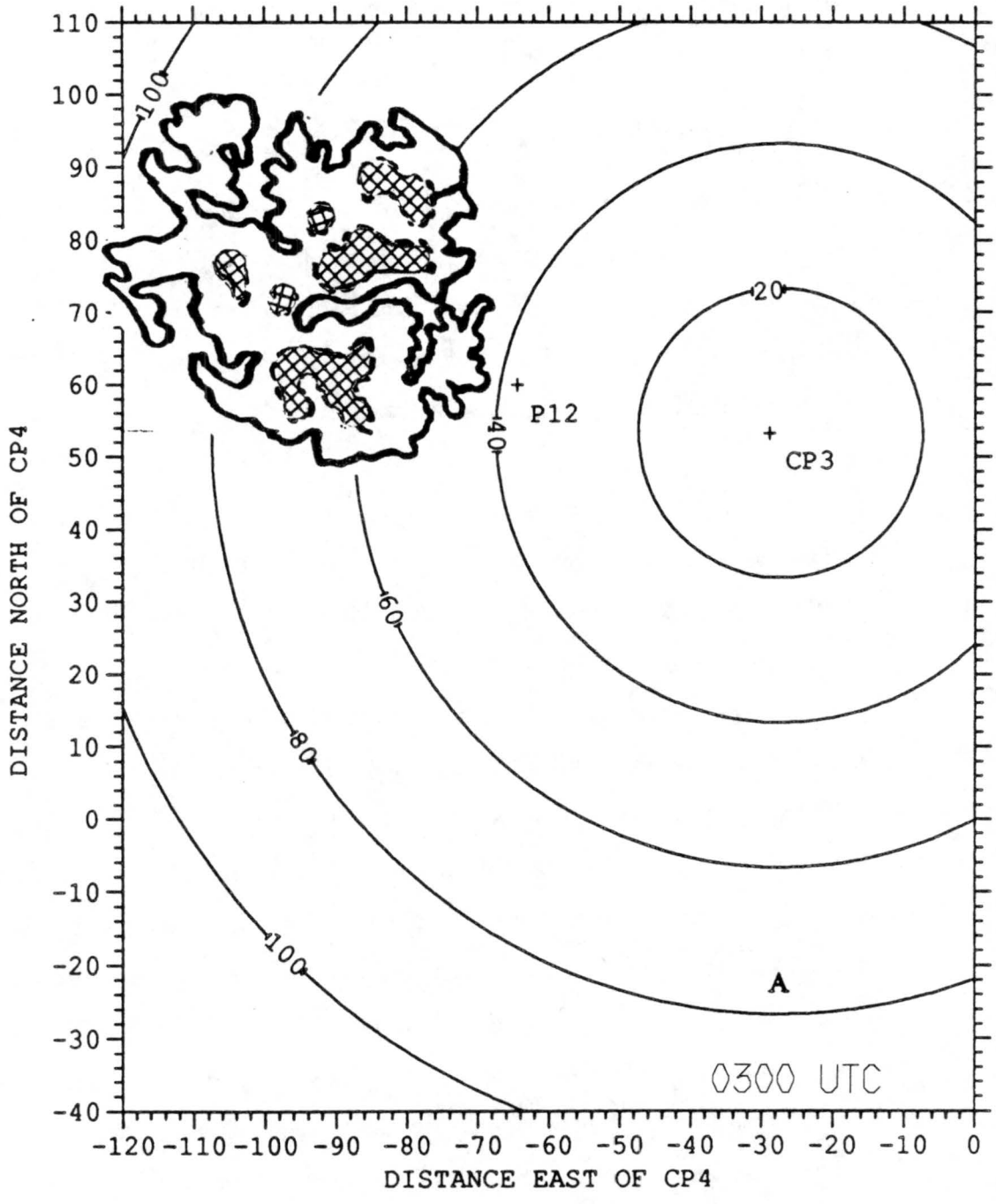

Figure 6.2: Radial velocity maxima from NCAR CP-3 Doppler radar at (a) 0300, (b) 0322, (c) 0340, (d) 0401, and (e) 0418 UTC, 24 June 1985. Solid contours represent radial velocities of 10 $m\ s^{-1}$, hatched areas represent radial velocities between 15 and 25 $m\ s^{-1}$, embedded black areas represent radial velocities exceeding 25 $m\ s^{-1}$. All contoured velocities were directed toward the radar.

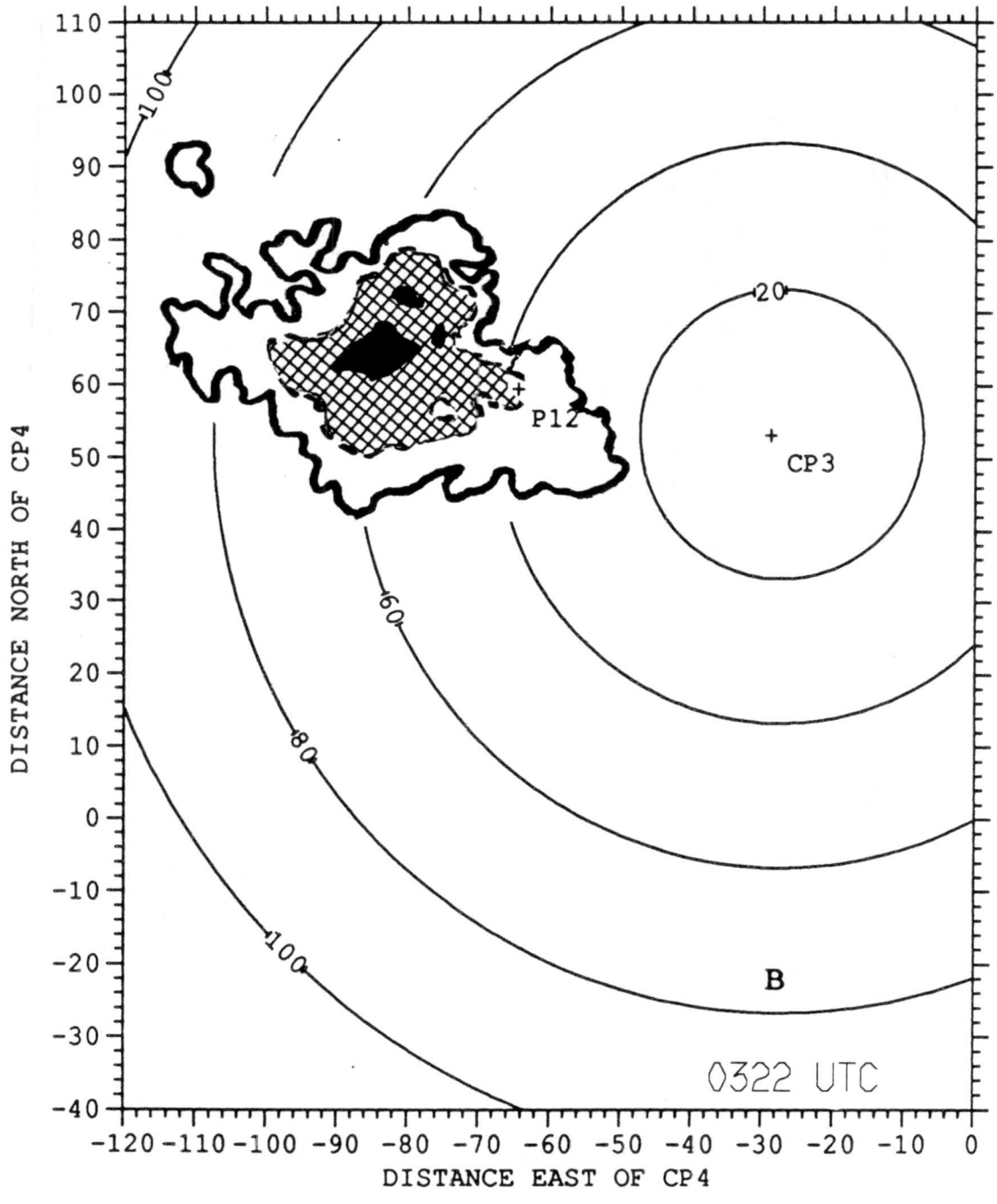

Figure 6.2: continued

folded radial winds decreased somewhat, but remained close to PAM-12 at this time (see Fig. 6.2c). At 0401 UTC the areal extent of the wind maximum decreased further, and only velocities between 10 and 15 $m\ s^{-1}$ remained over the station (see Fig. 6.2d). Station winds averaged 10.4 $m\ s^{-1}$ at 222°, with peak gusts to 13.7 $m\ s^{-1}$ at this time. Conditions at the station remained warm and dry, but no HBs were occurring then. By 0418 UTC the areal extent of the wind maximum increased, and again became positioned over station PAM-12 (see Fig. 6.2e). The second HB episode began there at approximately this time (0420 UTC). The station experienced an increase in average wind speed, and peak gusts reached 17.3 $m\ s^{-1}$ at 0425 UTC. By 0440 UTC, the area of folded radial velocities had almost completely dissipated, leaving only weak (less than 10 $m\ s^{-1}$) radial velocities over this region. Wind speeds measured at PAM-12 reflected this change, as they slowly decreased between 0425 and 0440. The second HB episode ceased soon afterward at 0455 UTC.

The association of the large area of high radial wind velocities and low reflectivity (depicted by the CP-3 radar and ICT WSR-57 radar, respectively) with the HB activity at PAM-12 is important, for it gives a strong indication that the HBs are linked to a fairly large scale source. A three-dimensional investigation of the precipitation and wind fields responsible for the formation of this large scale outflow region and the heat bursts associated with it will be the focus of two dual-Doppler syntheses.

6.3 Dual-Doppler Analyses

Dual-Doppler syntheses of data from the NCAR CP-3 and CP-4 radars were carried out for 0324 and 0415 UTC. These radar volumes were recorded just before the two HB episodes at PAM-12. Horizontal and vertical cross-sections were made through these data sets at elevations and through areas critical to the understanding of the formation of the heat bursts at the surface.

6.3.1 0324 UTC Dual-Doppler Synthesis

The first of the two dual-Doppler syntheses was performed for 0324 UTC, about 10 minutes before the onset of the first HB episode at PAM-12. This episode was the weaker

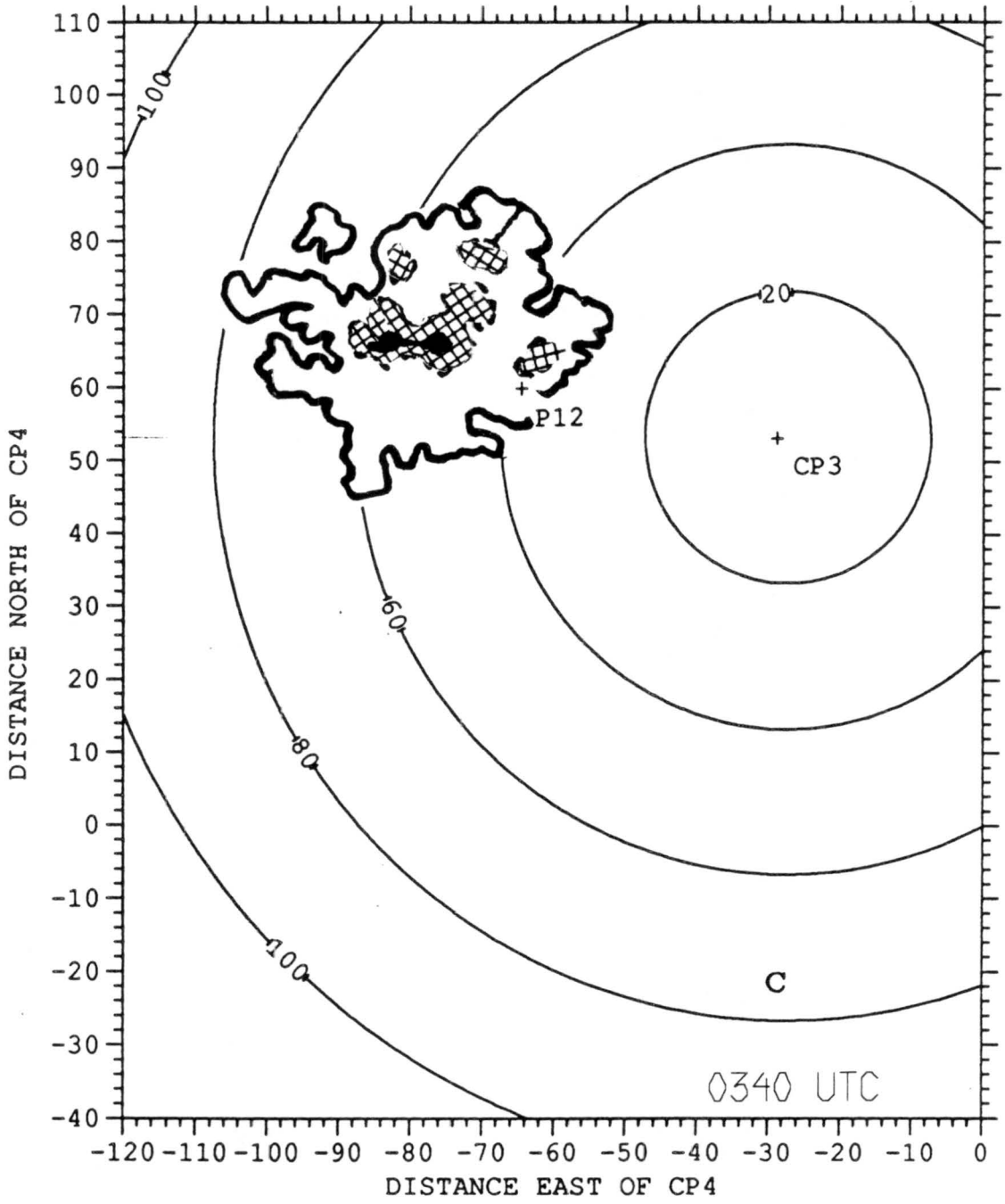

Figure 6.2: continued

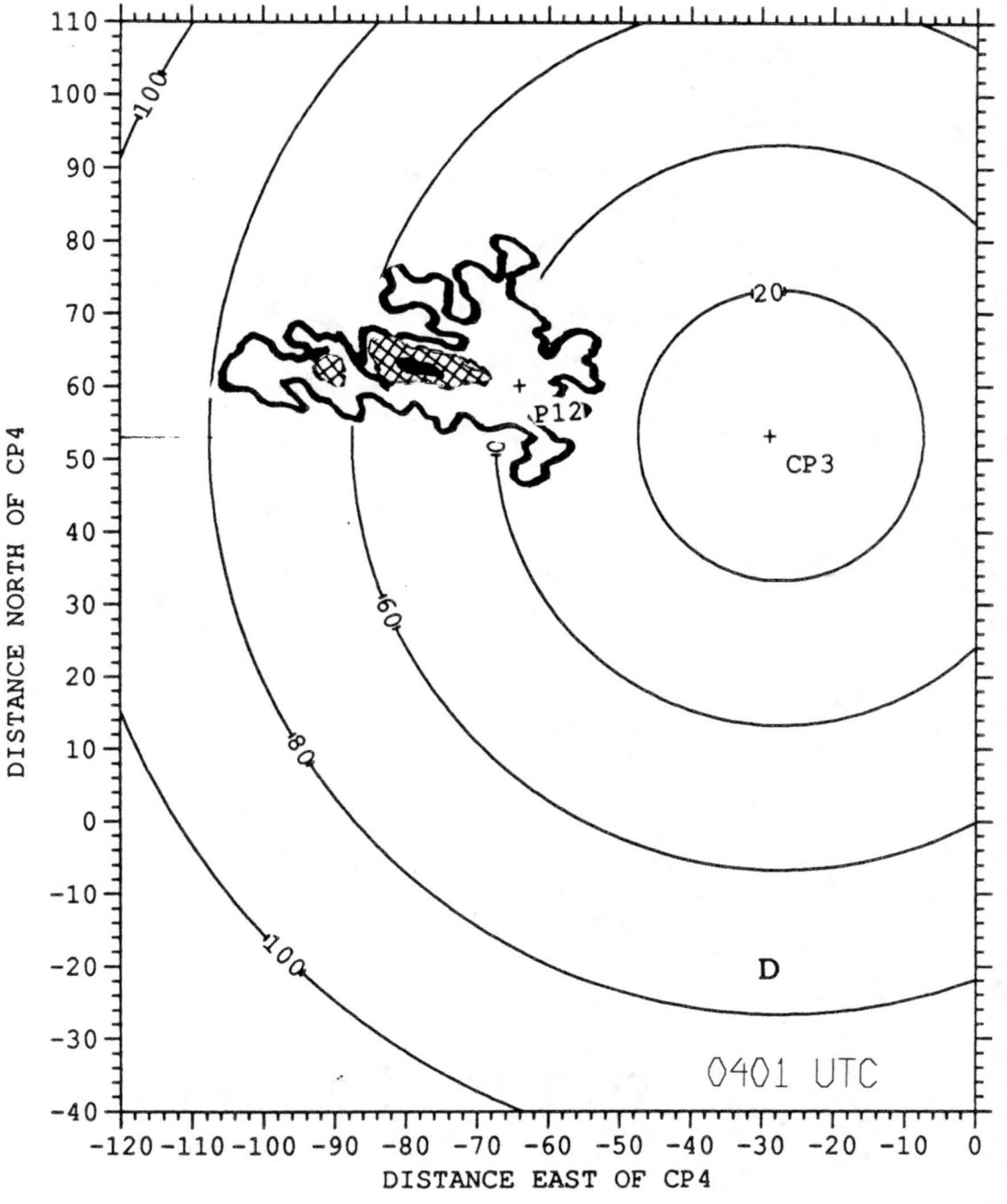

Figure 6.2: continued

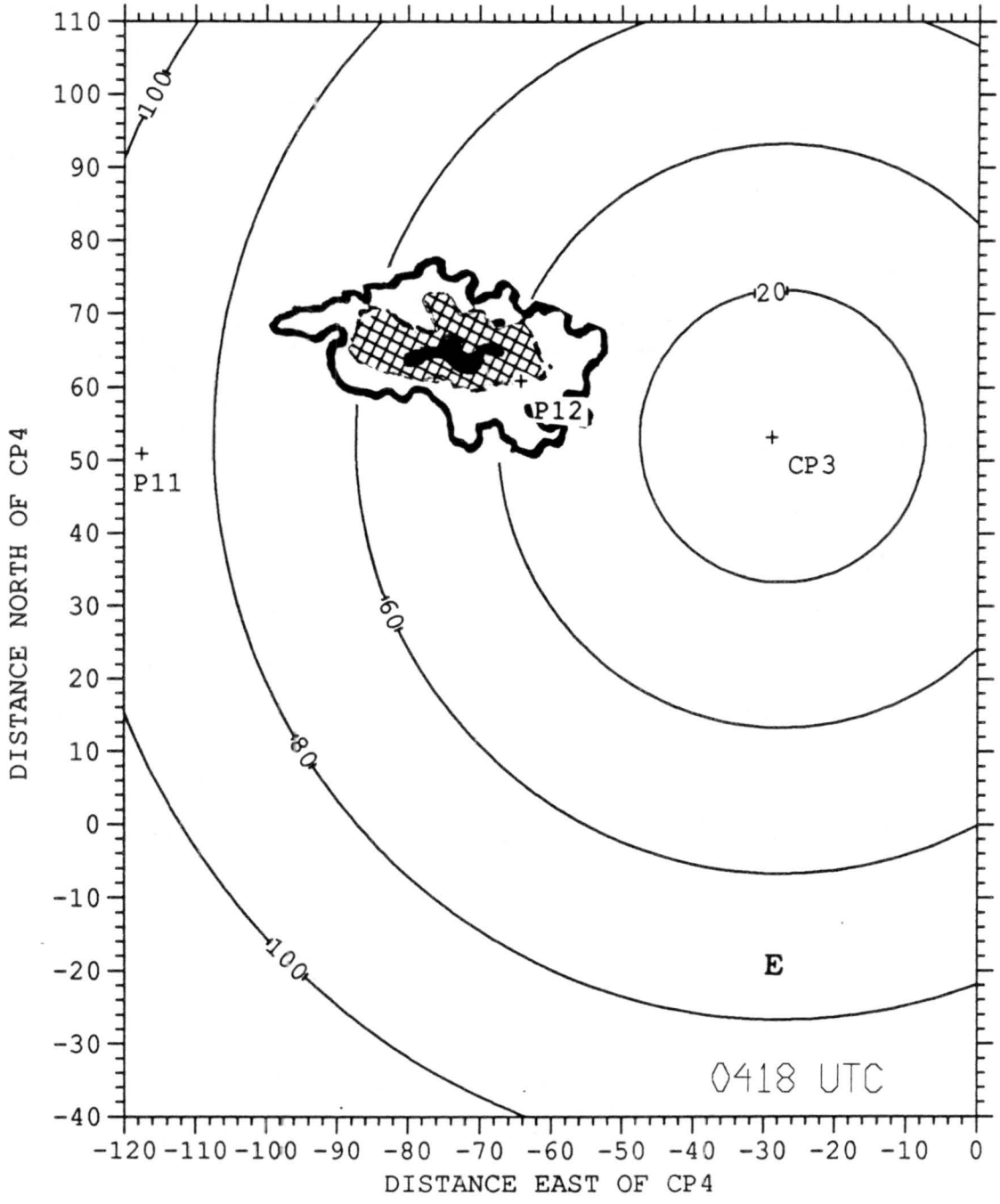

Figure 6.2: continued

of the two, as changes in the variables recorded at the surface station were relatively small (see Fig. 5.2). At this time, convective cells just to the southwest of PAM-12 were decaying, an area of low reflectivity and a large area of strong low-level winds 150 m above the surface were present just to the north and northwest of these cells. Horizontal and vertical cross-sections in this region of the MCS will reveal the three-dimensional structure of the precipitation and wind fields there.

Horizontal Cross-sections

Horizontal cross-sections of the MCS have been made at 1.4, 4.4 and 9.4 km (all radar indicated heights MSL) to give an indication of the precipitation and wind fields near the ground, at middle levels and at levels near the top of the storm. Ground levels at the CP-3 and CP-4 radars were 0.489 and 0.430 km, respectively, and storm top was approximately 11.4 km.

A low-level cross-section taken at 1.4 km (Fig. 6.3a) shows a number of decaying cells, represented by two areas of reflectivity greater than 30 dBZ. The larger of these areas was located approximately 40 km to the southwest of PAM-12, while the smaller cell was located 15 km to the southwest of this station. Just to the north of the smaller cell was the region of low reflectivity (less than 10 dBZ). The high wind area associated with this portion of the MCS is not apparent in the dual-Doppler data, as this region of low reflectivity at low levels could not be sampled by the CP-4 radar. Dual-Doppler derived winds at 1.4 km showed strong west-southwesterly winds, with velocities reaching 15 $m\ s^{-1}$ on the northern periphery of the cells closest to PAM-12, while weaker westerly and northerly flow was associated with the southern cells. The strong southwesterly wind velocities detected closest to PAM-12 coincided fairly well with the 12 $m\ s^{-1}$ average winds from 243° and 15 $m\ s^{-1}$ peak wind gusts measured at the station at the onset of the bursts.

A middle level cross-section taken at 4.4 km (Fig. 6.3b) depicts a reflectivity pattern similar to that seen at 1.4 km. The convective cells and low reflectivity (less than 20 dBZ) region close to PAM-12 were still present. The wind field showed a strong easterly and

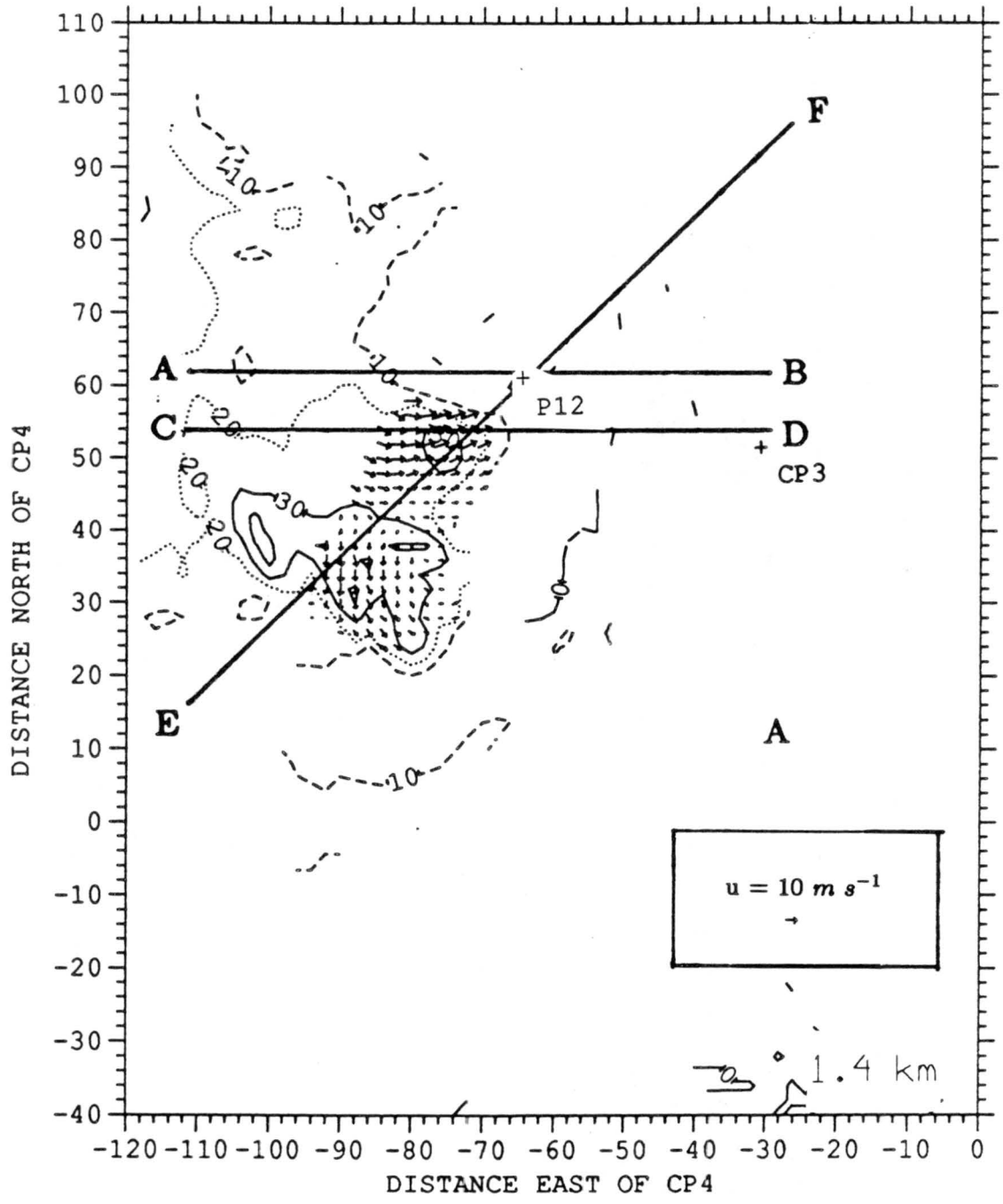

Figure 6.3: Horizontal cross-sections of dual-Doppler reflectivity and wind fields at (a) 1.4, (b) 4.4, and (c) 9.4 km MSL for 0324 UTC, 24 June 1985. Lines AB, CD and EF represent locations of vertical cross-sections in Fig. 6.4. Reflectivity contours are 10 (dashed), 20 (dotted) and 30 dBZ(solid).

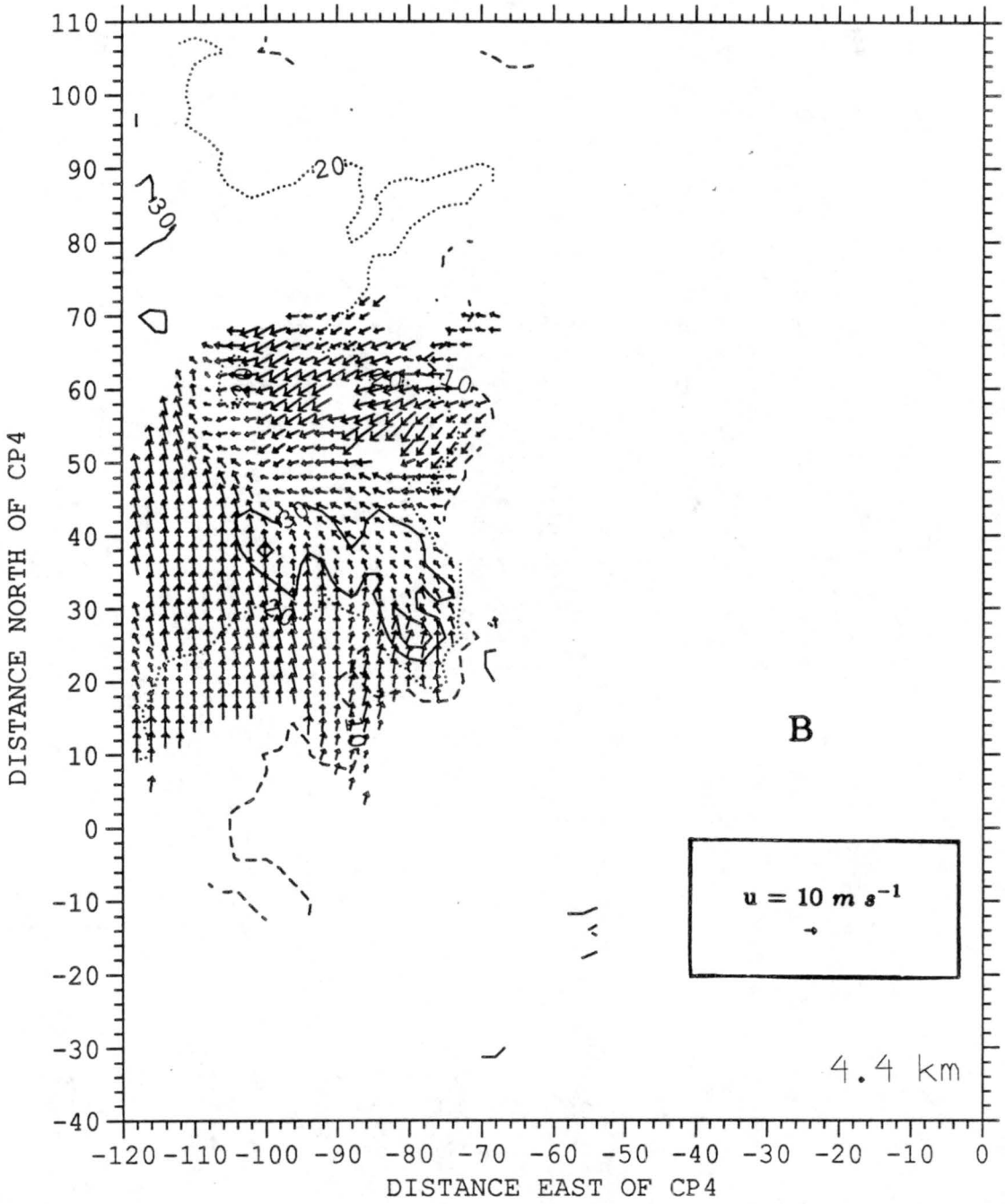

Figure 6.3: continued

northeasterly flow into this portion of the storm, with storm-relative velocities reaching 18 $m\ s^{-1}$ there.

An upper level cross-section made at 9.4 km (Fig. 6.3c) indicates a broad area of reflectivity between 10 and 20 dBZ, with a few small areas of reflectivity greater than 20 dBZ, which are associated with the convective cells seen at low levels. The wind field indicated divergence at the top of the convective cells, and overall broad scale divergence at this level. Winds were predominantly northwesterly in the southern half of the MCS, and southwesterly in the central and northern portions of the system. These winds indicate that the northeastward extension of stratiform precipitation associated with this MCS was formed by the advection of precipitation particles by southwesterly winds at upper levels. Some of the stratiform rainfall associated with this extension may have also been the result of in situ generation of new condensate by mesoscale updrafts which existed above the melting layer there, as well as by vapor deposition onto the ice particles which existed in this region of mesoscale upward motion (Brown, 1979; Ogura and Liou, 1980; Gamache and Houze, 1982; Smull and Houze, 1987; Rutledge and Houze, 1987; Johnson, et. al., 1989; Gallus and Johnson, 1990).

East-West Vertical Cross-sections

East-west vertical cross-sections of the precipitation and wind fields in close proximity to the HB activity were taken across and just to the south of station PAM-12 (see Fig. 6.3a for location of cross-sections). These sections traverse the region of strong low-level outflow detected by the CP-3 radar just to the northwest of PAM-12.

A cross-section (Fig. 6.4a) was taken along the line AB (Y = 62 km north of CP-4), approximately 2 km north of PAM-12, within the low reflectivity area described earlier. This section depicts an anvil structure existed there, as light precipitation extended toward the east with height. Radar reflectivities were predominantly between 10 and 25 dBZ. A sharp gradient of reflectivity existed at the edge of the precipitation at low levels. The wind field in this region indicated a strong easterly inflow, which descended along the base of the anvil, and spread outward at low levels. Peak downward motions calculated within this region reached 3 $m\ s^{-1}$. The outflow associated with this circulation did not likely

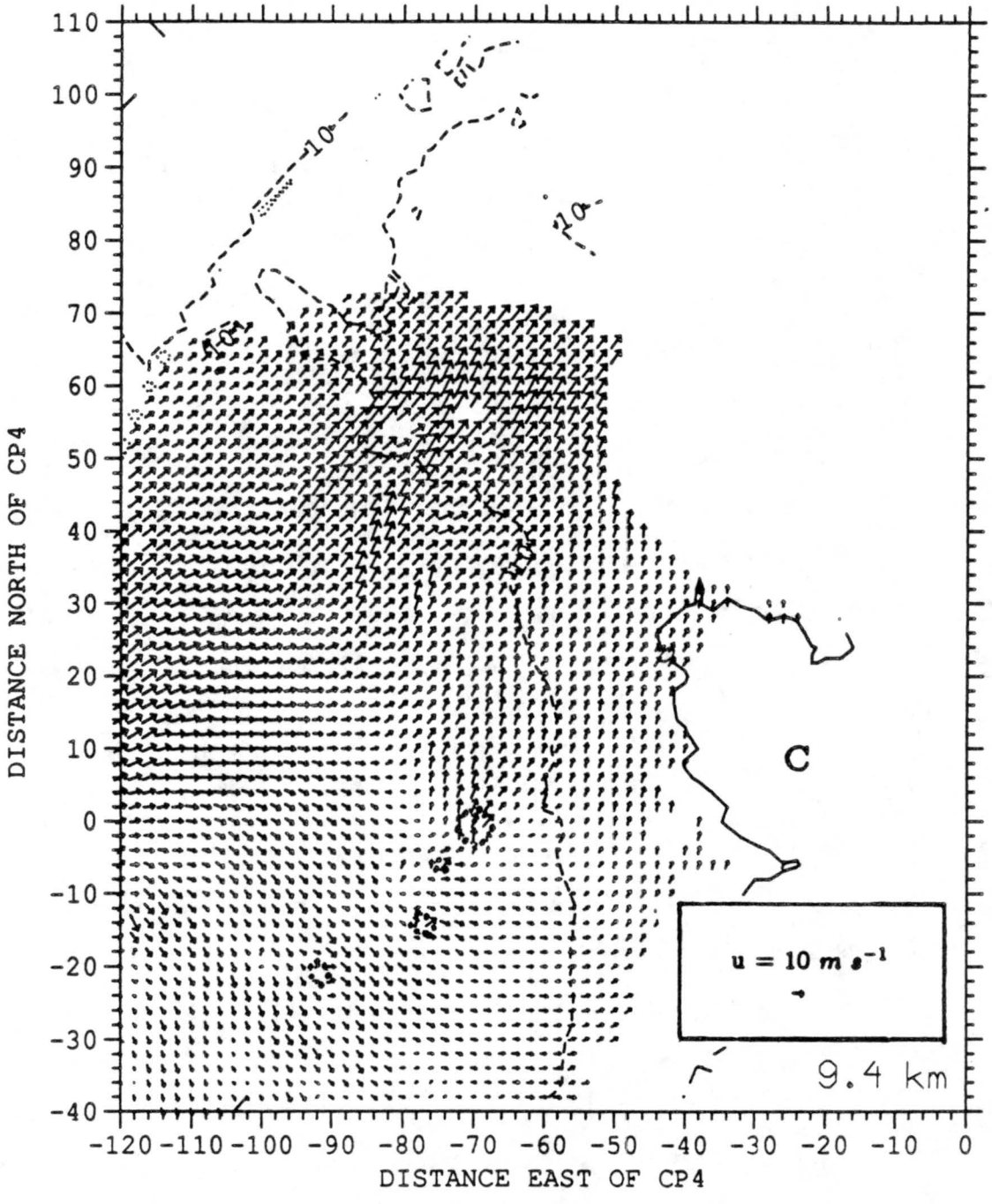

Figure 6.3: continued

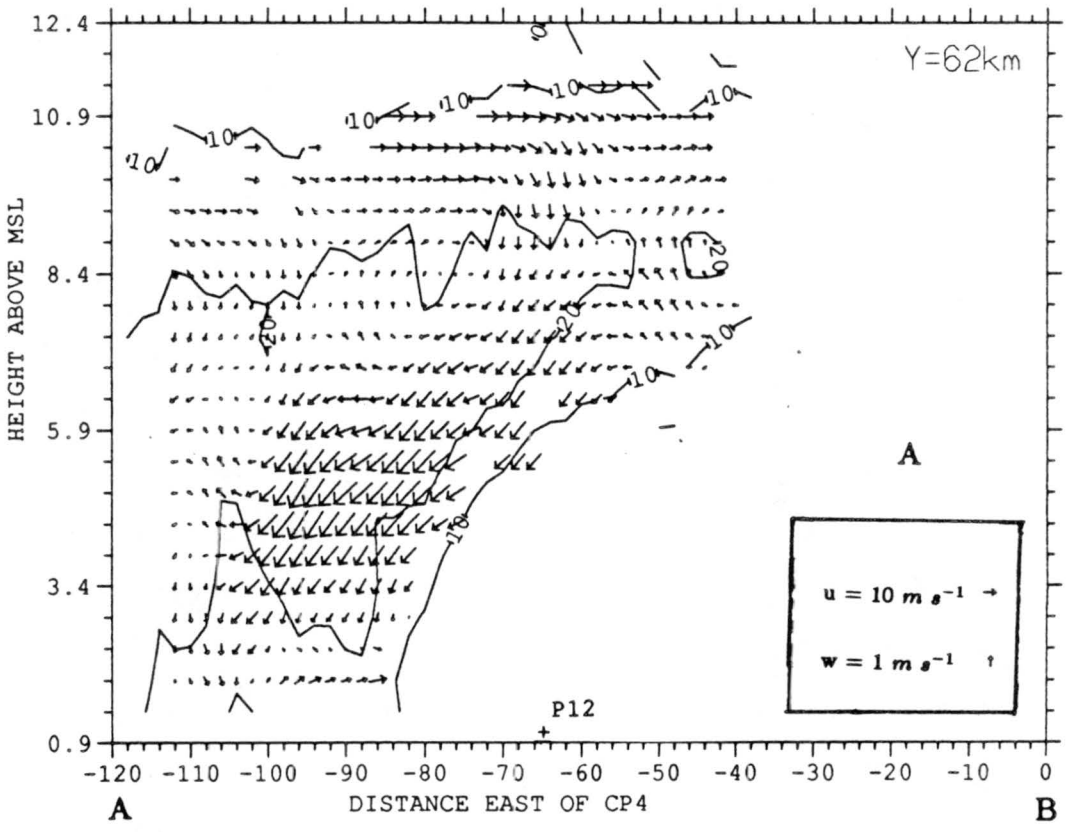

Figure 6.4: Vertical cross-sections of dual-Doppler reflectivity and wind fields along lines (a) AB, (b) CD and (c) EF for 0324 UTC. Reflectivity contours at 10, 20 and 30 dBZ.

reach PAM-12. It had a southerly component (see Fig. 6.3a), and exited the precipitation region 20 km nearly due west of the station. The circulation does appear to be associated with the wind maximum detected by the CP-3 radar, however, as the wind maximum was centered just to the northeast of the area of the strongest downdrafts and outflow at Y=62. As discussed in section 6.2, this wind maximum is linked to the HB activity at PAM-12.

Cross-sections taken to the northwest of PAM-12, such as Fig. 6.4a, revealed a structure similar to that which accompanies a rear inflow jet (e.g. Stumpf, et. al., 1990). However, the source region for the first, and weaker bursts at PAM-12 appears to be to the southwest of this station. This area coincided with the southeastern extreme of this strong outflow region, and therefore, the vertical structure of the precipitation and wind fields there will not be indicative of those associated with the HBs. A cross-section taken along the line CD, just to the south of PAM-12, reveals weaker inflow at mid-levels, and weaker downdrafts (see Fig. 6.4b). The strongest downdrafts were also located well within the precipitation area, while vertical velocities approached zero along the edge of the precipitation region. This does not indicate that strong evaporatively driven downdrafts existed just outside the precipitation area. Verification of was not possible as there was no reflectivity there to attain wind values. Previous studies have suggested that strong, evaporatively driven downdrafts outside the surface precipitation field were necessary to the formation of HBs.

As discussed earlier, northeasterly inflow existed at mid-levels and southwesterly outflow existed at low levels in the vicinity of PAM-12. A cross-section which more effectively displays the circulation associated with the winds reaching the station would be along the plane of this circulation, the line EF. This section (Fig. 6.4c) depicts a circulation somewhat similar to that seen in Fig. 6.4a, but through a shallower layer. Northeasterly inflow between the 3.9 and 5.4 km levels, downdrafts approaching 1 $m\ s^{-1}$, and southwesterly outflow are all evident. It is obvious, however, that the inflow jet signature is much weaker in this cross-section. This may help to explain the relative weakness of the first burst episode at PAM-12, when compared to those bursts experienced later.

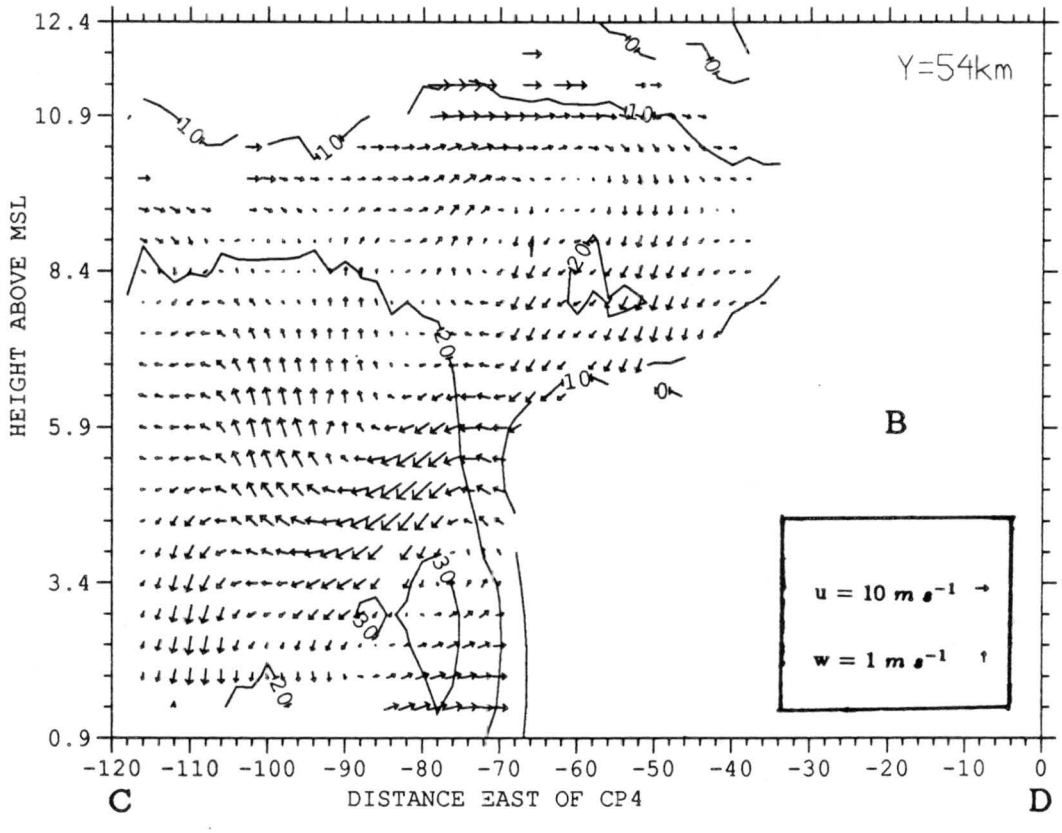

Figure 6.4: continued

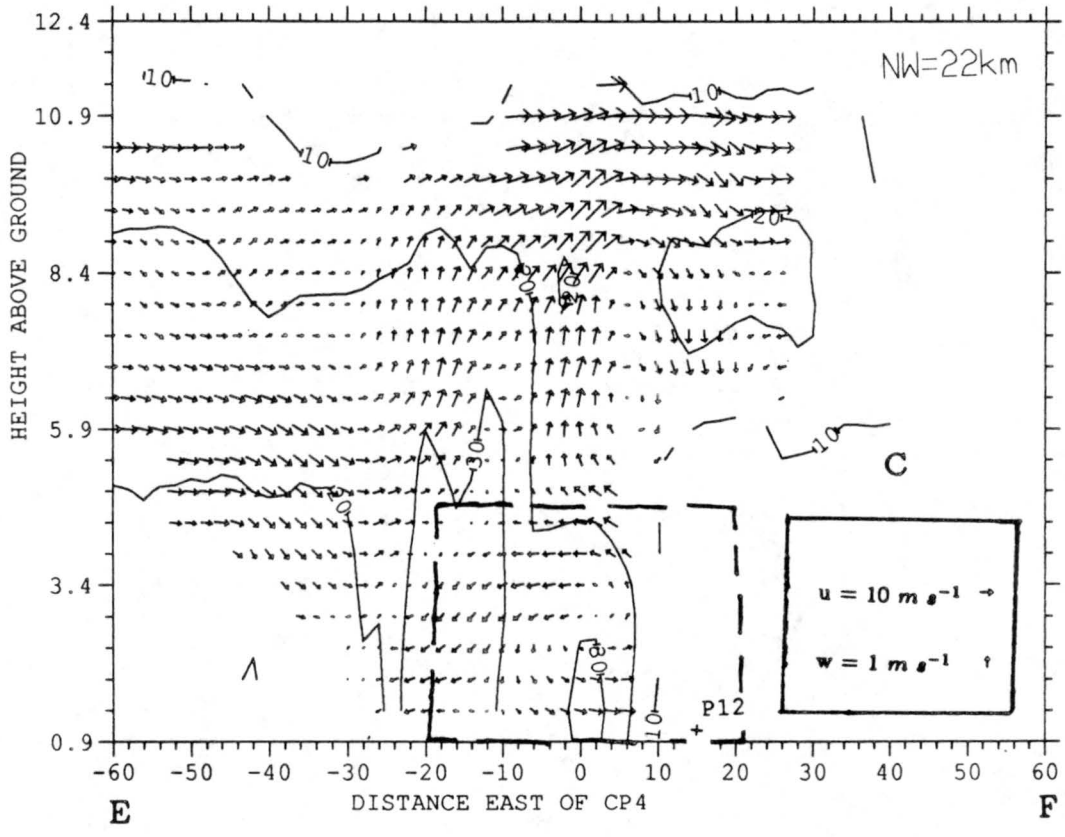

Figure 6.4: continued

6.3.2 0415 UTC Dual-Doppler Synthesis

The second of the two dual-Doppler syntheses was performed at 0415 UTC, approximately 5 minutes before the onset of the second episode of HBs at PAM-12. These bursts were more intense than those experienced during the first burst episode, as changes in the variables recorded there were more substantial (see Fig. 5.2). As discussed earlier, the convective cells which had formed to the southwest of PAM-12 had almost completely dissipated, and only a northeastward extension of stratiform precipitation existed to the west and northwest of the station by this time. The region of low reflectivity and the large area of high radial wind speeds detected by the CP-3 radar became positioned over PAM-12 (see Fig. 6.2h). The low-level wind maximum was not visible in the dual-Doppler synthesis, due to the inability of the CP-4 radar to sample activity close to the ground at far ranges (greater than 80 km). The focus of the second dual-Doppler investigation will be this low reflectivity area, and the three-dimensional structure of the precipitation and wind fields associated with it.

Horizontal Cross-Sections

Horizontal cross-sections of the MCS at 0415 UTC have been made at 1.4, 4.4 and 9.4 km to again give an indication of the precipitation and wind fields near the surface, at middle levels and near the top of the storm.

The 1.4 km cross-section (Fig. 6.5a) shows an area of convective cells approximately 70 km to the south-southwest of PAM-12. To the northwest and north of these cells, a large area of stratiform precipitation existed. This precipitation extended to just northwest of PAM-12, and had reflectivities predominantly between 10 and 30 dBZ. The strong reflectivity gradient noted earlier along the eastern edge of this precipitation (just west of PAM-12), as well as the high radial velocities associated with this portion of the MCS, persisted at this time. The sparse dual-Doppler derived winds in this area again showed strong southwesterly flow, with velocities reaching 15 $m\ s^{-1}$. These values were quite similar to the 10 $m\ s^{-1}$ average wind speed and 17 $m\ s^{-1}$ peak wind gusts measured at PAM-12 at this time.

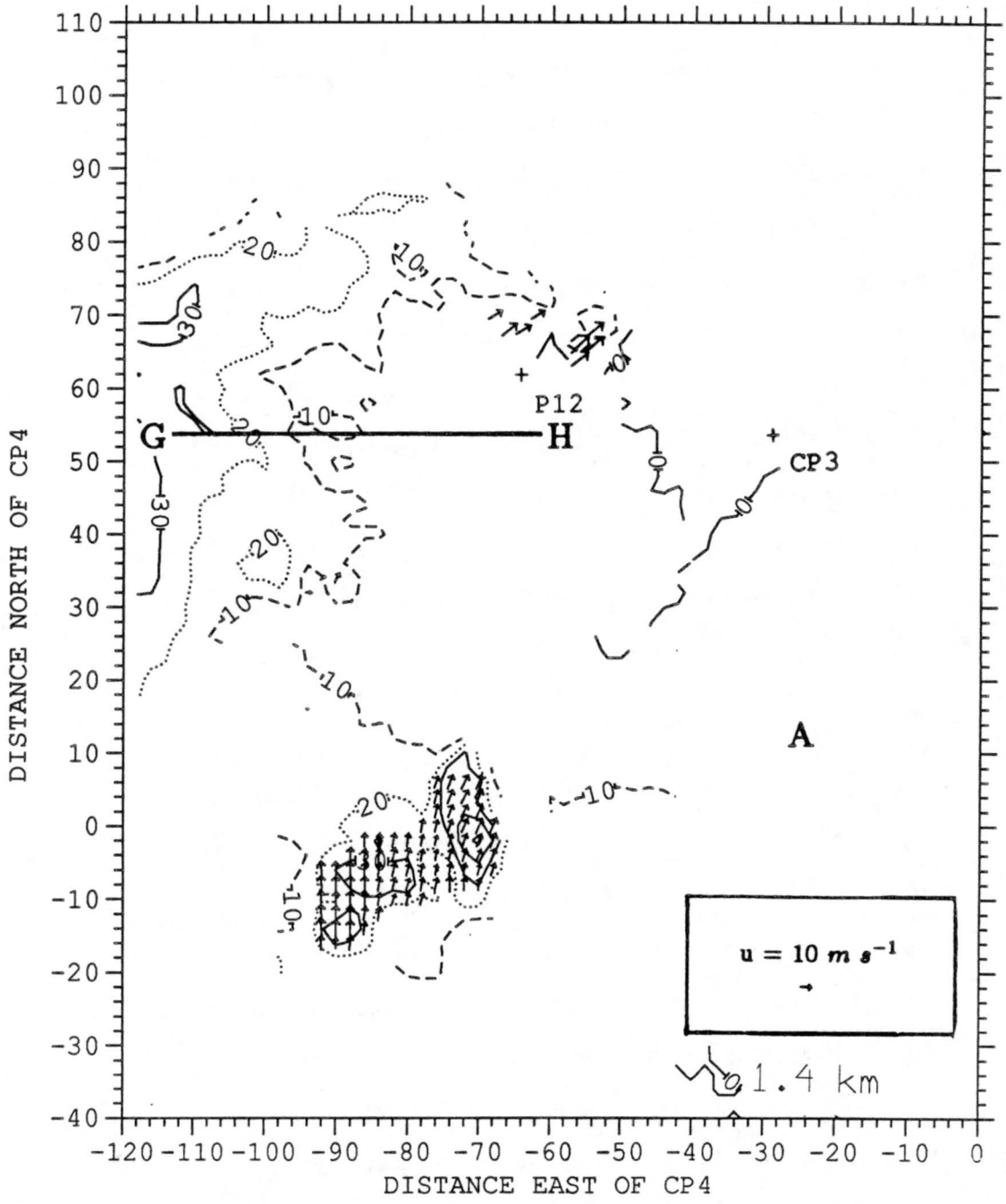

Figure 6.5: Horizontal cross-sections of dual-Doppler reflectivity and wind fields at (a) 1.4, (b) 4.4, and (c) 9.4 km MSL for 0415 UTC, 24 June 1985. Lines AB, CD and EF represent locations of vertical cross-sections in Fig. 6.4. Reflectivity contours are 10 (dashed), 20 (dotted) and 30 dBZ(solid).

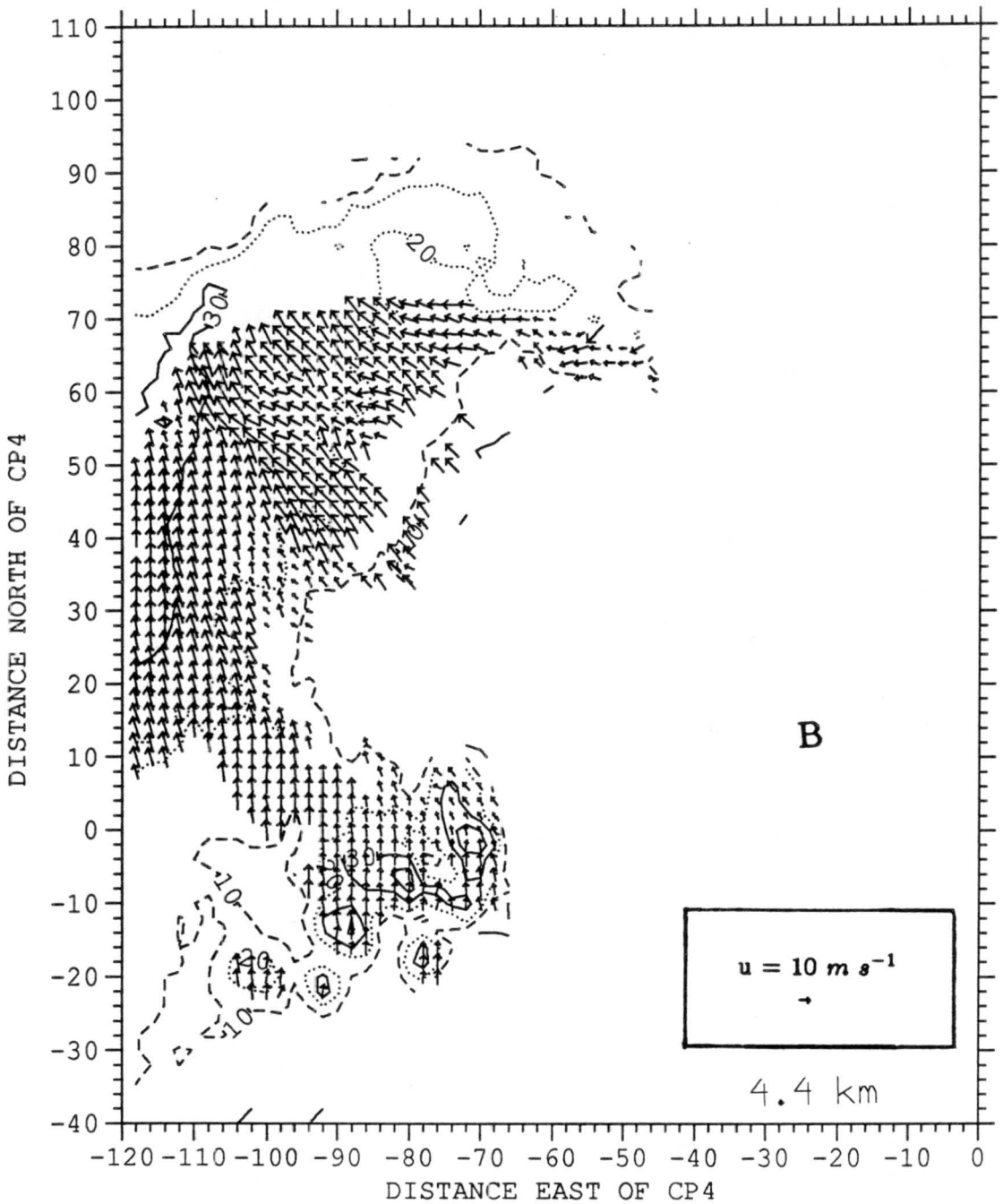

Figure 6.5: continued

The 4.4 km cross-section (Fig. 6.5b) displays a similar reflectivity pattern to that seen at the 1.4 km level. The main difference is the extension of the entire stratiform precipitation shield farther to the east over PAM-12. This trend continued with height, as the precipitation shield extended well to the north and east of PAM-12 at levels between 7.4 and 8.4 km (not shown). The low reflectivity area noted in the first dual-Doppler synthesis remained evident to the west and southwest of the surface station at both the 1.4 and 4.4 km levels. The wind field at 4.4 km showed that southeasterly and easterly flow was entering this portion of the MCS, with storm relative wind speeds reaching 15 $m\ s^{-1}$ there. This flow converged with an area of southerly flow from the convective cells, along a line just to the southwest of PAM-12. The position of this convergence line at 4.4 km coincided with that of the strong reflectivity gradient at 1.4 km.

The 9.4 km cross-section (Fig. 6.5c) again indicated a large area of precipitation with reflectivities between 10 and 20 dBZ, with a few areas of reflectivity greater than 20 dBZ associated with the convective cells to the south. The wind field continued to indicate the existence of broad scale divergence at this level, as winds were northwesterly at the southern edge of the MCS, and southwesterly and in the northern portion of this system. Divergence was also detected at the top of convective cells. These features are quite similar to those noted at this level at 0324 UTC, but they have moved southeast, along with the MCS.

East-West Vertical Cross-Sections

An east-west vertical cross-section of the precipitation and wind fields (Fig. 6.6) was taken just 6 km to the south of PAM-12, along the line GH (see Fig. 6.5a for location of cross-section). This section traversed the region just to the southwest of PAM-12. The winds measured at the station were from between 230° and 250°, and averaged between 7.7 and 10.0 $m\ s^{-1}$ during the bursts.

The precipitation structure in this region again had an anvil-like structure, with a strong reflectivity gradient at the edge of the low-level precipitation shield. The wind field had a deep layer of inflow with an easterly component, which descended along the base of the anvil cloud. Strong downward motions reaching 2.5 $m\ s^{-1}$ were present in

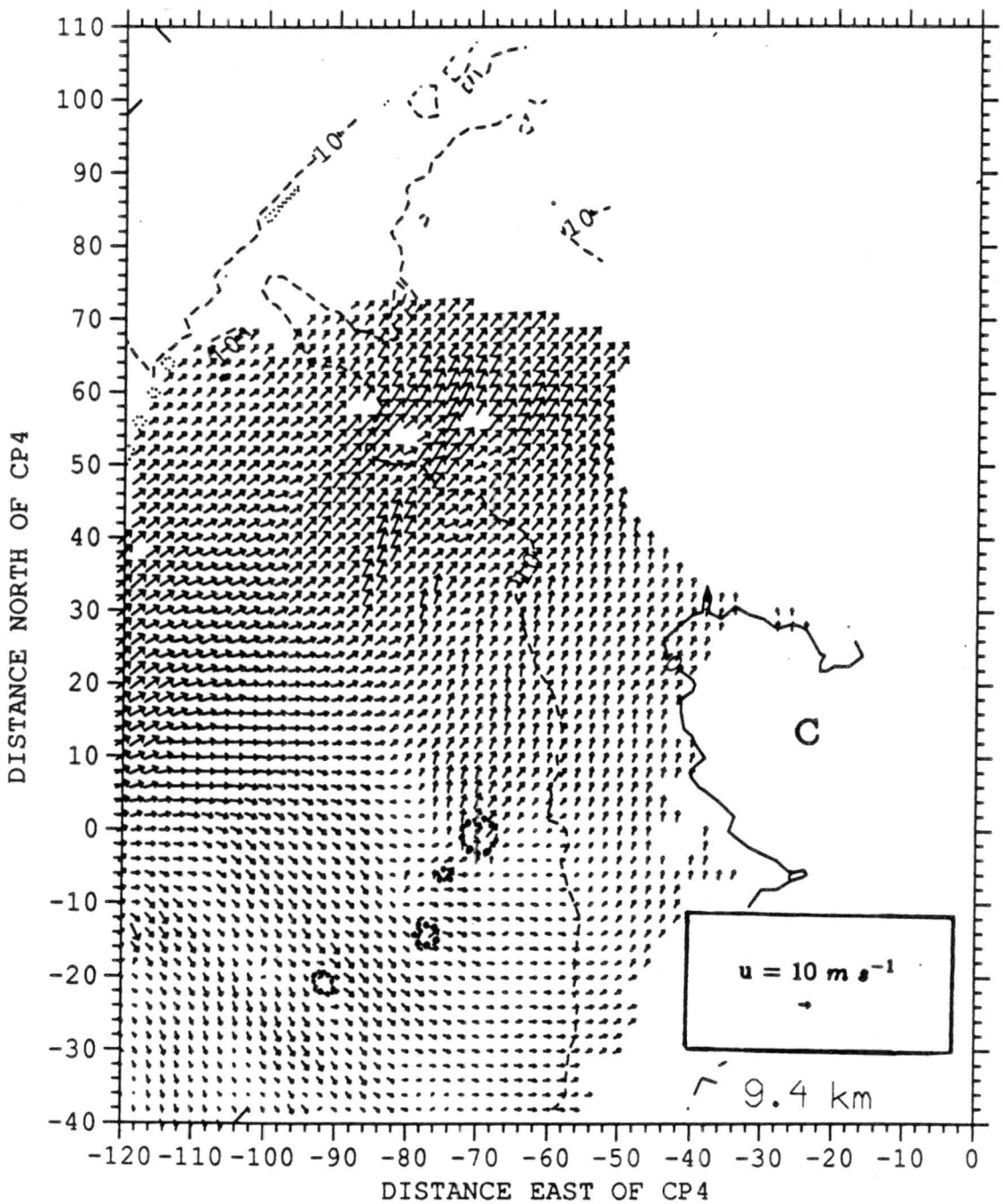

Figure 6.5: continued

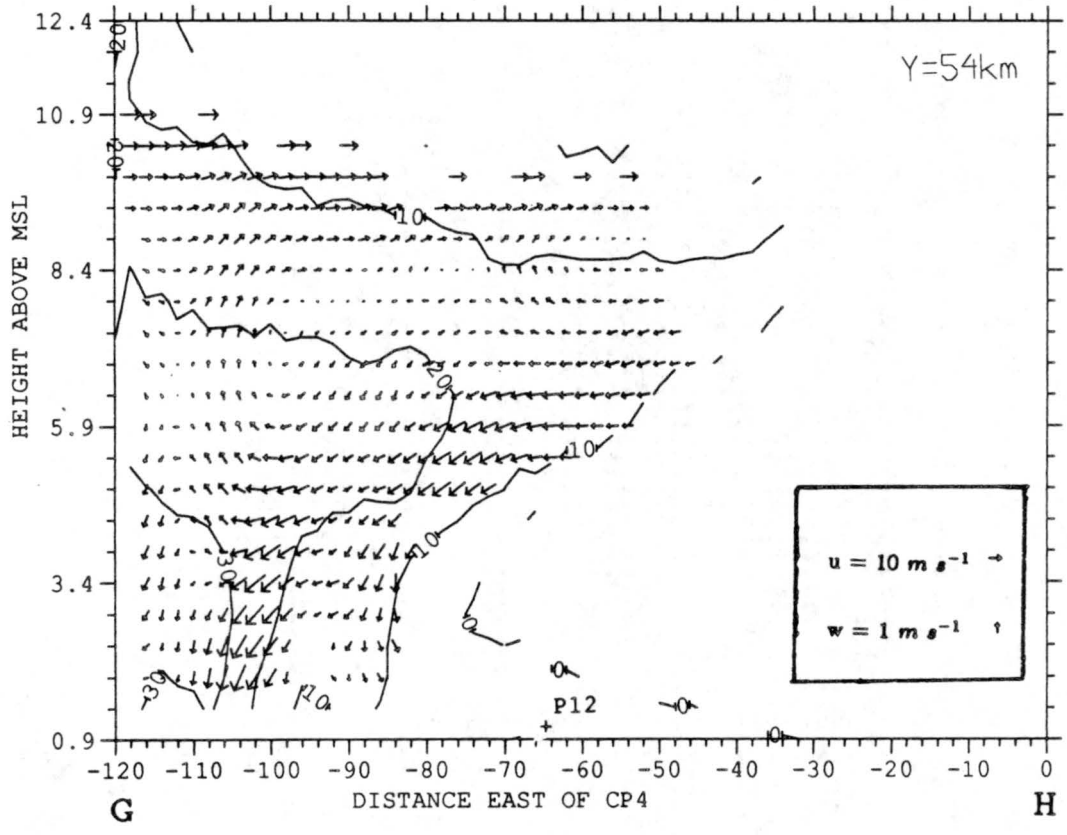

Figure 6.6: Vertical cross-sections of dual-Doppler reflectivity and wind fields along line GH for 0415 UTC. Reflectivity contours at 10, 20 and 30 dBZ.

the region of the strong reflectivity gradient, and indications of the southwesterly surface outflow were present at low levels. Velocities in this outflow reached 7 $m\ s^{-1}$. These winds were not detectable out to PAM-12, but an extension of weak low level reflectivity (less than 10 dBZ) beyond PAM-12 gives an indication that this outflow was indeed reaching the station (see Fig. 6.6). As discussed in section 6.3.1, this two dimensional wind and precipitation structure is similar to those documented in conjunction with rear inflow jets, however, rather than entering the rear of the MCS, the inflow jet was intruding into the stratiform precipitation region laterally.

6.4 Summary of Doppler Analyses

The combination of CP-3 single Doppler radial velocity analyses and dual-Doppler syntheses has revealed a distinct three-dimensional precipitation and wind structure associated with HBs. The region of surface HB activity is characterized by an area of low reflectivity and a strong horizontal reflectivity gradient at low levels, and an anvil structure at upper levels. A strong mid-level inflow entered this region from the east, descended along the base of the anvil and exited at the edge of the precipitation shield near the surface. The CP-3 radar detected a large area of strong low-level outflow just northeast of this precipitation, with velocities approaching 30 $m\ s^{-1}$, and size reaching nearly 600 km^2. The combination of these analyses has led to the conclusion that a lateral inflow jet existed at the edge of and in the precipitation-free region, immediately adjacent to the stratiform cloud system. It is this unsaturated, descending circulation just outside the precipitation shield which is likely to be responsible for both the large area of high winds, and the HBs at PAM-12, as the HB process is nearly dry adiabatic in nature.

6.5 A Heat Burst Conceptual Model

A conceptual model for the formation of HBs (Fig. 6.7) is proposed here, based on the results of this study. This model depicts heat burst occurrence as the result of the deformation of a shallow, cool, moist stable layer at the surface by a descending circulation of warm dry air, as proposed by Johnson, et. al. (1989). However, in contrast

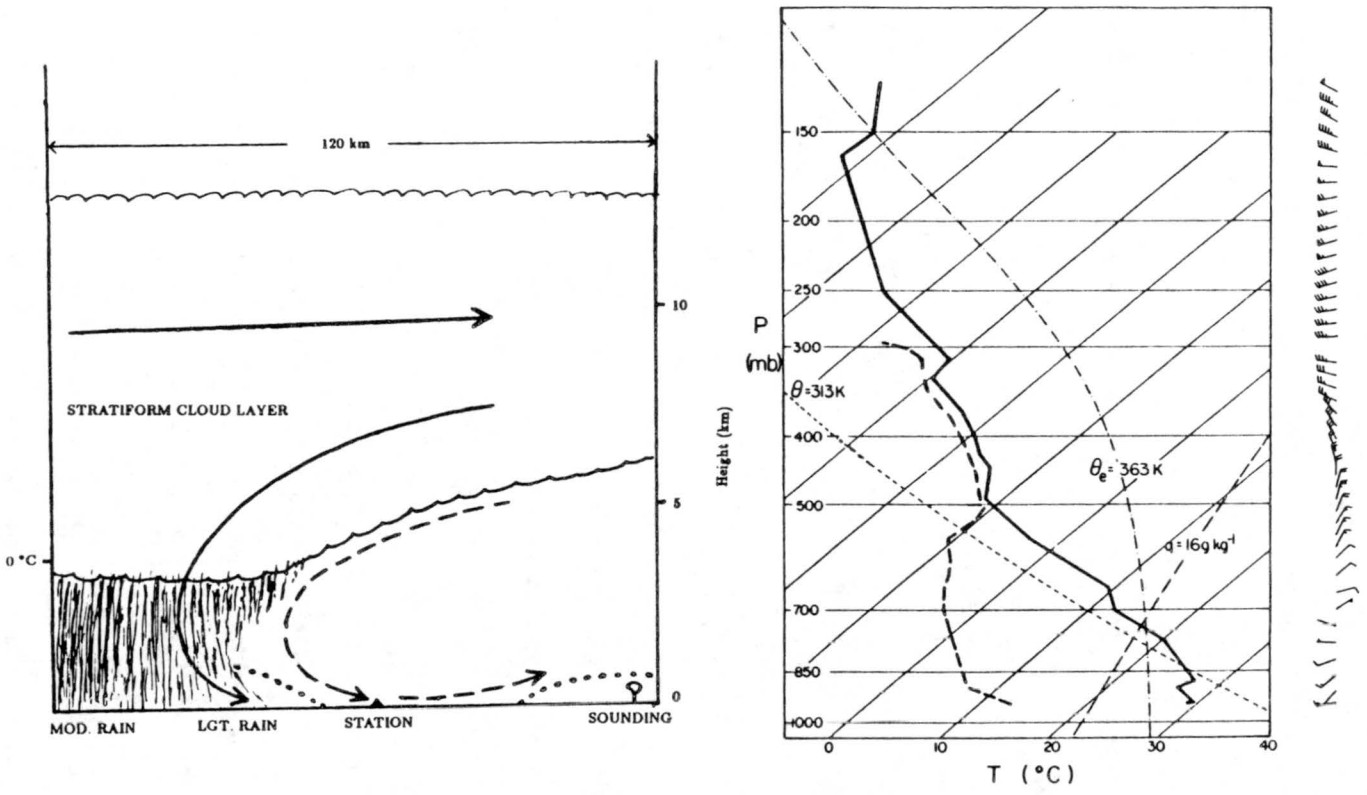

Figure 6.7: Conceptual model of a heat burst as a deformation of a shallow, cool, moist stable layer at the surface by a descending circulation of warm, dry air from aloft. Solid arrows represent winds verified by dual-Doppler data. Dashed arrow represents proposed heat burst wind. Dotted lines represent upper boundary of moist stable layer. Heat burst conceptual sounding adapted from 0440 UTC RSL sounding. Location of sounding and surface station are denoted.

to the microburst source for strong downdrafts proposed by Johnson (1983) and Johnson, et. al (1989), a lateral inflow jet appears to play a key role in the formation of strong downdrafts, at least in this instance. Both mechanisms rely on strong evaporation in a nearly dry adiabatic environment to force their respective downward motions. In this case, the dry air enters the stratiform region of the storm at middle levels, descends along the base of the anvil cloud, and exits the storm near the edge of the low-level stratiform precipitation shield. Downdrafts reaching 3 $m\ s^{-1}$ were detected in this region, but locally they may have been much stronger. Fig. 6.7 appears to represent the heat burst mechanism at PAM-12, but other mechanisms which produce strong downdrafts, such as microbursts, cannot be ruled out for heat bursts which occurred at other locations (e.g. PAM-3 and PAM-4).

Chapter 7

SUMMARY

The focus of this study was to extend the work done by Johnson, et. al. (1989) on the 23-24 June, 1985 PRE-STORM heat bursts (HBs). In their study and others which preceded it, it was discovered that HBs are often characterized at the surface by temperature rises, dewpoint and pressure falls, and are typically associated with regions of nocturnal thunderstorms having a nearly dry adiabatic lapse rate in the lower troposphere. A shallow stable layer with slightly elevated moisture content was also present in many HB soundings, including one taken in the vicinity of the HB activity in this case. Johnson, et. al. (1989) discovered that strong downdrafts were necessary to penetrate this stable layer. They suggested two possible mechanisms for the formation of these downdrafts: 1) Negatively buoyant, subsaturated air descending beneath virga shafts, similar to microbursts documented by Wakimoto (1983), attaining the momentum necessary to break through the surface stable layer, and 2) large scale descent in the vicinity of rear inflow jets causing a deformation of the stable layer, allowing the warm, dry air to reach the surface.

In this paper, further investigation of the surface characteristics linked to HBs was performed, and both single and dual-Doppler radar data were used to view the three-dimensional structure of the wind and precipitation fields in the vicinity of the bursts. The combination of these data with the results of Johnson, et. al. (1989) was used to offer a formation process to the 23-24 June, 1985 HB events.

The Oklahoma-Kansas PRE-STORM field project employed a sophisticated data collection network, which included a mesonetwork of 84 automated surface stations, seven digitized NWS WSR-57 10 cm radars, a network of rawinsonde sites, wind profilers and

four Doppler radars. At least six stations within the Kansas portion of the mesonetwork recorded HBs of varying intensity on 23-24 June. One station, PAM-12, received particularly strong HBs, and was located within the region of the dual-Doppler radar coverage supplied by the two NCAR radars in Kansas. A single nearby sounding from Russell, Kansas (RSL) was also available near the time of the HB occurrence at PAM-12.

The MCS which spawned the HBs formed just ahead of a dryline in western Kansas, and to the south of a synoptic scale stationary front positioned across southern Nebraska. As this system matured, a large stratiform region developed behind a southeastward progressing line of convective cells. Southwesterly flow aloft allowed for northeastward displacement of this light precipitation. The HB activity was all recorded in the vicinity of this stratiform precipitation extension.

The HB activity at surface station PAM-12 occurred in two distinct episodes, which lasted 15 and 30 minutes each. The episodes were marked by the following changes at the station: 1) a rise in temperature, 2) a fall in dewpoint, 3) a fall in relative humidity, 4) a fall in θ_e, 5) an increase in average wind speed, 6) an increase in peak wind gust speed, 7) a veer in wind direction, and 8) no change in surface pressure. The burst episodes were each followed by a period where conditions nearly returned to those which preceded the burst. Previous studies have documented the changes in temperature, dewpoint, relative humidity and pressure associated with HBs. Gusty, variable surface winds have also been reported during these events, but the impact of HBs on surface winds remained unclear. Winds at PAM-12 did show distinct changes in speed, gustiness and direction both during and following burst episodes. Changes in θ_e at the station, when used in conjunction with the RSL sounding, indicated the intrusion of air from levels between 480 and 700 mb during the bursts.

Single-Doppler data from the NCAR CP-3 radar were used to investigate the low level radial wind field in the vicinity of the HB activity. A large area (600 km^2) of high radial wind speeds was detected to the northwest of PAM-12. This wind maximum became well organized, and reached the station during two short periods. These periods coincided with those in which HBs occurred at the station. The relatively large scale of this feature

indicated that the PAM-12 HBs were the result of a feature much larger than that which would likely be associated with a small scale downdraft descending from a virga shaft.

Dual-Doppler investigations of the three dimensional precipitation and wind fields associated with the HB activity at PAM-12 revealed structures similar to those seen in the vicinity of rear inflow jets. An area of low reflectivity with a strong horizontal reflectivity gradient was clearly visible at low levels, and an anvil-like structure was present aloft. Strong storm-relative mid-level inflow entered the stratiform precipitation region laterally from the east, descended along and beneath the anvil precipitation, exiting the storm at low levels with a southwesterly wind direction (similar to the winds recorded at PAM-12 during the bursts). This direct circulation was likely to have been duplicated in the unsaturated air immediately adjacent to the precipitation structure there. This hypothesis is supported by the detection of a large area of high wind speeds just outside of the low-level precipitation shield by the CP-3 radar. These discoveries have led to the conclusion that the 23-24 June, 1985 PAM-12 HBs were the result of a descending lateral inflow jet associated with the stratiform region, which deformed the shallow surface stable layer in a large area near this station. This deformation, as suggested by Johnson, et. al. (1989) allowed for the formation of heat bursts at the surface. Stumpf, et. al. (1990) also reported deformation of the stable layer by a descending rear inflow jet, but no penetration to the surface was reported in their case.

This study points out the need for further investigation of the features associated with HBs. The bursts studied here only reflect one possible scenario for their formation. In the vicinity of the 23-24 June, 1985 MCS alone, HBs occurred at surface stations located in several completely different regions of the storm. The mechanisms for the production of the bursts which affected these stations may not have been similar to that proposed here for the PAM-12 bursts. Studies to date have only detected the motions within the precipitation shield which are associated with nearby HBs. To fully understand the circulations responsible for the formation of these bursts, a clear air detection device, such as Doppler lidar, would be required. Also, the intermittency of heat bursts remains unexplained.

REFERENCES

Battan, L. J., 1973: *Radar Observation of the Atmosphere* , University of Chicago Press, 324 pp.

Bedard, A. J., Jr., and T. T. LeFebvre, 1986: Surface measurements of gust fronts and microbursts during the JAWS Project: Statistical results and implications for wind shear detection, prediction and modeling. NOAA Tech. Memo. ERL WPL-135, 112 pp. [NTIS PB86-200847].

Bolton, D., 1980: The computation of equivalent potential temperature. *Mon. Wea. Rev.*, **108**, 1046-1053.

Brown, J. M., 1979: Mesoscale unsaturated downdrafts driven by rainfall evaporation: A numerical study. *J. Atmos. Sci.*, **36**, 313-338.

Brown, J. M., K. R. Knupp and F. Caracena, 1982: Destructive winds from shallow, high-based cumulonimbi. Preprints, 12th Conf. Severe Local Storms, San Antonio, Amer. Meteor. Soc., 272-275.

Cunning, J. B., 1987: The Oklahoma-Kansas Preliminary Regional Experiment for STORM-Central. *Bull. Amer. Meteor. Soc.*, **67**, 1478-1486.

Cunningham, D., 1989: Rapid changes of pressure and temperature, Guernsey, 31 July 1983. *Weather*, **44**, 131-133.

Froude, G., and J. Simmonds, 1965: Phenomenal temperature oscillations in Aden. *Meteor. Mag.*, **94**, 185-187.

Fujita, T. T., 1955: Results of detailed synoptic studies of squall lines. *Tellus*, **7**, 405-436.

Fujita, T. T., 1985: *The Downburst.* SMRP Research Paper Number 210, Dept. of Geophysical Sciences, University of Chicago, 122 pp. [NTIS PB-148880].

Fujita, T. T., and F. Caracena, 1977: An analysis of three weather related aircraft accidents. *Bull. Amer. Meteor. Soc.*, **58**, 1164-1181.

Gallus, W. A., Jr., and R. H. Johnson, 1990: Heat and moisture budgets of an intense midlatitude squall line. *J. Atmos. Sci.*, (in press).

Gamache, J. F., and R. A. Houze, Jr., 1982: Mesoscale air motions associated with a tropical squall line. *Mon. Wea. Rev.*, **110**, 118-135.

Houze, R. A., Jr., and S. A. Rutledge, 1986: A squall line with trailing stratiform precipitation observed during the Oklahoma-Kansas PRE-STORM experiment. Preprints, 23rd Conf. Radar Meteorology, Snowmass, Colorado, Amer. Meteor. Soc., J167-170.

Houze, R. A., Jr., S. A. Rutledge, M. I. Biggerstaff, and B. F. Smull, 1989: Interpretation of Doppler weather radar displays of midlatitude mesoscale convective systems. *Bull. Amer. Meteor. Soc.*, **70**, 608-619.

Johnson, B. C., 1983: The heat burst of 29 May 1976. *Mon. Wea. Rev.*, **111**, 1776-1792.

Johnson, R. H., and P. J. Hamilton, 1988: The relationship of surface pressure features to the precipitation and air flow structure of an intense midlatitude squall line. *Mon. Wea. Rev.*, **116**, 1444-1472.

Johnson, R. H., and J. J. Toth, 1986: Preliminary data quality analysis for May-June 1985 Oklahoma-Kansas PRE-STORM PAM II mesonetwork. Atmospheric Science Paper No. 407, Colorado State University, Dept. of Atmos. Sci., Fort Collins, Colorado, 41 pp.

Johnson, R. H., S. Chen, and J. J. Toth, 1989: Circulations associated with a mature-to-decaying midlatitude mesoscale convective system. Part I: Surface features-heat bursts and mesolow development. *Mon. Wea. Rev.*, **117**, 942-959.

Leary, C. A., and R. A. Houze, Jr., 1979: The structure and evolution of convection in a tropical cloud cluster. *J. Atmos. Sci.*, **36**, 437-457.

Leary, C. A., and E. N. Rappaport, 1987: The life cycle and internal structure of a mesoscale convective complex. *Mon. Wea. Rev.*, **115**, 1503-1527.

Meitín, J. G., and J. B. Cunning, 1985: The Oklahoma-Kansas preliminary regional experiment for STORM-Central (OK PRE-STORM), Volume I. Daily operations summary. NOAA Tech. Memo. ERL ESG-20, Dept. of Commerce, Weather Research Program, Boulder, Colorado, 313 pp.

Mohr, C. G., L. J. Miller and R. L. Vaughan, 1979: An economical procedure for Cartesian interpolation and display of reflectivity factor in three-dimensional space. *J. Appl. Meteor.*, **18**, 661-670.

Newton, C. W., 1950: Structure and mechanisms of the pre-frontal squall line. *J. Meteor.*, **7**, 210-222.

Ogura, Y., and M. T. Liou, 1980: The structure of a midlatitude squall line. *J. Atmos. Sci.*, **37**, 553-567.

Pedgley, D. E., 1962: A meso-synoptic analysis of the thunderstorms on 28 August 1958. *Brit. Meteor. Off., Geophys. Mem.*, **No. 106**, 74 pp.

Rutledge, S. A., and R. A. Houze, Jr., 1987: A diagnostic modeling study of the trailing stratiform region of a midlatitude squall line. *J. Atmos. Sci.*, **44**, 2640-2656.

Rutledge, S. A., R. A. Houze, Jr., M. I. Biggerstaff and T. Matejka, 1988: The Oklahoma-Kansas mesoscale convective system of 10-11 June 1985: Precipitation structure and single-Doppler radar analysis. *Mon. Wea. Rev.*, **116**, 1409-1430.

Sloan, Y. T., 1966: An unusual temperature fluctuation at Midland, Texas. Southern Region Rep. 3, U.S. Weather Bureau, Washington, DC, 9-12. [NTIS PB170757].

Smull, B. F., and R. A. Houze, Jr., 1986: The rear inflow jet in mesoscale convective systems. Preprints, 23rd Conf. Radar Meteorology, Snowmass, Colorado, Amer. Meteor. Soc., J163-166.

Smull, B. F., and R. A. Houze, Jr., 1985: A midlatitude squall line with a trailing region of stratiform rain: radar and satellite observations. *Mon. Wea. Rev.*, **113**, 117-133.

Smull, B. F., and R. A. Houze, Jr., 1987: Rear inflow in squall lines with trailing stratiform precipitation. *Mon. Wea. Rev.*, **115**, 2869-2889.

Stensrud, D. J., and R. A. Maddox, 1988: Opposing Mesoscale Circulations: A Case Study. *Wea. and Forecasting*, **3**, 189-204.

Stumpf, G. J., 1988: Surface pressure features associated with a mesoscale convective system in O. K. PRE-STORM. M.S. Thesis, Colorado State University Dept. of Atmos. Sci., 148 pp.

Stumpf, G. J., R. H. Johnson, and B. F. Smull, 1990: The wake low in a midlatitude mesoscale convective system having complex convective organization. *Mon. Wea. Rev.*, (in press).

Wakimoto, R. M., 1985: Forecasting dry microburst activity over the High Plains. *Mon. Wea. Rev.*, **113**, 1131-1143.

Williams, D. T., 1963: The thunderstorm wake of May 1961. Natl. Severe Storms Proj. Rep. 18, U.S. Dept. of Commerce, Washington, DC, 23 pp. [NTIS PB168223].

Wood, R. A., 1966: A thunderstorm "warm wake" at Midland, Texas. Southern Region Rep. 3, U.S. Weather Bureau, Washington, DC, 1-7. [NTIS PB170757].

Zipser, E. J., 1969: The role of organized unsaturated convective downdrafts in the structure and rapid decay of an equatorial disturbance. *J. Appl. Meteor.*, **8**, 799-814.

Zipser, E. J., 1977: Mesoscale and convective-scale downdrafts as distinct components of squall line structure. *Mon. Wea. Rev.*, **105**, 1568-1589.

Appendix A

PROCESSES USED ON DUAL-DOPPLER RADAR VOLUMES TO ATTAIN FINAL FIELDS

The procedures used to attain the final reflectivity field and the u, v and w components of the wind field from the synthesized NCAR CP-3 and CP-4 Doppler radar data were as follows:

1. Eliminated u and v fields where radars were at crossing angles less than 22° or greater than 158° (where 2 $csc^2\beta = (3.75)^2$). This allowed for a standard deviation of 1.875 $m\ s^{-1}$ in the u and v wind components.

2. Created reflectivity values for each grid point in radar volume as the maximum of those recorded by CP-3 and CP-4 radars for each grid point. This served to eliminate holes in the reflectivity data where false echoes were removed for one radar.

3. Created V_t (terminal velocity) field from reflectivity data, taking into account whether precipitation was frozen or melted. This was done using the following equation:

$$V_t = -\left[\frac{1}{exp(-0.1z)}\right]^{0.4} c_1\ Z^{c_2}$$

where c_1 and c_2 are set accordingly for melted (2.6, 0.107) and frozen (0.817, 0.063) precipitation, and V_t is negative by convention. This was done so that with w (vertical velocity) assumed to be zero, V_t could be used as a first estimate of W (= w + V_t). This allowed for the computation of u an v at every point in space by simultaneously solving the radial wind equation

$$V_{Rn} = R_n^{-1}\left[(x - x_n)u + (y - y_n)v + z(w + V_t)\right]$$

for the two radars, where n denotes the number of the radar and V_{Rn} is the radial velocity detected by each radar (Battan, 1973).

4. Patched V_t using a global patch. This gave values of V_t at all points in the grid, so no points within the precipitation area lack a V_t value.

5. Corrected u and v fields for V_t (patched version), using the 2-Radar Horizontal Wind Recomputation. This process eliminated the vertical component of the u and v fields that was due to the inclusion of V_t .

6. Patched V_t-corrected (w-corrected for later iterations) u and v fields into temporary fields, using a local patch. This process filled all gaps in the data field within and along the edges of the available wind data, thus allowing for the calculation of convergence at every point within the wind field.

7. Filtered the patched V_t-corrected (w-corrected for later iterations) u and v fields using a 2-step Liese filter. This process eliminated small scale features in the wind fields which were not important to this study.

8. Created convergence field using 3-point convergence of the V_t-corrected (w-corrected for later iterations) u and v fields.

9. Patched convergence field using a global patch.

10. Eliminated patched convergence field where the patched and filtered u field was not present (no data). The combination of the last two processes allowed for the availability of convergence values at every point where horizontal winds were available, thus allowing the calculation of all three components of the wind field at these locations.

11. Performed a top-down vertical integration of the convergence field, using w = 0 $m\ s^{-1}$ as a boundary condition one level above the highest level with good convergence values. A first guess (new estimate of the) vertical velocity (w) field resulted. Top down integration was used to minimize errors due to poor sampling of the convergence field near the surface.

12. Corrected V_t-corrected u and v fields for most recent estimate of w field (similar reasoning as used when correcting for V_t).

13. Calculated absolute value of the difference between the original V_t-corrected u and v fields and u and v fields corrected for the most recent estimate of w.

14. Repeated items 6 through 13 until the layer mean difference between the original V_t-corrected u and v fields and u and v fields corrected for the most recent estimate of w did not exceed 10 $cm\ s^{-1}$ in any horizontal layer (e.g. z = 4.4 km).

15. Adjusted most recent estimate of w to a lower kinematic boundary condition of w = 0 $m\ s^{-1}$. This was done by distributing excess divergence through the lowest few layers of each column, then recalculating w using a top down integration of the adjusted convergence field.

16. Corrected u and v fields for adjusted w field.

17. Subtracted out storm motion (5 $m\ s^{-1}$ at 330 degrees) from u and v fields to get storm relative winds.

Appendix B

LIST OF SYMBOLS

β	Radar beam crossing angle
°C	Celsius temperature
°F	Fahrenheit temperature
g	Gravity
K	Absolute temperature
m	Meter
mb	Millibar
P	Pressure
P_s	Surface pressure
R_d	Gas constant for dry air
s	Second
t	Time
T	Temperature
T_d	Dew point temperature
T_v	Virtual temperature
θ_e	Equivalent potential temperature
θ_w	Wet bulb potential temperature
u	x component of velocity

UTC	Universal time (Greenwich mean time)
v	y component of velocity
V_R	Radial velocity
V_t	Terminal velocity
w	Vertical component of velocity
x	Eastward distance
y	Northward distance
z	Upward distance
Z	Universal time (Greenwich mean time)
Z	Radar reflectivity
dBZ	10 log_{10} Z